Low Cost Optoelectronic Sensors for Gas Monitoring in Diverse Environments

BY

Yu Chen

A dissertation submitted in partial fulfillment
of the requirements for the degree of
Doctor of Philosophy
in
Electrical Engineering
at
TUFTS UNVERSITY
August 2017

ADVISER:

Professor Sameer R. Sonkusale

Copy right

It will be complete later

Signature of Author ……..……..……Yu Chen

Department of Electrical and Computer Engineering

Certified by ……..Sameer Sonkusale

Professor,

Electrical Engineering,

Tufts University

Thesis Supervisor

Certified by ……...……...Eric Miller

Professor,

Electrical Engineering,

Tufts University

Certified by …….……..…John Durant

Associate Professor,

Civil Engineering,

Tufts University

Certified by ……,Mehmet R.Dokmeci

Instructor,

Harvard Medical School

ABSTRACT

Gas sensors are used extensively in monitoring of the environment. Many volatile organic compound gases found in the environment severely impact the health of an individual. Volatile organic compounds are also present in food odors (i.e. fruits, coffee, poultry) and we believe sensing them using gas sensors may provide an effective indicator of food freshness. For these sensors to be used en masse, they need to be affordable, sensitive, user-friendly, easy to fabricate, and ecofriendly. Thus the objective is design, fabricate, test and validate low-cost optoelectronic sensor arrays for some targeted application in medical diagnostics and food quality monitoring.

Towards this goal, cellulosic paper is among the most promising substrates, since it is inexpensive, flexible, lightweight, portable and biodegradable. Several paper-based gas sensor platforms functionalized with different gas sensitive elements (e.g. chemo-responsive dyes, conductive nanomaterials) have been presented for gas detection in diverse environments. In one work, a paper-based microfluidic platform functionalized with an array of chemo-responsive dyes is built. Selective sensing of dissolved ammonia and carbon dioxide is achieved with ppm level sensitivity. In another work, a disposable food sensor is made on paper substrate with colorimetric microbeads arrays arranged as a geometric barcode to monitor the food spoilage. The sensor is fabricated through a stamping process, which is easy and highly reproducible. This barcode sensor can distinguish hourly change of food freshness at room temperature. Another paper based optoelectronic platform with combined optical and electrical chemi-resistive sensor arrays is used for sensing and discriminating several volatile gases and mixtures. By combining the optical and electrical

approaches, a unique optoelectronic signature is generated for each gas analyte and its mixtures. Using support vector machine (SVM) based machine learning approach enables accurate classification of these gases from the combined use of both optical and electrical sensor responses.

Another part of work includes a couple of sensor platforms with dye-contained colorimetric microbeads as the core sensing element. These works include an optical fiber sensor functionalized with colorimetric beads for the detection of gastric gas at ppm level; a microfluidic sensing platform incorporating colorimetric beads for detection of ammonia concentration in saliva with sub-ppm sensitivity; the colorimetric beads embedded hydrogel fiber used to monitor the pH of the skin for wound healing.

In summary, several optoelectronic sensor platforms have been developed, which combine the advantages of clean room free fabrication, low-cost paper-based substrate material with highly sensitive sensing materials such as chemoresponsive dyes. These as-fabricated cost-effective and highly reproducible sensor platforms have been used to realize gas sensing in diverse environments.

菩提本无树，明镜亦非台。

本来无一物，何处惹尘埃。

Science is not only a disciple of reason but, also, one of romance and passion.

---- Stephen Hawking

ACKNOWLEDGEMENTS

I would like to express my deepest gratitude to my advisor, Dr. Sameer R. Sonkuale, for his excellent guidance, patience, and support during the entire period of my graduate study. He has always provided me with timely help whenever we came across any difficulty in our research. He has always shown complete understanding whenever we are suffering from any obstacle. He is the one that has evoken my passion in science and has intiated me into the field of multi-disciplinary research. More than that, his charming personality and warm encouragement has always boosted my confidence to continue on as a researcher.

I would also like to thank Dr. Eric Miller, Dr. John Durant and Dr. Mehmet R. Dokmeci for serving as the committee members for my PhD defense and for giving me their valuable time and feedback.

I would like to thank Dr. Vishesh Vikas for providing valuable guidance and support on a variety of technical problems and offering useful advice for improvements during his postdoctoral years at Tufts University. I would also thank Dr. Shideh Kabiri Ameri for her help and contribution on some of my projects. I want to thank many other Nano Lab members, including Dr. Saroj Rout, Dr. Yael Zilberman, Guoqing Fu, Meera Punjiya, Aydin Sadeqi, Robbie D'Angelo, Wei Wang and Dr. Arif Zeeshan for their help during my Ph.D years. I would also thank Dr. James Vlahakis, who is the lab manager of Tufts Micro-fabrication Lab, for his technical support in microfabrication process for my projects. I want to also thank Ms. Stacie Simon, the lab secretary of Advanced Technology Lab who always provided timely help with packages and lab issues for our lab.

Many thanks to all the faculties and staff in the department of Electrical Engineering, and all other members of Tufts University for their time and efforts in helping me with coursework and administration issues during my study at Tufts University.

Finally, I would like to sincerely thank everyone in my family for their selfless love, support and consideration for me during all these years when I am staying abroad. I would like to express my deepest love to my mom who has enlighten my entire life by giving me the freedom and opportunity to explore this wonderful yet complicated world.

LIST OF FIGURES AND TABLES

TABLE OF CONTENTS

CHAPTER 1

Introduction

1.1 Motivation

Our atmosphere plays an important role in the survival of all living things. Due to urbanization, there is a growing need to monitor air quality in various environments, including industry, indoors, roads, mining, petroleum and gas refineries etc. The overarching need to maintain a sustainable environment has motivated researchers to develop gas sensors, early generation of which were used primarily for detection of toxic or/and combustible gases, such as methane, carbon monoxide and carbon dioxide [1]. Later the use of gas sensors were extended to monitoring of the industrial toxic wastes, odiferous compounds and many other volatile organic compounds [2][3]. Recently, researchers have found correlation between exposures to some environmental gases to their presence in body fluids impacting human health. Beyond environmental monitoring, patients with cancers (i.e. lung, breast, colorectal and prostate cancers) have shown disproportionate levels of certain volatile organic compounds (VOCs) present in either breath, saliva, sweat or other body fluids [4][5]. Thus, these VOCs have great potential to serve as biomarkers for detecting underlying cancers and other diseases. Based on these understandings, it is promising to incorporate gas sensors into the point-of-care (POC) diagnostic platform for health care applications.

In another application, gas sensors sensitive to VOCs have also emerged as a quality monitoring technique in the food industry to “smell” the aroma of different products, including fruits, coffee, poultry, and determine the food freshness [6][7][8]. Furthermore, the efforts on exploring new materials and novel sensing mechanisms for gas sensing has greatly

improved the detection limit of these sensors and expanded the categories of detectable gases, making it even more practical for routine monitoring of environments in regular and extreme conditions [9][10][11].

Thus the new generation of gas sensors will not only be used for monitoring air conditions in living and working space, but will be extensively used in health care diagnostics and food industry [12][13]. Meanwhile, there is also an increasing need for gas sensors in resource-limited environments. More considerations will therefore need to be taken into account when developing gas sensors for resource-limited environments. For instance, all the sensing techniques developed for POC diagnostic platform need to meet the generic requirements of World Health Organization (WHO), described under the criteria defined as ASSURED (Affordable, Sensitive, Specific, User-friendly, Rapid, Equipment free, Delivered to those who need it) [14]. Additionally, it is critical to make the sensor eco-friendly. The cost of making them should also be substantially lower using locally resourced materials. In essence, the next generation of gas sensors used in diagnostic platform should be low-cost, easy to fabricate, easy to use, accurate and biodegradable. To fulfill all the requirements, we have explored cellulosic paper as a substrate with low-cost fabrication process for printing sensing materials on them, and subsequent ease of sample delivery, readout and use.

During the past two decades, researchers have spent a lot of efforts on exploring possible substrate materials for fabricating gas sensors. Silicon wafer was used as an early generation of substrate material for making metal oxide based chemiresistive sensor arrays [15][16]. In this case, electrode and metal oxide deposition can be realized using microfabrication techniques, which makes the fabrication process highly compatible with

traditional CMOS fabrication procedure [17]. Given the relative high expenses and complexity of applying microfabrication techniques for sensor fabrication, cheaper materials, including glass, plastic, polymer films [18][19][20], and simpler fabrication techniques, such as inkjet printing and dielectrophoresis (DEP) assembly have been employed to fabricate low cost sensors [21][22]. With the advancement of optical communication, optical fiber has also emerged a promising platform for building optical gas sensors [23]. Optical fibers have several attractive features, including its light transmission capability over the entire visible wavelength, lightweight, biocompatibility and flexibility [24]. Optical fiber based gas sensors have already been successfully used for detection of hydrogen, oxygen, hydrocarbons and many other vapors [25].

In recent years, there is an increasing interest in developing paper-based sensors for chemical and bio-sensing applications [26][27]. Paper substrate possess the merits of being inexpensive, flexible, lightweight, portable and environmental friendly [28]. So far, paper based platform have been used for building lateral flow assays (LFAs) and microfluidic analytical devices [29][30]. Some examples of successfully commercialized paper based sensors include pregnancy test and urine test [31]. Paper substrate is highly compatible with most of the biological and chemical sensing ingredients based on its cellulous structure, therefore serves as one of the most promising platform for building new generation of integrated sensing system, which can fulfill all the WHO requirements for making affordable, sensitive and user-friendly diagnostic sensors.

In our work, several optoelectronic platforms based on low cost substrates (e.g. paper) coated with different gas sensitive elements (e.g. chemo-responsive dyes) have been built for gas detection under diverse environments. These optoelectronic sensor platforms include

paper-based microfluidic gas sensor, functionalized optical fiber gas sensor, disposable gas sensing tag, and other polymer supported sensing platforms. These sensor platforms are tested under both gaseous and aqueous environments and exhibit good sensitivity and adaptability. These sensor platforms have the potential to be used for a variety of applications, including medical diagnostics and food quality monitoring.

1.2 Contributions

In this dissertation, several low cost optoelectronic sensing platforms for gas monitoring are presented with the main applications in health diagnostics, food industry and environment monitoring. The design, fabrication and testing of the sensors are described in details. The key contributions of this dissertation are summarized as follows.

(a) *Use of economically inexpensive fabrication methodologies for sensor fabrication.* We explore several low cost fabrication methods for making sensors to avoid use of expensive clean room facilities or the use otherwise expensive equipment. Silicone spray based hydrophobic patterning is used on native hydrophilic substrate to define microfluidic regions on paper for inking dyes or delivery of analytes. This method is highly producible while minimizing the fabrication time. In another example, stamping based fabrication technique is used to print hydrophobic sensing elements onto paper substrate. It has the advantage of transferring complicated patterns onto paper substrate for deposition of several sensing elements simultaneously. The stamp is reusable for making batches of sensors.

(b) *Use of spectrometer, flat-bed scanner or smartphone for optical readout*. We have employed different detection methods in capturing optical signals, including USB spectrometer, flab-bed scanner and smartphone. USB spectrometer has the advantage

of distinguishing the color at nanometer wavelength resolution; flat-bed scanner can only extract three channels (i.e. Red, Green, Blue) which is shown to be sufficient for sensing applications. Smartphone is also emerging as portable and user-friendly tool for POC diagnostics however it suffers from background illumination variability. These detection methods are used under different circumstances for different applications based on their sensitivity and usability;

(c) *Capability in sensing in both gas or liquid.* We have demonstrated the capability of doing gas sensing under both gaseous and aqueous environments without any further modification in the sensor configuration. This is important in enabling sensing in an environment where gas is present in either gaseous form or dissolved state, such as in stomach environment.

(d) *Seamless integration into existing sensing platforms.* We have shown the potential of our sensors to be integrated into other existing sensing platform. The paper based sensors can be incorporated into other paper based diagnostic platform for disease screening; the functionalized fiber sensor can be easily integrated the endoscope capsule to assist visual inspection of the inner lining of the esophagus and the stomach.

1.3 Organization

The dissertation is divided into eight chapters. Chapter 1 provides brief introduction of this thesis. Chapter 2 covers a brief review on the significance of gas sensing in healthcare and discusses available sensing techniques. Sensing mechanisms of various sensors, as well as the corresponding detection methods are discussed in details. In chapter 3, a paper-based platform for colorimetric sensing of ammonia and carbon dioxide is described. In this work,

we are exploring a low-cost, flexible and reliable method to effectively pattern paper for capturing optical dyes and for flow-based delivery of target samples for colorimetric chemical sensing. We target the detection of ammonia (NH_3) and carbon dioxide (CO_2), two of the important environmental and health biomarkers. By functionalizing the paper platform with diverse cross-reactive dyes sensitive to NH_3 and CO_2, their selective sensing within a certain pH range, as well as their detection at different concentrations can be achieved. Chapter 4 discusses a flexible optical fiber sensor for sensing gastric gas with spectrometer detection. We present a gastric gas sensor based on conjoined dual optical fibers functionalized with sensitive optical dyes for sensing gases in both fluidic and gaseous environments. In chapter 5, a disposable colorimetric barcode sensor for food quality monitoring is presented. The barcode sensor is embedded in the food packaging to monitor the change of pH and volatile organic compounds (VOCs) during food spoilage. The sensor fabrication is low-tech and easy to perform. A smart phone provides a non-contact metric of food freshness/spoilage. In chapter 6, the realization of optical and electrical measurements on paper based sensors for gas sensing is introduced. In this work, optical and electrical sensor arrays are on the same paper substrate. This sensor platform can capture the change of optical and electrical signals when sensing a variety of gas analytes and clearly discriminate these gases. Chapter 7 lists some other biomedical applications using optical dyes as the sensing elements. Chapter 8 is a conclusion of this thesis with a short discussion on the possible improvement on sensor design, fabrication and measurement.

CHAPTER 2

Background

A gas sensor is a device used to detect the presence of a specific gas, as well as determine its concentration. During the past few decades, gas sensors have been widely used in environmental monitoring [1]. The increasing need of sensitive and cost-effective gas sensors has promoted the exploration of more efficient sensing principles and of more reliable sensor fabrication techniques [32]. There are different methods to realize gas sensing, including gas chromatography [33], optical techniques [34], and acoustic wave related mechanism[35]. Among these technologies, electronic nose, which is proposed as a method to mimic the smell discrimination functionality of mammalian olfaction system, has drawn widespread attention due to its relative simplicity and sensitivity to various gases [36]. An electronic nose detects different gas species and concentrations through monitoring electrical change of diverse sensing elements, thus it is also regarded as chemiresistive sensor [37]. Similarly, the concept of colorimetric nose has been proposed as a promising technique for making artificial olfaction system, which has comparable or even better sensitivity when compared with electronic nose, while overcoming some shortcomings of the existing electronic nose technology [38]. The colorimetric nose is based on various chemoresponsive dyes, the color of which will change significantly when interacting with targeted gas. In the following sections, the principle of chemoresponsive dyes, their applications in gas sensing, the measurement of optical signals, and the comparison between colorimetric nose and electronic nose, as well as some other gas sensing techniques will be discussed.

2.1 Classification of chemo-responsive dyes

The chemo-responsive dyes used in building colorimetric sensors are those containing an interaction center strongly coupled with an intense chromophore, which is responsible for the significant color change when the dye is interacting with analytes. This inter-molecular interaction between dye molecule and analyte molecule is usually stronger than van der Waals interation. Based on the types of interaction, the chemo-responsive dyes can be further classified into three categories, namely (a) Lewis acid/base dyes; (b) Brønsted acidic or basic dyes; (c) dyes with large permanent dipoles. The chemical constructions of different categories of chemo-responsive dyes are shown in Figure 2.1 [39] [40] [41].

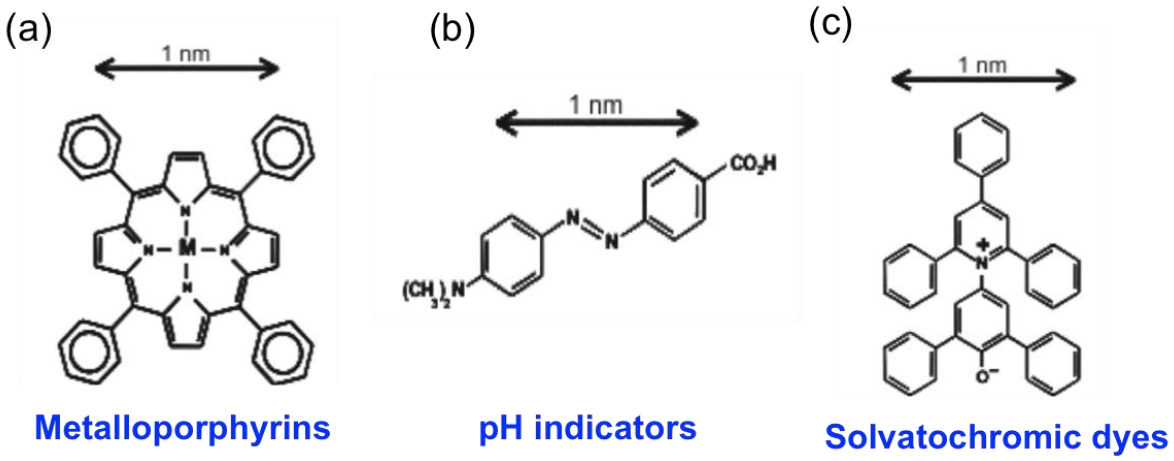

Figure 2.1: A schematic of typical chemical structures of three categories of chemo-responsive dyes. [41]

2.1.1 Metalloporphyrins

Lewis acid/base dyes described here refer to metalloporphyrins formed by the combination of porphyrins and metal ions. Metalloporphyrins have several open coordination sites allowing metal-ligand binding, which matches perfectly with the fact that a number of odiferous compounds are excellent ligands for metal ions. Some examples of metalloporphyrins are Zinc tetraphenylporphyrin (Zn-TPP), Copper tetraphenylporphyrin (Cu-TPP), Nickel tetraphenylporphyrin (Ni-TPP) and Cobalt tetraphenylporphyrin (Co-TPP), to name just a few. The ligation process between metalloporphyrins and odiferous compounds usually results in large spectral shifts. In Figure 2.2, the resulting spectral change of Zn-TPP upon exposure to ethanol and pyridine is presented. It is shown that the variation of ligands, in this case, ethanol and pyridine, will cause a difference in coloration, which naturally distinguishes different gas analytes [42].

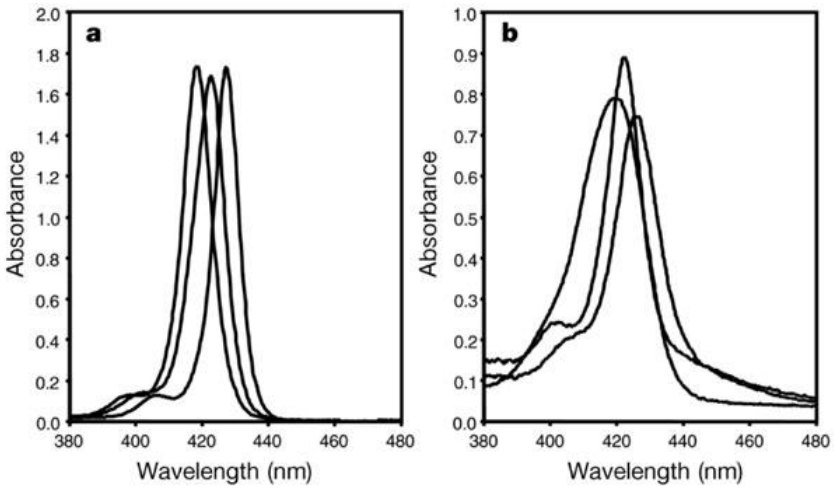

Figure 2.2: Comparison of spectral shifts observed on Zn-TPP upon exposure to ethanol and pyridine. (a) in methylene chloride solution; (b) on the reverse phase support. [42]

2.1.2 pH indicators

Brønsted acidic or basic dyes (pH indicator dyes) are weak acid or weak base. It is a halochromic chemical compound, which is sensitive to the concentration of hydrogen ions. The color of a pH indicator dye is determined by the relative concentration ratio of the conjugate base of this dye and the hydrogen ions, thus serves as the indicator of different pH values. There are a large number of pH indicator dyes, of which some commonly used ones are cresol red, methyl red, bromocresol purple, bromothymol blue, brilliant yellow, phenol red, phenolphthalein, etc. Figure 2.3 lists the chemical structures of several commonly used pH indicators dyes [43]. Usually, each pH indicator is sensitive to certain pH range, for instance, bromocresol green is responsive between pH 3.8 to 5.4; cresol red changes color at from pH 7.2 to 8.8, etc.

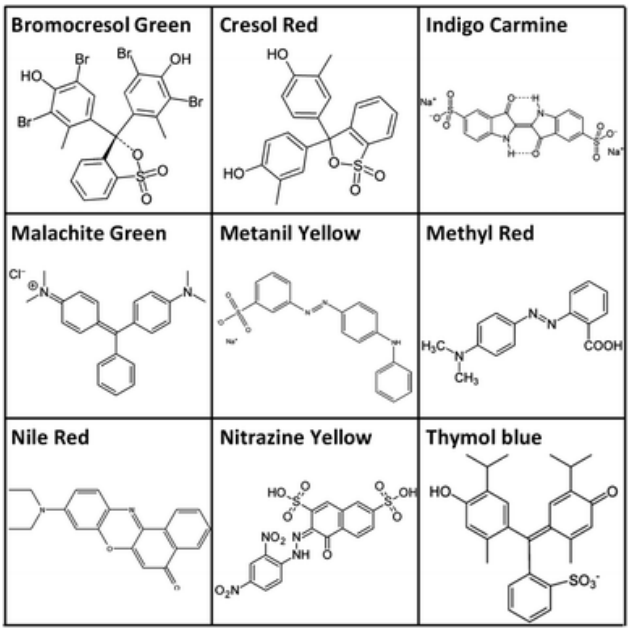

Figure 2.3: Some examples of pH indicator dyes. [43]

2.1.3 Solvatochromic dyes

Solvatochromic compounds are regularly used as polarity indicator of different solutions. The change of solvent polarity will strongly affect the absorption spectrum of solvatochromic dyes in the UV/Vis/near-IR range, with either blue shift (increasing solvent polarity) or red shift (decreasing solvent polarity). Figure 2.4 demonstrates the examples of the color variation of two solvatochromic compounds in several organic solvents. The fact that most of the organic solvent have different degree of polarity and this polarity can be visualized through the interaction with solvatochromic compounds paves the way for the application of solvatochromic dyes in sensing various gaseous organic compounds, thus making it a great candidate for building colorimetric nose. [44]

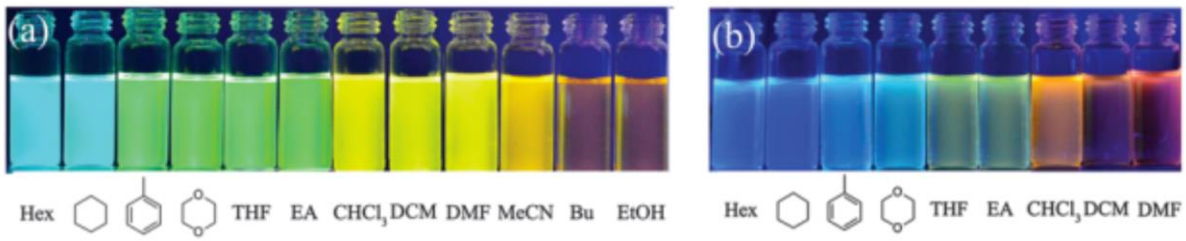

Figure 2.4: Fluorescence photographs of two solvatochromic compounds in a number of organic solvents (From left to right: hexane, tetrahydrofuran, ethyl acetate, dichloromethane, dimethylformamide, acetonitrile, n-butanol, ethanol): (a) BDPA-TXO and (b) BTPA-TXO. [44]

2.2 Gas sensing applications of chemo-responsive dyes

In the previous section, the properties and sensing mechanisms of typical types of chemo-responsive dyes are explained. Briefly, these chemo-responsive dyes are chemically reactive to a variety of gas compounds through intermolecular interaction. The chromophore

coupled active center of each chemo-responsive can react fiercely with specific gas molecules to induce a large spectral shift which results in a color change of this chemo-responsive dye [41]. This color changing property of chemo-responsive dyes provides a simple way to visualize the existence of a wide range of gas species [39]. Optical sensors incorporating a specific chemo-responsive dye have been developed to target specific gas compounds and shown ppm level sensitivity [45]. To increase the discriminatory power of such optical sensors, an array of optical sensors based on various chemo-responsive dyes have been built. By combining the responses of all chemo-responsive dyes, non-overlapping color patterns will be generated for each gas analyte, thus serves as an optical fingerprint for any targeted gas [43]. By using optical sensor arrays, one can not only clearly differentiate diverse gas species, but also distinguish different gas mixture. This discriminative power can be simply enhanced by increasing the number of chemo-responsive dyes used [46]. So far, these optical sensor arrays have exhibited excellent sensitivity and efficiency in sensing a number of volatile organic compounds (VOCs), toxic gases and aqueous solutions. Some applications using these optical sensor arrays will be discussed as examples to verify the sensing power of chemo-responsive dyes.

2.2.1 Detection of volatile organic compounds (VOCs)

Volatile organic compounds (VOCs) are ubiquitous and abundant in our environment, which are generated naturally by the metabolic activities of plants and animals. However, some of those VOCs are harmful to human health when excessive amount are presented in the air [47]. Given the effect of chronic toxicity due to long term exposure to VOCs, it is necessary to monitor the concentrations of different VOCs in the environment. So far, the detection and discrimination of various VOCs are most accurately realized by using gas

chromatography mass spectroscopy (GC-MS) technique [48] and later by using electronic nose built on chemi-resistive materials to meet the requirement of preforming real time measurement and enhancing the portability of the device [49].

Recently, optical sensor arrays with chemo-responsive dyes are recently being proposed as a portable, highly sensitive, cost-effective method for VOCs detection. As shown in Figure 2.5, Janzen et al. have built a disposable colorimetric sensor arrays containing metalloporphyrins, pH indicator dyes and solvatochromic dyes (totally 36 dyes) [39]. The detection of gas is realized by comparing the color of dye arrays before and after its exposure to different VOCs and by generating a color difference map. The color difference map is created by subtracting the RGB values of each dye center before and after gas exposure. The sensor responses to 24 representative VOCs are visualized in color difference maps in Figure 2.6. In these color maps, it is observed that these colorimetric sensor arrays can generate a unique color pattern for each VOC. The same set of colorimetric sensor arrays can easily discriminate more 100 VOCs which covers a broad range of VOCs under interest.

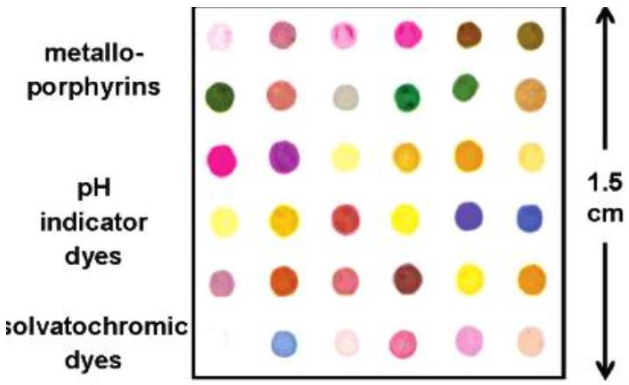

Figure 2.5: A typical image of as-fabricated colorimetric sensor array built with three classes of chemo-responsive dyes, namely, metalloporphyrins, pH indicator dyes and solvatochromic dyes. [39]

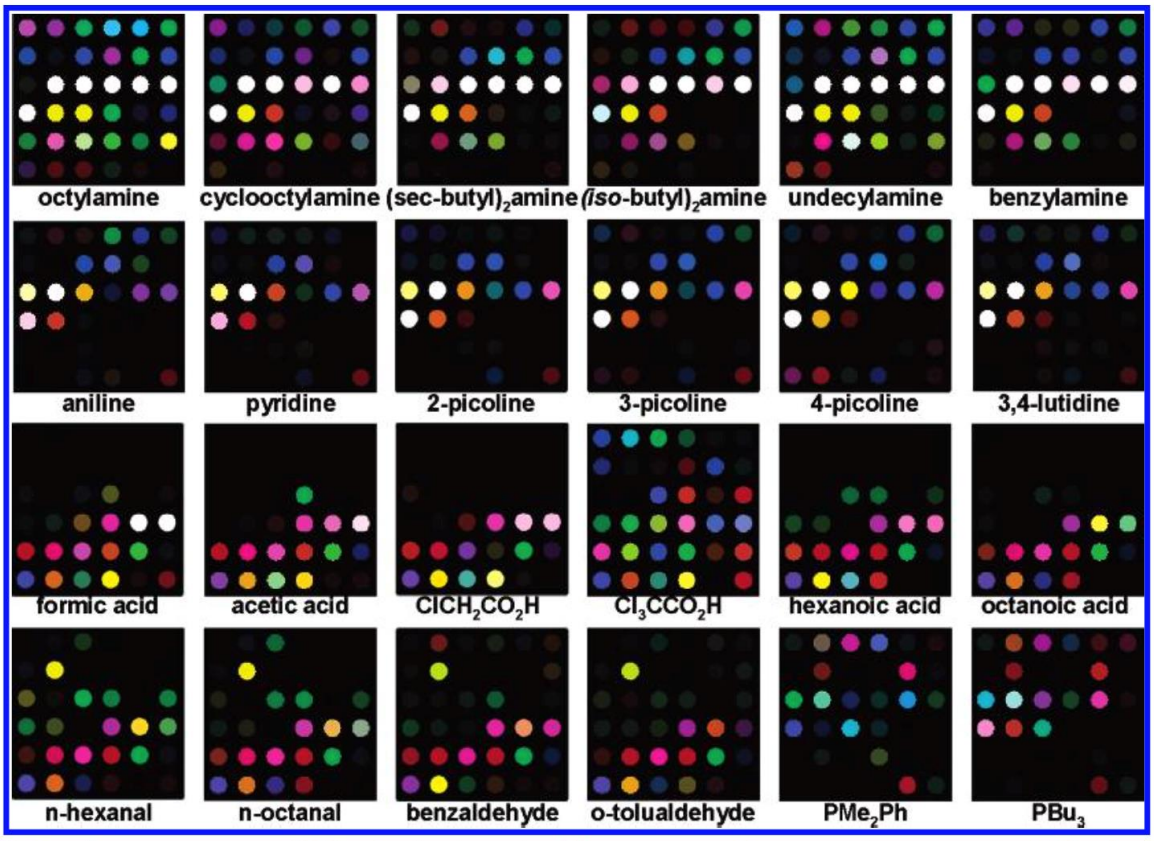

Figure 2.6: The proposed colorimetric array used to detect a number of VOCs. The sensing responses are visualized as color difference maps. [39]

The successful detection and discrimination of VOCs using colorimetric sensing arrays offers a reliable method for real-time monitoring VOCs. Moreover, the application of these colorimetric sensing arrays in VOCs detection is not limited to air quality monitoring. Long-term study of cancer inducing diseases have unveiled the relationship between body released VOCs and the actual condition of body health. For instance, by examining the VOCs presented in the exhaled breath, it is found that the amount and types of presented VOCs can serve as natural biomarker patterns to predict the health status of human body. This biomedical discovery has attracted attentions on developing sensors for VOCs detection in exhaled breath. Among these techniques, colorimetric sensor arrays also justify its suitability

in breath testing. Figure 2.7 presents a colorimetric sensor arrays with 24 cross-reactive dyes sealed in a disposable cartridge for breath testing [50]. The colorimetric testing information obtaining from healthy volunteers and volunteers with lung cancers can be combined with other clinical parameters to build a statistical model to estimate the health condition.

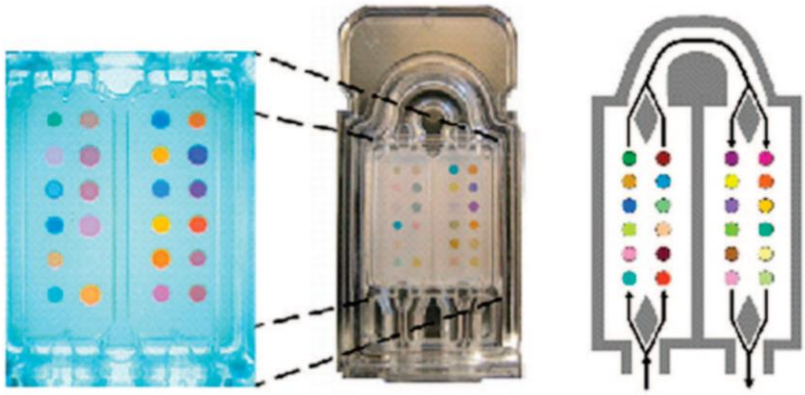

H2TPP+TsOH	CoTPP	Malachite Green	Methyl Red with NaOH
Zn2,6-F2PP	ZnTPP	Chlorophenol Red	Bromophenol Red + NaOH
Reichardt's Dye RD1	ZnTPP	Nile Red	Chlorophenol Red + NaOH
Malachite Green	F2S8 ZnTMP	Bromophenol Blue	Chlorophenol Red (higher conc.) + NaOH
Reichardt's Dye RD3	Lead Acetate	Bromocresol Green	Cresol Red+ NaOH
Copper Neodecanoate	Bromophenol Red+TsOH	Thymol Blue	Cresol Red+ NaOH (more plasticizer)

Figure 2.7: Colorimetric sensor with 24 chemo-responsive dyes used for breath testing on a disposable cartridge. [50]

2.2.2 Detection of toxic gases in environment

The functionality of colorimetric sensor arrays based on chemo-responsive dyes is not limited to VOCs sensing, but can be expanded to examine industrial toxic gases, fuels and combustion residues. Li et al. have employed an optical sensor array with 36 chemo-responsive dyes to distinguish 20 commonly used automobile fuels. As shown in Figure 2.8, under same concentration, different brands of gasolines can be recognized by its own color

pattern. The sensing results indicate that these optical sensor arrays can be used as a simple visualized indicator to discriminate the composition of a number of gasolines [51].

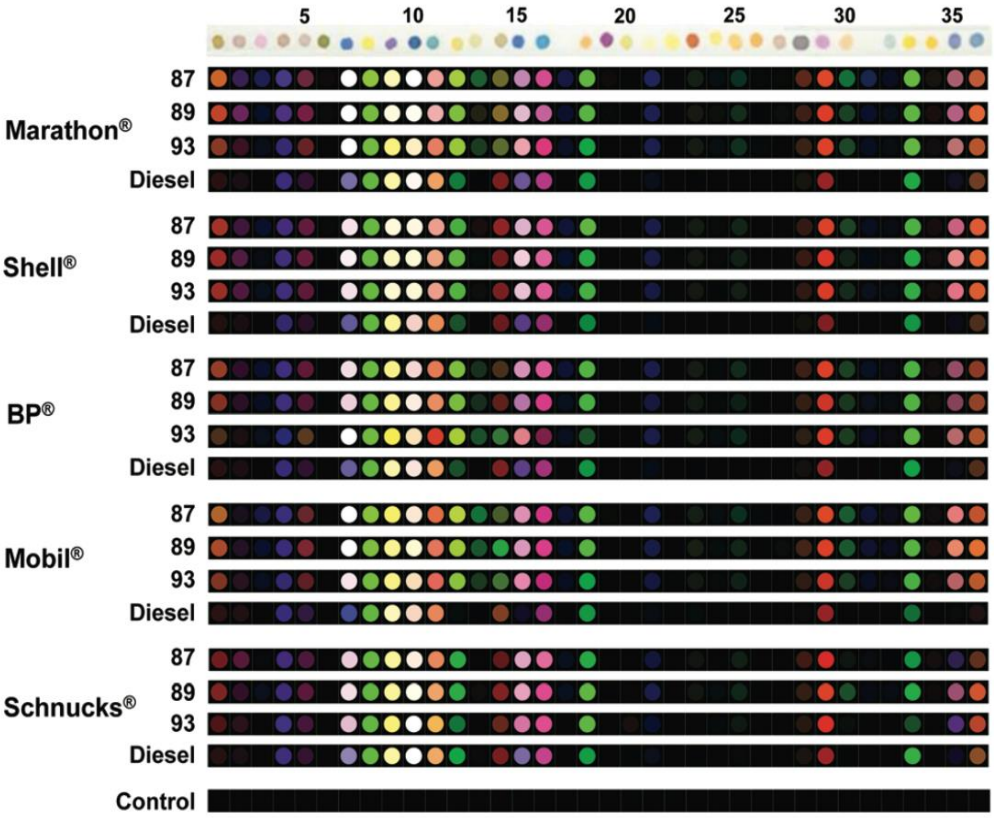

Figure 2.8 Colorimetric sensor arrays used for sensing 20 automotive fuels after pre-oxidation. The resulting color difference maps shows visible difference when the sensor strip is exposed to different fuel. [51]

Another example shown in Figure 2.9 illustrates the application of optical sensor arrays in testing three common types of industrial toxic wastes [52]. The optical responses of ammonia, chlorine and sulfur dioxide are highly distinguishable. Moreover, for each analyte, the variation in the concentration can be obtained by checking the resulting color map. For some analyte, such as chlorine, sub-ppm sensitivity can be achieved. The capability of dyes based optical sensor arrays to test analytes at varying concentrations with sub-ppm sensitivity

makes it a very promising technique for environmental monitoring, especially for the identification of toxic gases under permissible exposure limit [53].

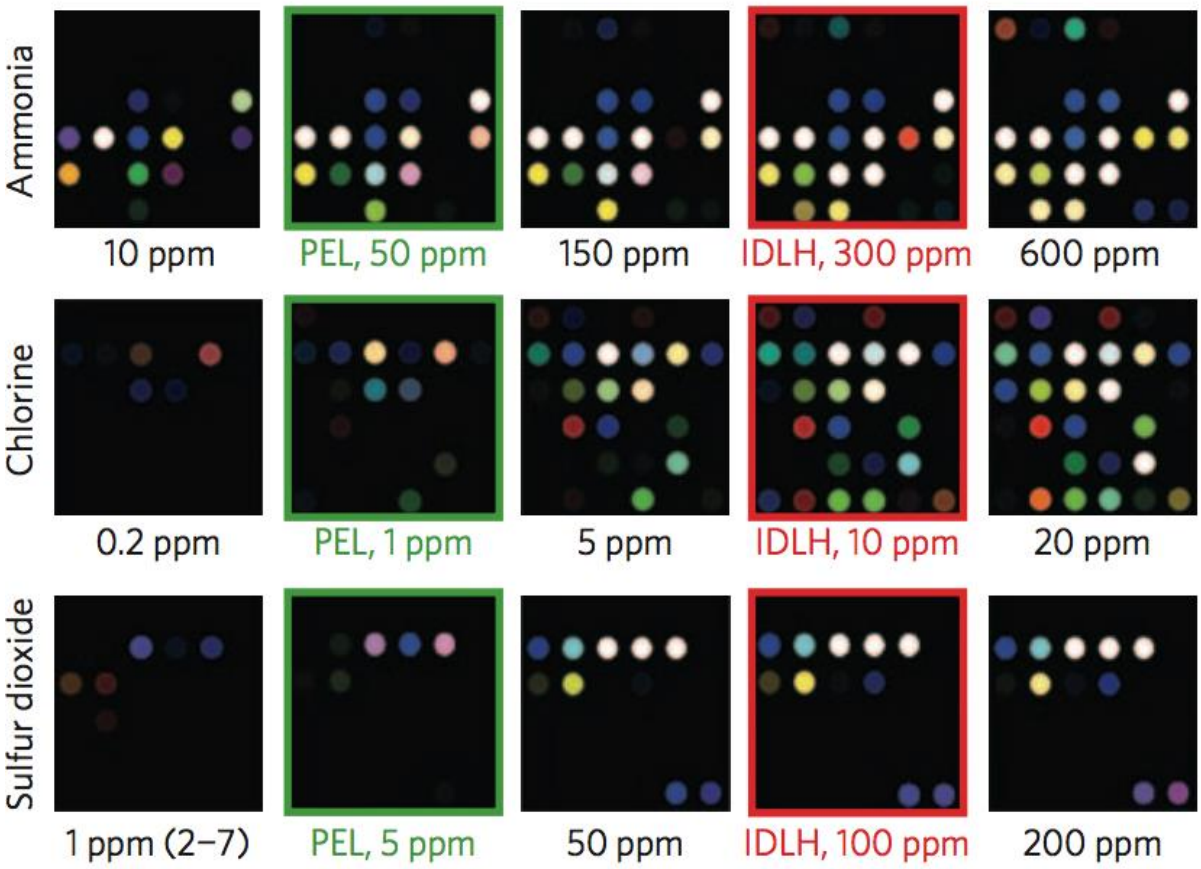

Figure 2.9: The sensing results of colorimetric sensor arrays for sensing different concentrations of ammonia, chlorine and sulfur dioxide. The colorimetric sensor arrays are able to detect ammonia, chlorine and sulfur dioxide at sub-ppm level concentration. [54]

2.2.4 Detection of complex mixture of odorants in food

As discussed in the previous examples, chemo-responsive dyes based colorimetric sensor arrays have been applied to detect health-related VOCs, air pollutants and industrial toxics. Given the powerful sensing ability, researchers have also explored the possibility of

applying the same set of colorimetric sensor arrays to detect the odorants emitted by a variety of food. Zhang et al. use colorimetric sensor arrays to examine the mixture of odorants in 14 common soft drinks (Figure 2.10) [55] and again demonstrate clear difference in the resulting color maps. Similar method is used to differentiate natural and artificial sweeteners (Figure 2.11) [56].

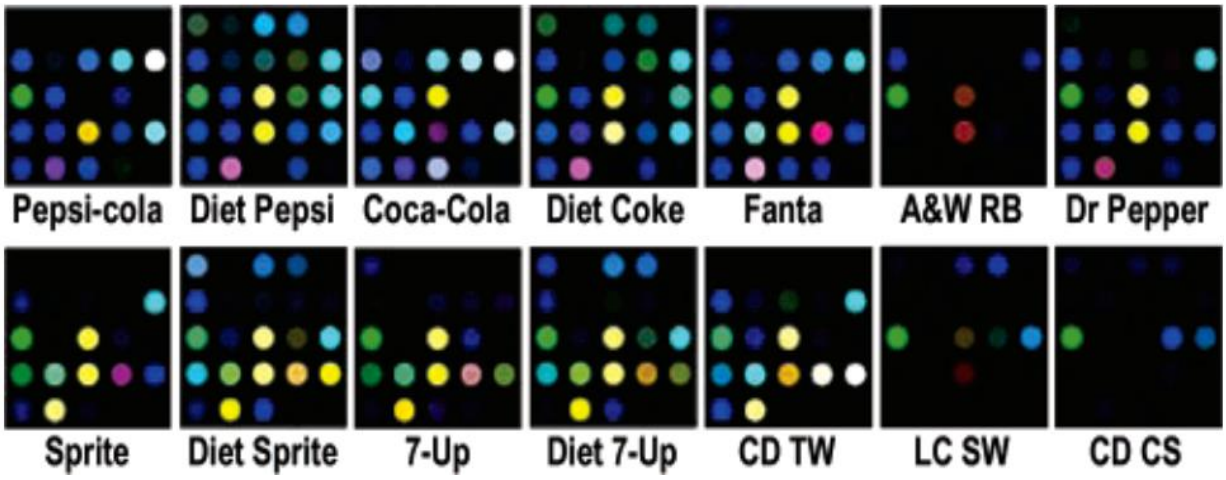

Figure 2.10: Use of colorimetric sensor arrays to detect the odor of 14 common soft drinks. The odors of 14 common soft drinks can be clearly distinguished. [55]

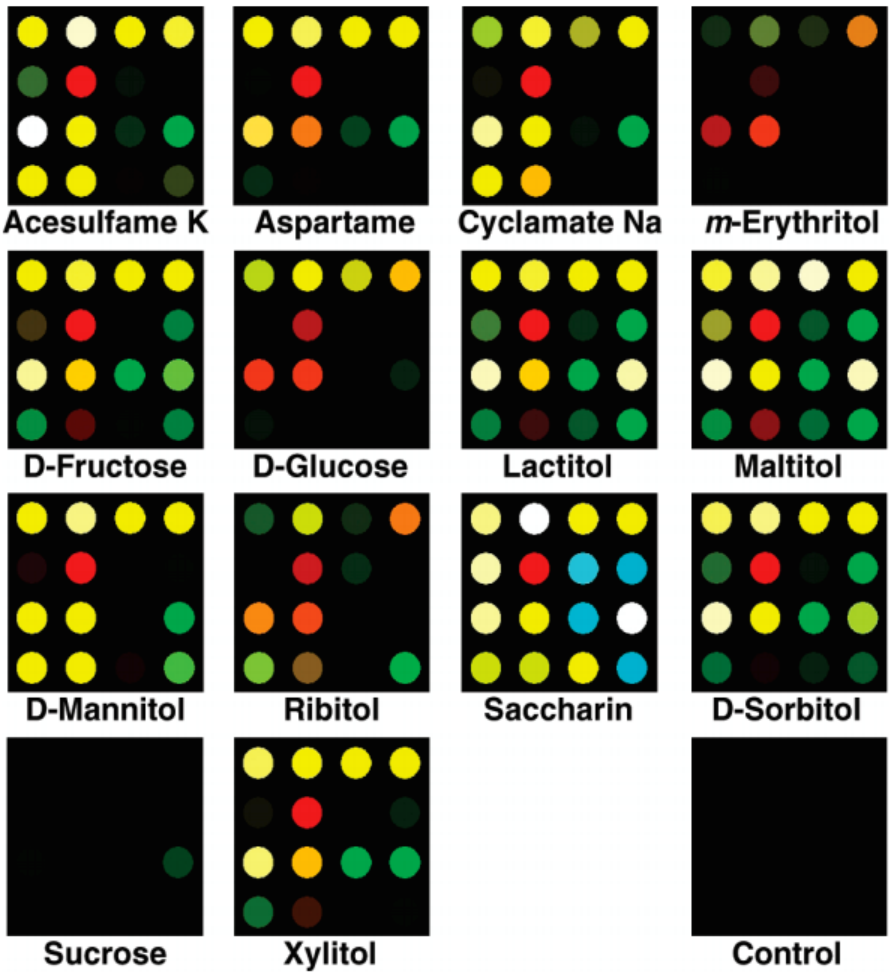

Figure 2.11: Use of colorimetric sensor arrays to differentiate 14 natural and artificial sweeteners of same concentration (25 mM concentration, except sucrose at 75 mM). [56]

In the work of Suslick et al, the colorimetric sensor arrays are used to discriminate the aromas of a batch of commercially available coffee products [57]. The aroma of coffee is a mixture of compounds and the difference between these aromas is very minute. In Figure 2.12, the vapors of 10 commercial coffees are examined by the same sensor arrays. Although there is similarity in the overall pattern of all the color maps, the difference is apparent to distinguish one set of aroma from another. These works have verified the adaptability of these colorimetric sensor arrays to be used in food industry for quality monitoring, where the

capability of discriminating very similar complex mixture is highly valued. It is a very promising technique to be use for food quality control and assurance during the production line and during the consumption.

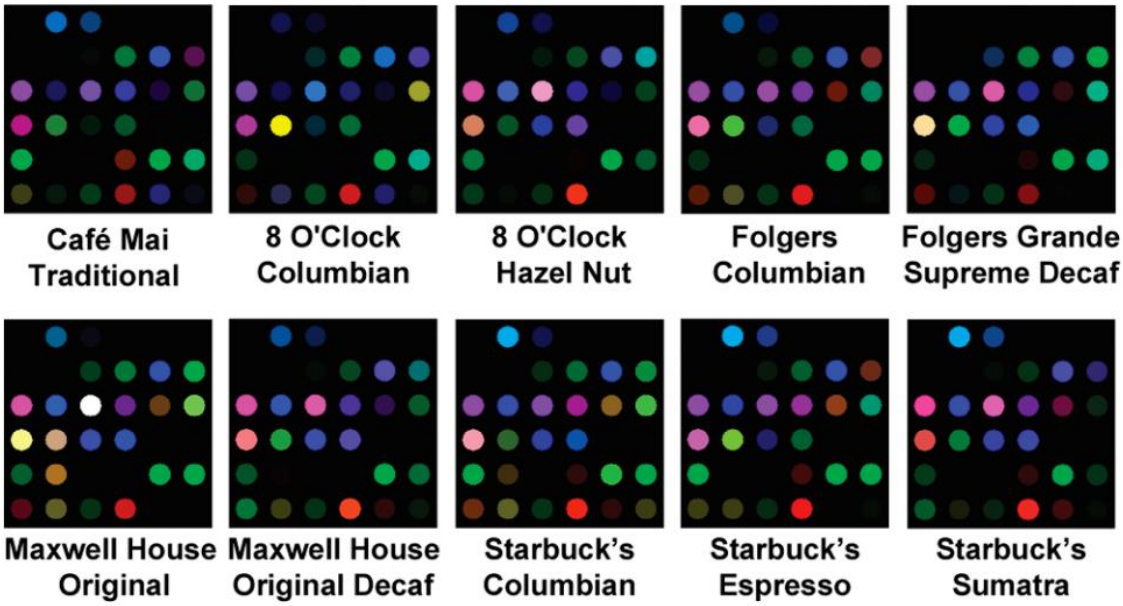

Figure 2.12: Use of colorimetric sensor arrays to sense the vapor of 10 representative commercial coffees. All the measurements are done after exposing colorimetric sensor arrays to the saturated vapor for 2 min. [57]

2.3 Optical signal read-out and processing

The previous section describes the applications of colorimetric sensor arrays in health care diagnostics, environmental monitoring and food quality testing. For all these applications, it is crucial to capture the color change of these sensor arrays, and convert it into a quantitative value. The most natural way of storing color information is through obtaining the images of the sensor. In most of these prior arts, flatbed scanner is employed as the most convenient tool to record the image and obtain color information by monitoring R,

G and B values of each pixel in the image [58]. There are some advantages of using flatbed scanner as the read-out for colorimetric sensor arrays. First, flatbed scanner based imaging can efficiently minimize the ambient light induced background variation and maintain the same level of color uniformity in all the images. This uniformity guarantees that the extracted color change accurately reflects the change of analyte. Moreover, flatbed scanner is relatively cheap, easily accessible and simple to operate.

Another widely used color detection tool is the optical spectrometer, which is commonly used to split light into a color spectrum [59]. An optical spectrometer can detect light signal ranging from ultra violet to infrared. The resulting spectrum is comprised of a series of spectral lines deciphering the wavelengths and corresponding intensities of a specific light signal. Unlike the situation of using flatbed scanner to capture color image, where all color information is eventually decomposed into R, G, B values through further image processing, using optical spectrometer can directly extract the characteristic spectral fingerprint of a specific color signal with nanometer wavelength resolution. This function is especially beneficial for characterizing the color feature (peaks in spectrum) of various chemo-responsive dyes before sensing, as well as capturing the shift of spectrum peaks after sensing. In another word, optical spectrometer offers the best accuracy and the most informative analysis of a color signal in a real-time measurement. However, spectrometer based measurement usually requires additional light source and any slight shake or mechanical movement may affect the spectrum. It is suitable to be used in a fixed set up with no moving parts.

In recent years, there is a growing interest in using the functionalities of smart phone for scientific applications [60]. It is shown that the smartphone-based detection method can

capture both the color change and pattern change on paper-based sensors. Even though smartphone-based detection cannot achieve the nanometer wavelength resolution as spectrometer, it can visualize the color change by recording the image of sensor arrays; moreover, unlike flatbed scanner, the images taken by smartphone usually have varying background illumination, which requires more effort in image processing to overcome the nonuniforminity. Regardless of these imperfections, smartphone-based detection still has great advantages when serving as an optical read-out for a sensor. Compared to flatbed scanner, smart phone is highly portable, with the functionality to realize direct color processing using an imbedded app; in comparison with spectrometer, smart phone is cost-effective, user-friendly, and realizing training-free operation. The successful use of smartphone provides more opportunities for empowering general public to use sensor technology with phone and an app as a substitute for expensive scientific instrumentation.

2.4 Colorimetric nose vs. electronic nose

In section 2.2, the implementation of colorimetric nose for gas sensing in different fields is thoroughly reviewed, with a detailed description of the sensing mechanism and sensing performance under each scenario. The success of the colorimetric nose relies on the idea of building an optical sensor arrays with various chemo-responsive dyes to enhance its power in discriminating chemically similar/dissimilar analytes [61]. However, the concept of using multielement arrays for selective gas sensing has already been implemented in electronic nose technology [62]. Electronic-nose technology, due to its relative simplicity and high sensitivity, has been developed for several decades to meet the increasing demands of gas sensing in industry and life science field [63]. An electronic nose incorporates a number of chemiresistive materials to build multielement arrays that is capable of sensing a specific gas

or other complex gas mixtures [64]. The development of innovative nanostructured materials, such as graphene [65], carbon nanotube [66], conductive polymers [67], has greatly broaden the choices of chemiresistive materials for building electronic nose. Given the similarity of electronic nose and colorimetric nose in terms of their basic concept and targeted applications, it is necessary to make a comparison between these two technologies and summarize their respective advantages.

2.4.1 Chemiresistive sensors

In our discussion, chemiresistive sensors refer to gas sensors built with sensing elements (e.g. nanomaterials) that change resistance upon chemical stimulation [68]. There are three common types of materials utilized for building chemiresistive sensors, namely, metal oxide[69] [70], carbon [71] and conductive polymer [72]. An electronic nose is realized through integrating chemiresistive sensor arrays with different sensing materials onto one platform to increase its gas recognition capability. Figure 2.13 shows an example of chemiresistive sensor arrays based on SnO_2, WO_3 and In_2O_3 for examining some volatile organic compounds [73]. Gas detection is realized through monitoring the electrical properties (e.g. resistance) of each chemiresistive sensor to obtain a collective response. In Figure 2.14, the electrical responses of nine chemiresistive sensors to four different gas analytes are recorded for comparison [72]. All the chemiresistive sensors demonstrate similar trend in the characterization curves but with different response amplitudes for the same gas analyte. The collective electrical responses of nine chemiresistive sensors form different patterns for different analytes. The amount of resistance change, which in this case is quantified by the change of voltage drop, is used to analyze the presence and respective amount of the specific gas analyte.

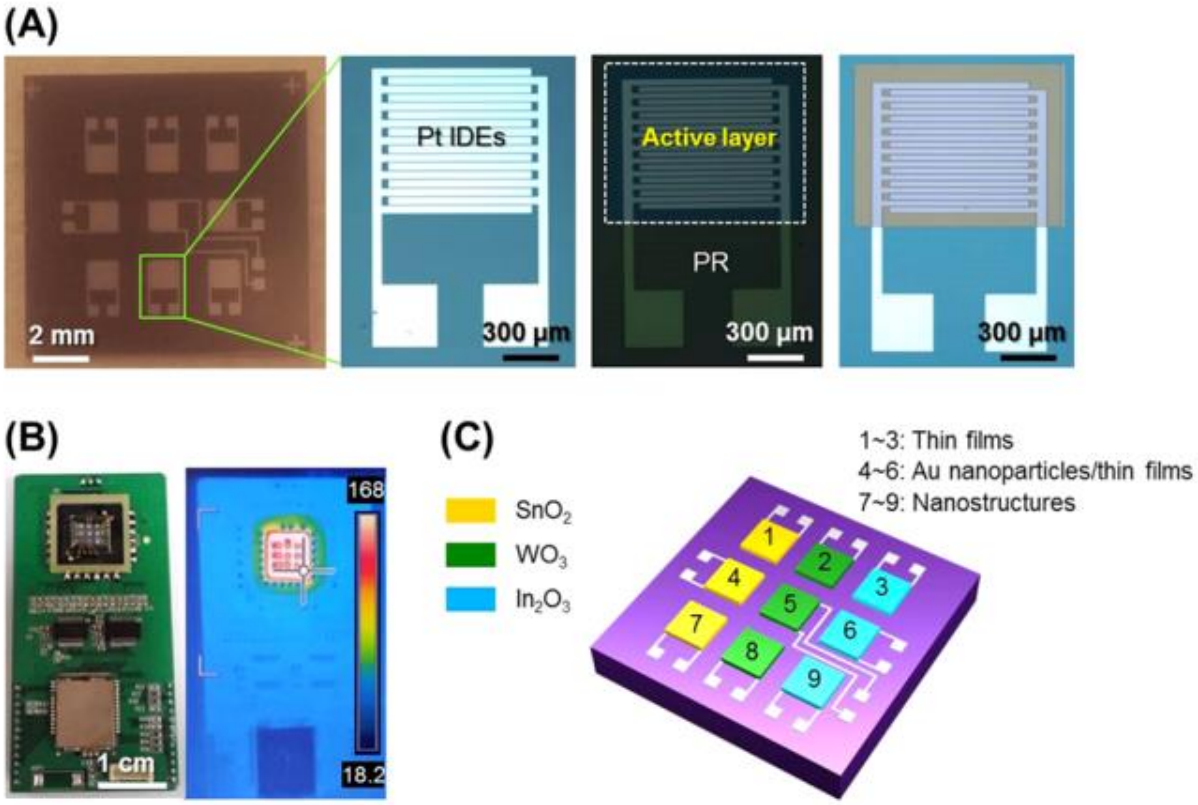

Figure 2.13: An electronic nose made of a number of metal oxides (SnO_2, WO_3, In_2O_3): (A) Microscope images of as fabricated electronic nose; (B) Image of the sensor platform and signal processing; (C) Schematic of the as fabricated electronic nose. [73]

The gas discrimination power can be further enhanced by incorporating different types of sensing materials in the electronic nose platform, which does not increase the complexity and difficulty from the fabrication viewpoint. For example, MacNaughton et al. has integrated different types of sensing materials (Carbon nanotube, graphene oxide, copper oxide, polypyrrole) onto a single chip through dielectrophoresis (DEP) assembly to form an electronic sensor arrays for VOCs sensing, as shown in Figure 2.15 [74].

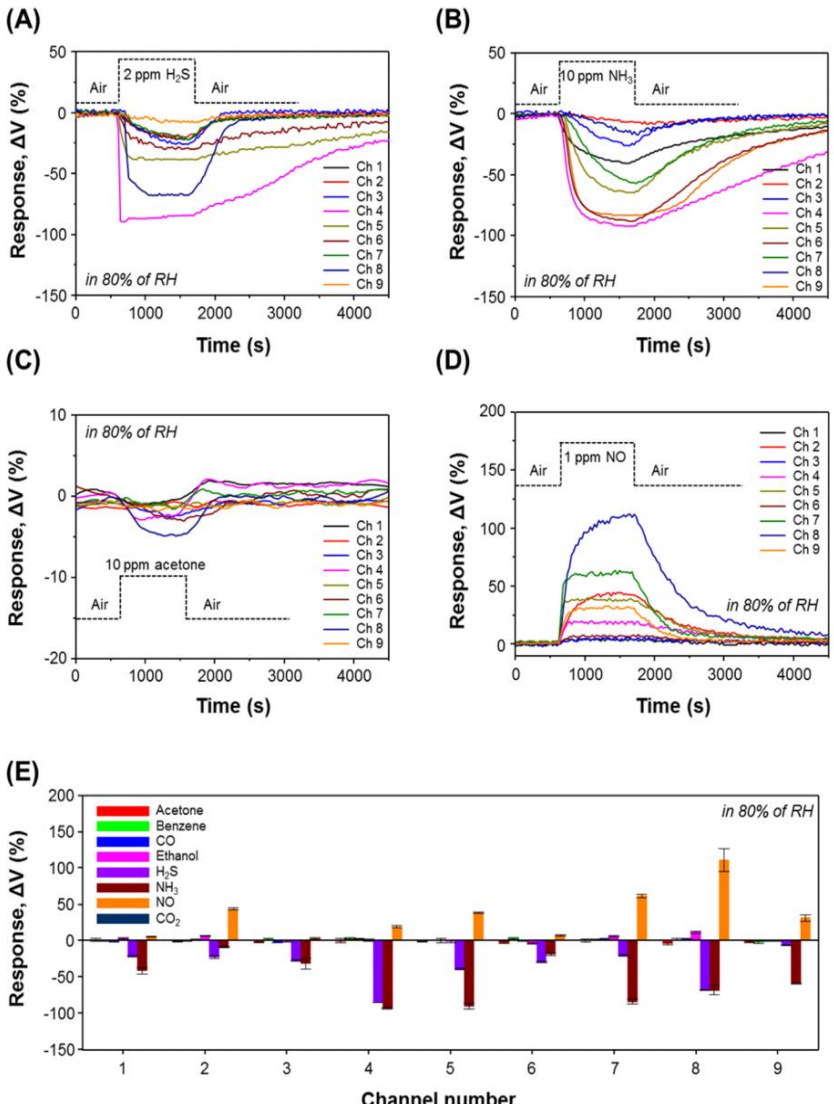

Figure 2.14: Electrical responses of chemiresistive sensors towards several analytes (A−D) Real-time response of each chemiresistor to 2 ppm H_2S, 10 ppm NH_3, 10 ppm acetone, and 1 ppm NO in 80% relative humidity; (E) summary of response pattern. [73]

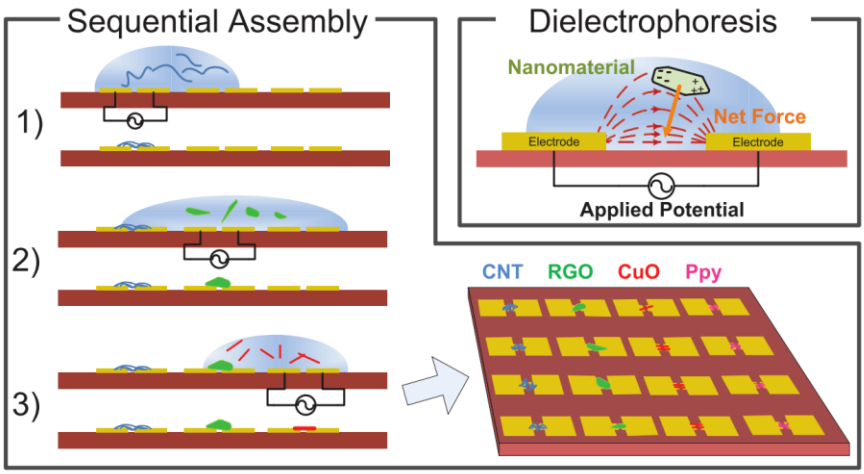

Figure 2.15: Electronic sensor arrays built with Carbon nanotube, graphene oxide, copper oxide, polypyrrole through dielectrophoresis (DEP) assembly [74].

The sensitivity of chemiresistive sensor arrays keeps increasing due to the advancement in synthesizing novel nanostructured materials [75]. The earlier generation of chemiresistive sensor arrays is mainly based on metal oxide thin film or nanoparticles [76][77]. Later on, carbon materials, including carbon nanotubes and graphene, and conductive polymers [78], such as polypyrrole [79] , polyaniline [80][81] and poly(3,4-ethylene-dioxythiophene) [82], have also been employed for building electronic sensing platform and greatly enriched the choices of sensing elements for making chemiresistive sensor arrays. In recent researches, functionalizing nanomaterials (e.g. nanowire, nanoparticles) with various molecular groups to form novel gas sensing elements has gradually become popular due to the improved stability and sensitivity [83][84][85][86]. In the work of Peng et al., gold nanoparticles are capped with different thiol groups (e.g. dodecanethiol, butanethiol) and used to build sensor arrays for breath testing. These sensor arrays can be used in real breath testing to distinguish normal breath and breath from lung cancer patients with ppb level sensitivity, as shown in

Figure 2.16 [87]. In another work, molecularly modified silicon nanowires based field effect transistor is used for VOCs sensing and achieved excellent selectivity towards each gas species [88]. The excellent performance of these nano-sensors are promising for cancer diagnostics, including lung, breast, colorectal and prostate cancer [89]. All these developments have very positive effects on the continuous advancement of electronic nose technology.

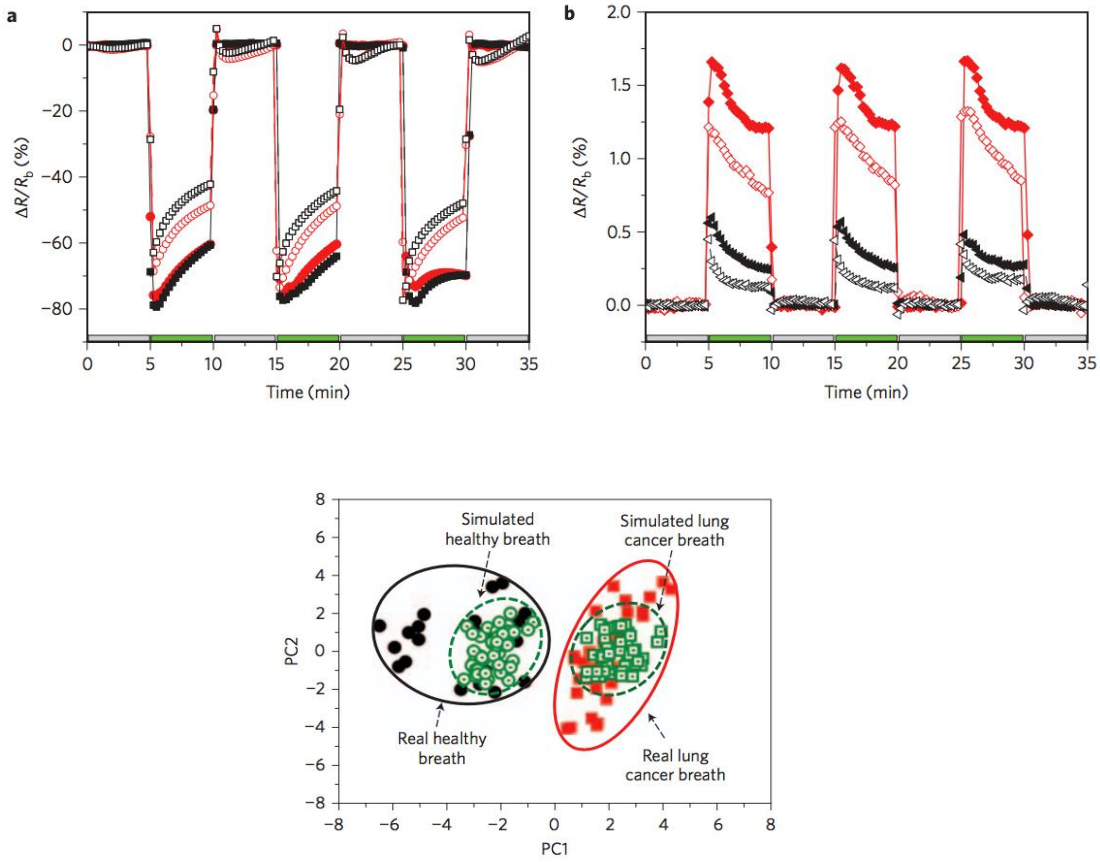

Figure 2.16: Electrical responses of 4 different thiol-capped gold nanoparticles when exposed to breath from lung cancer patients [87].

2.4.2 Comparison of colorimetric nose and electronic nose

Electronic nose and colorimetric nose, regarded as two of the most promising techniques for gas sensing, exhibit similarity in some aspects, including employing the idea of building cross-reactive sensing arrays to improve selectivity, the targeted types of gas specifies and fields of applications. Given the outstanding performance and exhibited similarity of both technologies, it is interesting to put them side by side and make a comprehensive comparison. In this section, colorimetric sensing technology will be compared with electronic nose technology at the following aspects:

(a) Application fields: both colorimetric sensor arrays and electronic nose technology have been applied for environment monitoring, medical diagnostics and food quality testing. As discussed in section 2.2, colorimetric sensor arrays have been used for sensing a variety of volatile organic compounds (VOCs), industrial toxic wastes, exhaled breath and the aroma of food. Similarly, utilization of electronic nose based on chemiresistive sensor arrays in cancer diagnostics (sensing VOCs) [87][90][89][91], sensing corrosive gases (e.g. H_2S, NO_2) and food emanating gas product has been testified in a number of prior arts [92][93][94][95].

(b) Complexity of fabrication: The fabrication process of colorimetric sensor arrays and that of chemiresistive sensor arrays are completely different. Usually, fabrication of chemireisistive sensor arrays is a multi-step process, including patterning of electrodes on designated substrate, preparation of nanomaterials and assembly of nanomaterials onto patterned substrate [96]. Patterning of electrodes (e.g gold, platinum) is commonly done through photolithography procedure to achieve micrometer or nanometer precision. Fabrication of nanomaterials is mostly done through a few methods, such as chemical vapor

deposition, physical vapor deposition and electroplating [97][90]. Some common ways to assemble nanomaterials onto the patterned electrodes include e-beam evaporation [98], dielectrophoresis (DEP) [99] and inkjet printing [100], to name just a few. In general, the fabrication of chemiresistive sensor arrays is a high-tech process that requires sophisticated microfabrication techniques and is time-consuming. By comparison, the process of making colorimetric sensor arrays is much simpler and time-efficient [101]. Most of the optical dyes are commercially available and can be used directly as received. Additionally, synthesis of some complicated dye compounds can be realized through a tool free process, such as mixing the raw materials, agents and solvents, filtering, heating and phase extraction [102]. The colorimetric sensor arrays are simply made by immobilizing different optical dyes onto some supporting substrate (e.g. PET) through a sol-gel procedure [103]. Compared with the fabrication process of chemiresistive sensors, which requires expensive tools and costly nanomaterials, the procedure of making colorimetric sensor arrays is much easier and cost-effective, which has great potential for mass-production at low cost.

(c) Sensing condition: both colorimetric nose and electronic nose can be utilized to sense gaseous analytes under room temperature. For the application of electronic nose, the sensing temperature and humidity condition in the sensing environment need to be strictly controlled, since some nanomaterials (e.g. metal oxide) have varying sensitivity under different temperature and most of the nanomaterials (e.g. carbon nanotube) are responsive to the water vapor, the amount of which will affect the magnitude of electrical response [104]. By contrast, colorimetric sensor arrays, which are used under room temperature and have more resistivity to humidity due to its own hydrophobicity, have less restriction to the sensing environment. Moreover, while the sensing application of electronic nose is limited to

gaseous analyte, colorimetric sensor arrays can not only be used to sense gaseous analytes, but also are suitable for sensing aqueous analytes, which further expends its application in monitoring targeted analyte under a complicated environment.

(d) Sensitivity: colorimetric sensor arrays are known to have high sensitivity towards a variety of gases with sub ppm concentration [105]. In the example of employing colorimetric sensor arrays for monitoring toxic gases, the observed limit of detection (LOD) values are as low as 25 ppb for HCN and 250 ppb for SO_2 and NH_3 [53]. On the other hand, the sensitivity of electronic nose experiences continuous improvement thanks to the innovation of nanomaterials [106][107][108]. In one prior work of using chemiresistive arrays of metal oxide thin films, metal-catalyzed thin films, and nanostructured thin films to detect exhaled breath, the estimated detection limit of H_2S, NH_3 and NO are 2.87 ppb, 42.29 ppb and 2.06 ppb, respectively, as shown in Figure 2.17 [73]. In short, colorimetric nose and electronic nose have comparable sensitivity level (sub-ppm) in sensing gaseous anayltes.

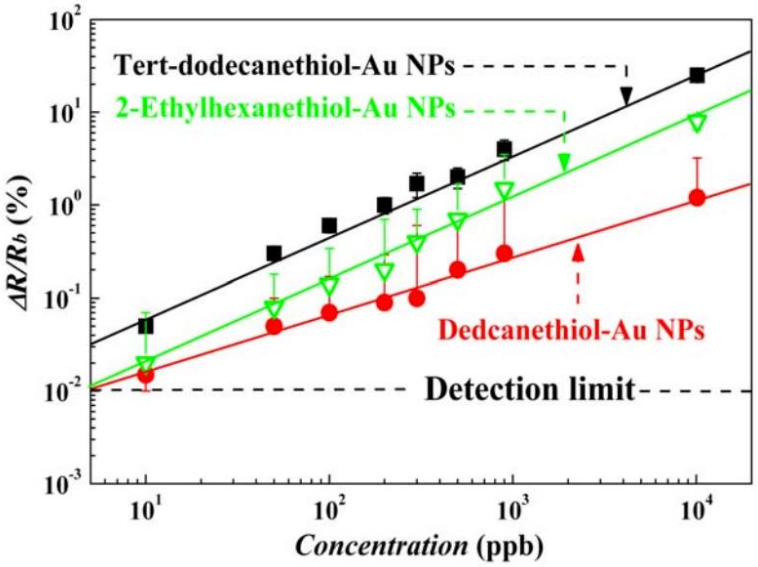

Figure 2.17: Detection limit of proposed electronic nose. [73]

(e) Detection methods: The sensor responses of electronic nose are quantified by the change of conductance of chemiresistive materials, which are usually recorded through external circuitry. In the case of colorimetric sensor arrays, the sensing responses are represented as color change of various cross-reactive chemo-responsive dyes. As discussed in section 2.3, several techniques, such as flat-bed scanner, optical spectrometer and smart phone, can be used to capture the colorimetric signal [109] [110]. Additional signal processing is required to quantify the detected color information [111]. In terms of detection methods, electronic nose and colorimetric nose has same level of complexity. Compared with electronic nose, one advantage of colorimetric nose is its capability to visualize the sensing result. Users can simply see the color change wirelessly to judge the existence of a specific analytes.

(f) Cost: last but not least, the costs of electronic nose and colorimetric nose are briefly discussed to complete a relatively comprehensive comparison. The cost of fabricating electronic noses covers but is not limited to the following aspects of expenses: mask design and fabrication; microfabrication tools; packaging, nanomaterials [112]. Relatively, to produce colorimetric nose, the main cost is the expense of purchasing optical dyes (most of which are no more expensive than nanomaterials), solvents and substrate materials [113]. Given the much higher cost of micro fabrication, making colorimetric sensing arrays is considered to be more cost-effective than making an electronic nose. However, with continuous efforts on exploring cheaper fabrication methods for making electronic nose, such as employing inkjet printing technique for depositing both electrodes and nanomaterials, the cost of an electronic nose can be further lowered, nevertheless with a trade-off between device reliability and cost.

2.5 Other gas sensing techniques

There are some other existing gas sensing techniques based on different sensing mechanisms, including gas chromatography (GC), mass spectroscopy (MS) and surface acoustic wave (SAW) technology. Gas chromatography aims at gas separation based on the variation of gas transit time through a specific medium. This variation is due to the interaction between the gas molecule and the stationary phase of the medium. Gas chromatography is known for its power in gas separation accuracy and is mostly used in laboratory to characterize the gas components of a volatile gas mixture. Mass spectroscopy generates a mass spectrum of ionized chemical species to distinguish them by their mass to charge ratio. It is commonly combined with gas chromatography as a complete tool (GC-MS) for gas separation and identification [114]. Surface acoustic wave device detects gas through monitoring the change of resonator's natural frequency due to absorption of gas specifies [115]. It has good selectivity towards different gas species and can achieve very high sensitivity (sub ppb), with the help of an ultrasonic wave generator and a detector [116]. These techniques have gained certain popularity in different fields. However, in this dissertation, we will focus on the works of optoelectronic gas sensors and their sensing capability under varying environments.

CHAPTER 3

Paper based microfluidic platform for colorimetric sensing of dissolved gases

Objective: The objective of this work is to show a paper based microfluidic platform for sensing dissolved ammonia and carbon dioxide. The sensor is fabricated using a low-cost, highly reproducible method. The detection of gases is realized by capturing the colorimetric signal using flatbed scanner.

Paper, a cheap and ubiquitous material, has great potential to be used as low-cost, portable and biodegradable platform for chemical and biological sensing application. In this work, we are exploring a low-cost, flexible and reliable method to effectively pattern paper for capturing optical dyes and for flow-based delivery of target samples for colorimetric chemical sensing. This in done in the context of an important application that of detection of ammonia (NH_3) and carbon dioxide (CO_2) which are an important biomarkers for health. By functionalizing the paper platform with diverse cross-reactive dyes sensitive to NH_3 and CO_2, their selective sensing within a certain pH range has been demonstrated, as well as their detection at different concentrations has been achieved. The images of paper based device were captured by flatbed scanner and processed in MATLAB® using RGB model and PCA for quantitative analysis. Paper based devices with readout using ubiquitous consumer

electronic devices (e.g. smartphones, flatbed scanner) are considered promising approaches for disease screening in developing countries with limited resources.

3.1 Motivation

Paper based microfluidic device has emerged as a new research field and gradually been showing its potential in a variety of applications such as health diagnostics, food quality testing and environmental monitoring [117]. Paper has several good reasons to be popular: it is a ubiquitous material in our daily life; its cellulose property allows functionalization of different biological and chemical reagents on it [118]; meanwhile, liquid can flow through paper's hydrophilic fiber matrix by capillary force without using any external pumps for force; furthermore, the hydrophilicity of paper can be altered by different treatments to create microfluidic channels on paper, resulting in effectively confining and transporting liquid flow in desired manner [119]. Paper-based microfluidic device can be mass produced and easily made into different shapes and thicknesses; therefore they are low-cost, disposable and flexible. These devices, when coupled with readout using ubiquitous commercial electronic devices (e.g. cell phone, PC web camera, flatbed scanner etc.) are considered promising approaches for disease screening in developing countries with limited resources [120].

Considering the merits that paper substrate holds, many exciting developments have been recently reported. Martinez et al. has fabricated paper based microfluidic devices by stacking layers of lithography patterned paper and double-sided adhesive paper for glucose and protein measurements [121]. Dungchai et al. demonstrated electrochemical detection of glucose, lactate and uric on paper by adding silver electrodes into the detecting zone on lithography patterned paper [26]. Although lithography can produce high resolution of

microfluidic channels, the disadvantages of this method are that it requires several fabrication steps, it needs different instruments, and it uses several chemicals for development. There are other paper patterning methods such as inkjet printing [122], plasma treatment [119], laser treatment [123] and later wax printing. Wax printing was introduced by Whitesides group and other research groups as a low cost way to create a microfluidic channel. Designed patterns could be printed onto paper by a wax printer and followed by heating to melt the wax [121]. However, wax printing still needs a specialized instrument in the form of a wax printer. Although it is simple and fast, the paper needs to be heated before use, and the dimension of the channel is subjected to spreading of wax [124]. Laser treatment approach discussed by Chitnis et al. begins with hydrophobic paper and uses laser-based direct writing to pattern hydrophilic regions. Direct writing process are inherently slow and can only be used for low volume manufacturing. Moreover it requires access to high powered laser source which may be inaccessible for many in developing regions of the world.

So far, paper based devices have been used for glucose monitoring, protein detection and other applications [125] [117] using variety of biological fluids such as blood, urine etc. Here we present an easy and effective method for hydrophobic–hydrophilic patterning of paper by applying commercially available hydrophobic silicone spray instead of laser or wax treatment, while maintaining low-cost and environmental friendly materials and processing. We also demonstrate the potential of this paper platform for colorimetric sensing of dissolved gas, for example, dissolved CO_2 and NH_3. NH_3 and CO_2 are important indicators in health monitoring and disease diagnostics [126]. No expensive fabrication equipment is required to make these paper based sensing devices. To avoid using bulky and expensive detecting and analyzing methods, optical responses of the dyes on paper were captured by flatbed scanner

[127]. The quantitative analysis of the scanned images can be done using MATLAB where the data can be imported into computer through USB device, Internet or wireless transmission.

3.2 Patterning of hydrophilic paper

In this experiment, two types of paper were chosen as the patterning substrate, A4 printing paper and cellulose paper. The hydrophobic patterning agent used here is a commercially available hydrophobic silicone water repellant spray. The desired pattern was designed in computer and transferred onto paper by printer, followed by hydrophobic patterning. The detailed fabrication procedure is described in Figure 3.1.

In Figure 3.1(a), desired pattern was designed in computer by using Microsoft PowerPoint; the designed pattern was transferred onto the paper substrate using a laser printer; Figure 3.1(b) showed the printed paper platform with desired pattern; in Figure 3.1(c), hydrophobic barriers were made by painting a hydrophobic agent dipped cotton swab uniformly on all the area outside the printed pattern (grey area in the Figure 3.1c). The paper was heated after the hydrophobic agent was applied to prevent the undesired spreading of hydrophobic agent into the desired pattern. In Figure 3.1(d) and (e), the paper platform were functionalized with different dyes and then target analytes were added to the reservoirs; Figure 3.1 (f) showed the post-sensing image acquisition and processing method; Figure 3.1 (g) showed the real images of as-fabricated paper platforms.

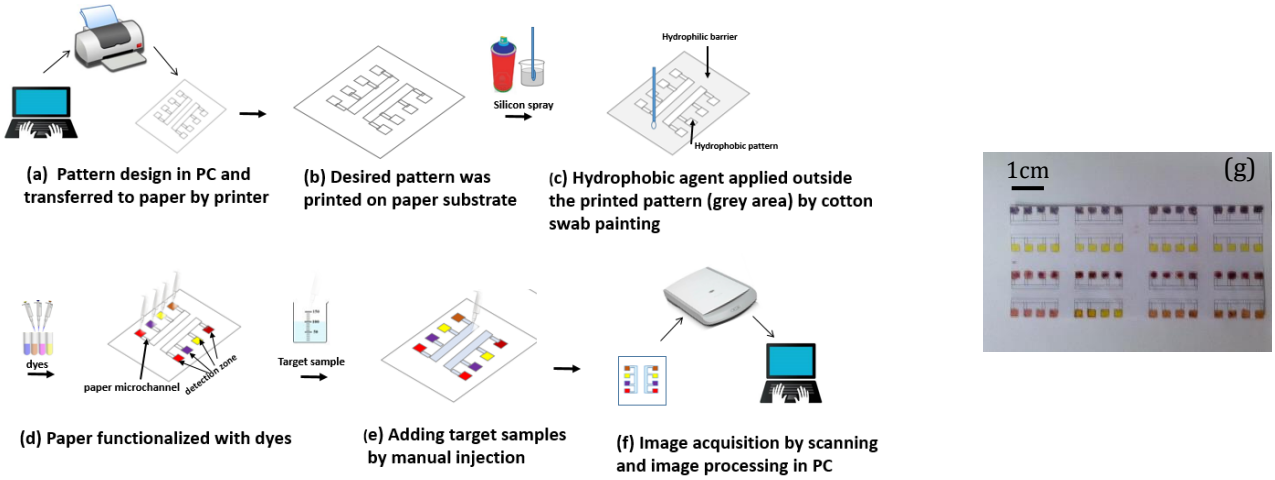

Figure 3.1: Device fabrication process: (a) designed pattern is printed on paper; (b) printed paper with desired pattern; (c) hydrophobic-hydrophilic patterning by painting hydrophobic agent dipped cotton swab in the grey area; (d) dyes injected into the square sensing area (colorful squares); (e) target sample is injected into the reservoir (long rectangle in light blue); (f) image acquisition of the paper platform by flatbed scanner and image processing in PC; (g) as-fabricated dye functionalized paper platform. Dyes deposited from top to down are: cresol red ion pair, pyranine ion pair, Zn-TPP, methyl red)

3.3 Methods

The paper based CO_2 and NH_3 sensing platform is prepared by functionalizing paper platform with CO_2 and NH_3 sensitive dyes [128] [124]. The dyes used are methyl red, Zinc Tetraphenylporphine (Zn-TPP) and phenolphthalein for NH_3 sensing, while cresol red ion pair and pyranine ion pair for CO_2 sensing. All used chemicals were purchased from Sigma-Aldrich, US.

3.3.1 Dye preparation

Methyl red solution: 25 mg of methyl red powder was dissolved in 1 mL of ethanol and 2 mL of DI water, and the mixture was stirred for 10 min followed by 10 min of sonication. The sonication step is to guarantee the uniformity of dye solution.

ZnTPP solution: 25 mg of ZnTPP powder was dissolved in 3mL of toluene. Similarly, the mixture was stirred for 10 min followed by 10 min of sonication.

Phenolphthalein solution: 25 mg of phenolphthalein powder was dissolved in 3mL of ethanol.

Cresol red-ion pair (CR-IP) and pyranine-ion pair (P-IP): 24 mg of cresol red (or pyranine) powder was dissolved in 22.5 mL of 0.1mol NaOH (solution A). Then 37.39mg tetraoctylammonium bromide (ToABr) was dissolved in 3mL of toluene to make solution B. Solution A and B were mixed together and stirred on magnetic stirrer for 30 min. After that, the organic phase (the upper layer) of the mixture was extracted and washed two times with 3 mL of 0.1 mol NaOH, the resulting solution is containing pure ion pair dissolved in toluene. [124]

3.3.2 Platform preparation and dye deposition

Two different designs of paper platforms for CO_2 and NH_3 sensing were prepared, as shown in Figure 3.4 (a) and Figure 3.5 (a). The platform in Figure 3.4 (a) had different testing units and each unit was deposited with four different dyes. The other platform shown in Figure 3.5 (a) had four blocks of sensing arrays and each block has one type of dye. The prepared dye solutions were manually injected into the hydrophilic sensing areas on the paper platform.

3.3.3 Analyte preparation

For paper platform in Figure 3.4(a): NH_3 solution (0.1 mol), NaOH solution (0.1 mol)

and $NaHCO_3$ solution (0.1 mol) were diluted with DI water until their pH were equally 10. The corresponding concentrations of NH_3, NaOH and $NaHCO_3$ in the solutions were 17 ppm, 4 ppm, 8.4 ppm, respectively. Carbon dioxide solution was made by bubbling pure CO_2 gas into DI water for 30 min to attain saturated carbon dioxide solution. The pH of the saturated CO_2 solution is around 4.25 and its concentration is 352 ppm. HCl (0.1 mol) solution was diluted with DI water until its pH increased to 4.5 and the corresponding concentration is 1.2 ppm.

For paper platform in Figure 3.5(a): The saturated CO_2 solution was further diluted by DI water into three solutions with different concentrations. The corresponding CO_2 concentrations of the three diluted CO_2 solutions were 147 ppm, 14.7 ppm and 1.47 ppm, respectively. The NH_3 solution (0.1 mol) was diluted with DI water into three solutions with different concentrations. The corre- sponding NH_3 concentrations were 1700 ppm, 17 ppm and 0.17 ppm, respectively.

3.4 Image acquisition and data processing

3.4.1 Flatbed scanner based image acquisition

For quantitative analysis, accurate information from the post-sensing paper platform is extracted by taking images of colorimetric sensing platform and analyzing its color change. Taking advantage of the flexibility of the paper substrate, the images of the post-fabricated and dye functionalized paper platform was scanned by an office-use flatbed scanner before and after sensing. The acquired images have the merit of uniform lighting background compared with the images taken by smartphone or digital cameras. (Martinez et al. 2008b)

3.4.2 MATLAB® based data processing

The images of the pre- and post-sensing paper platform were imported into MATLAB^S for quantitative analysis. The RGB model was used to extract the color information from the scanned images. The RGB model in MATLAB^S can decompose the color of an image into three components (red, green, and blue) and can calculate the respective intensity of these three components in the image. The color information extracted from all the sensing areas was used for evaluating the performance of the paper based sensing platform. In this way, the color change of different dyes upon adding different analytes and the relation between color change and analyte concentration can be quantized and compared.

3.4.3 Principal Component Analysis (PCA)

Discrimination among different analytes can be done by applying principal component analysis (PCA) in the Matlab. Principal component analysis (PCA) is a statistical process using an orthogonal transformation to convert a set of possibly correlated observations into a set of principal components, the values of which are linearly uncorrelated [129]. In the sensing experiment, there are a number of sensors with several sharing parameters. When PCA is performed on the data extracted from all the sensors, the resulting values of principal components correspond to the responses of different sensors combining all parameters. Usually, the first principal component has the largest possible variance, and each succeeding component in turn has the highest variance possible under the constraint that it is orthogonal to the preceding components. In this experiment, three sets of parameters R, G and B were extracted from four different sensors (i.e. four different sensing dyes). PCA was performed

on the values of four different sensors to discriminate CO_2 and NH_3 responses.

3.5 Testing of paper based platform

In the following experiments, hydrophobicity of as-patterned paper platform was tested. The as-patterned paper platform was used for selectively sensing CO_2 and NH_3. Furthermore, the sensing ability of as-patterned paper platform for detecting dissolved NH_3 and CO_2 of different concentrations (in the ppm range) was demonstrated. For all sensing platform, the RGB information of all the sensing areas was collected and analyzed. Finally, discrimination of the responses of CO_2 and NH_3 was performed by PCA.

3.5.1 Hydrophobicity of as-patterned paper platform:

In Figure 3.2(a), the effectiveness of hydrophobic spray patterning was tested on cellulose paper. A piece of cellulose paper was divided into two regions by a dotted line. The left part of this paper was painted with the hydrophobic agent and dried, while the right part remained unprocessed. The cross-section view of paper in Figure 3.2(b) showed the high aspect ratio of water drop on patterned paper. The contact angle changed from 0° to 148° before and after hydrophobic spray coating. Figure 3.2(c) also further proved this hydrophobicity. When the patterned paper was totally immersed in water, water only flowed within the patterned hydrophilic areas. In Figure 3.2(d), when the dye (e.g. methyl red) functionalized paper platform was immersed in analyte (e.g. NH_3), analyte could be absorbed and transported through the specified channel into the sensing area, causing a color change of the dye. No manual injection or pumps/valves are required.

There are several advantages associated with this hydrophobic spray patterning method, including the flexibility in pattern design, excellent hydrophobicity and high reproducibility.

Unlike other paper patterning techniques, which require additional equipment (e.g. laser cutter) to create desired pattern, by using this method, arbitrary pattern can be designed for paper substrate using various available software, such as Microsoft PowerPoint or AutoCAD. In our experiment, the size of pattern is within the range of 1 cm. By applying this hydrophobic agent on paper, effective hydrophobic barriers can be made on designated area in seconds and this hydrophobicity is stable and long lasting. Furthermore, spray-patterned paper platform is highly reproducible. The desired pattern can always be precisely duplicated and effective hydrophobic boundary can always be made in the same condition. Thus, this fabrication procedure is easy, fast, low-cost and highly repeatable on paper.

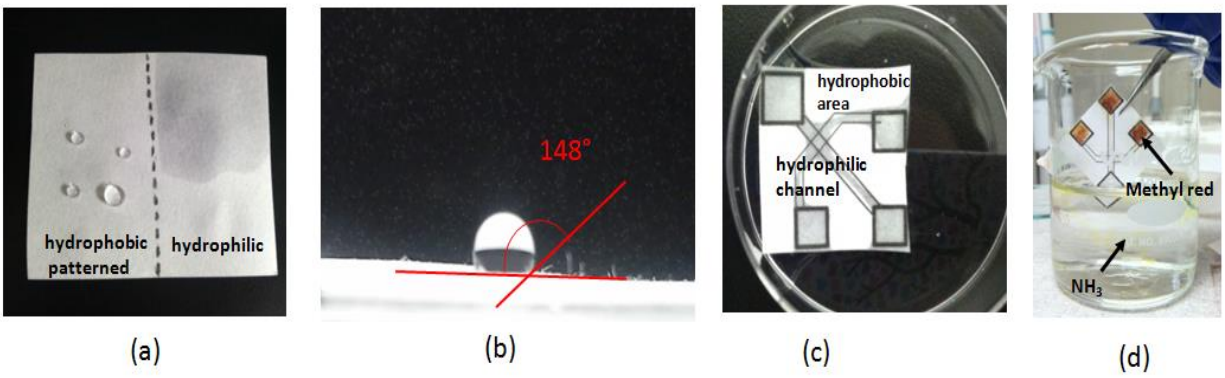

Figure 3.2: Hydrophobicity test on hydrophobic silicone spray patterned paper platform: (a) comparison of patterned (left) and unprocessed (right) paper; (b) cross-section view of water drop on hydrophobic paper in (a); (c) water transportation in the patterned area; (d) sample device immersed in ammonia solution;

3.5.2 Reproducibility of the testing platform:

The as-fabricated paper platform can be used as a general sensing platform. In our experiment, the paper platform was functionalized by halochromic dyes for CO_2 and NH_3 sensing. Figure 3.3(a) shows the scanned image of as-functionalized paper platform. The reproducibility of the sensing platform was tested using eight testing units, which

functionalized with four different dyes. Four dyes, methyl red, Zn-TPP, pyranine ion pair, cresol red ion pair were manually injected into four sensing areas of each unit. The injected volume of each dye is 2 mL. In Figure 3.3(b)–(e), color information of all sensing areas in eight testing units was ex- tracted and plotted. The standard errors of each dye using this readout were calculated accordingly: methyl red (R 4.65, G 6.16, B 6.48); Zn-TPP (R 3.37, G 4.10, B 3.17); pyranine ion pair (R 0.62, G 2.73, B3.55); cresol red ion pair (R 4.11, G4.86, B4.14). The numbers here indicate the minimum distinguishable R, G, B change in range from 0 to 256. By comparing the RGB color intensity distribution in all the units for each dye, a high degree of color uniformity was observed for all the deposited dyes.

Usually, it is difficult to uniformly deposit dyes onto paper by manual injection. This inaccuracy is mainly due to the fact that the amount of solution could not be precisely controlled by using the laboratory pipette. In our experiment, the errors of dye migration by manual injection measured in all the sensing areas are 10% for the 3mm by 3mm sensing area and 8% for the 5mm by 5mm sensing area. Although subjected to this inaccuracy, a satisfied uniformity was obtained on this paper platform. The use of flatbed scanner for image acquisition and sonication for dye preparation all attributed to the uniformity of this as-functionalized paper platform.

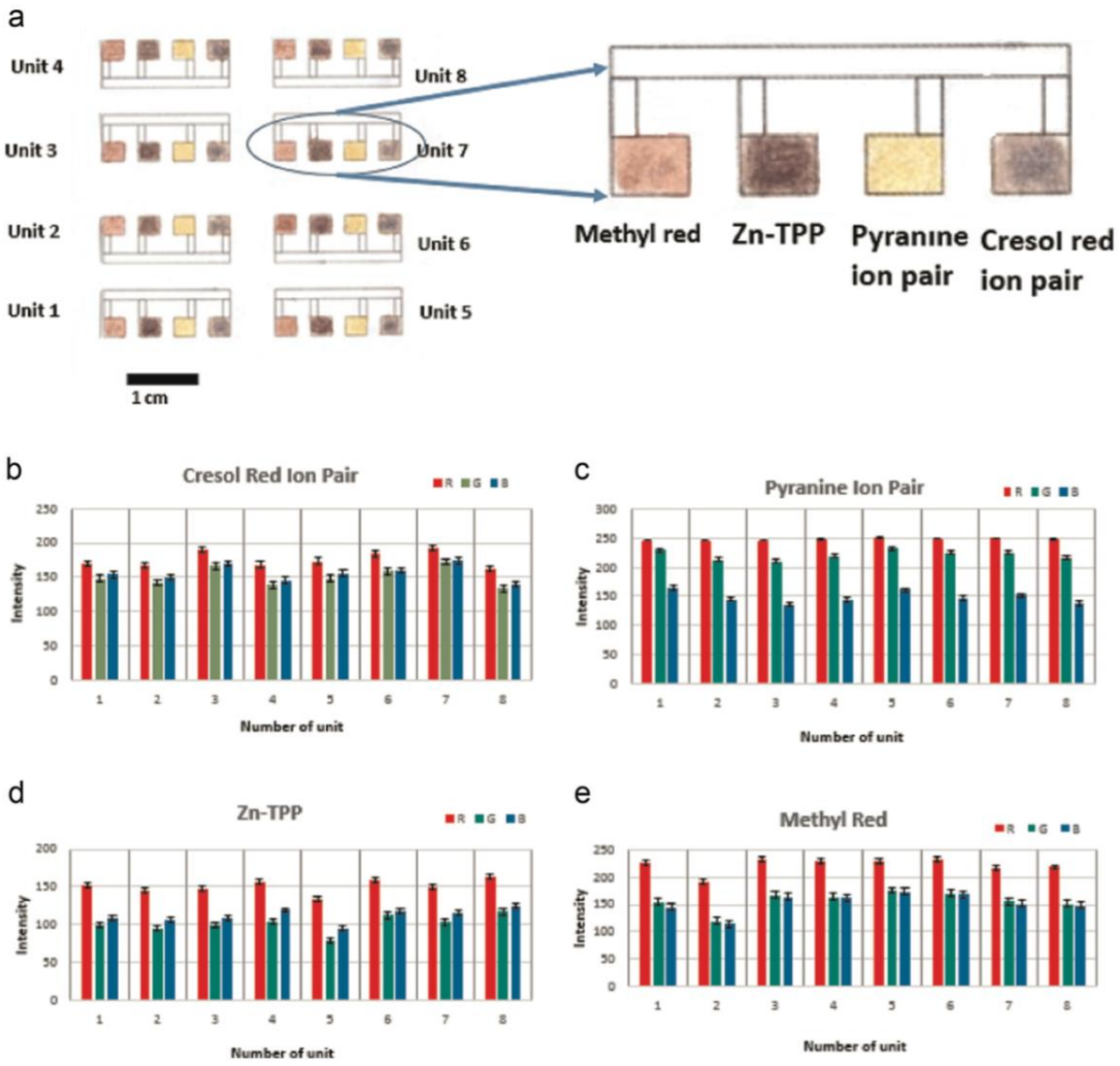

Figure 3.3: Reproducibility of dye functionalized paper platform before sensing: (a) scanned image of dye functionalized paper platform. In each unit, four dyes were deposited in a sequence from left to right: methyl red, Zn-TPP, pyranine ion pair, cresol red ion pair; (b) cresol red ion pair color distribution in eight testing units; (c) pyranine ion pair color distribution in eight testing units; (d) Zn-TPP color distribution in eight testing units; and (e) Methyl red color distribution in eight testing units. From the color distribution plots for four dyes in eight testing units, it is found that this dye functionalized paper platform can be reproduced with sufficient accuracy.

3.6 Paper based platform for sensing CO_2 and NH_3

3.6.1 Selective sensing of CO_2 and NH_3

It is important to demonstrate selectivity to CO_2 and NH_3. In order to demonstrate selective sensing, it is necessary to compare the sensitivity of selected dyes towards different acid and base analytes. Selective sensing of CO_2 and NH_3 was performed on the dye-functionalized paper platform. The image of post-sensing paper platform is shown in Figure 3.4(a). NaOH, $NaHCO_3$ were selected for comparison with NH_3, while HCl was compared with CO_2 solution. In Figure 3.4(a), unit 1 was left without adding analyte as the reference, and units 2–6 were injected with CO_2, HCl, NaOH, $NaHCO_3$ and NH_3, respectively. The RGB color information of each dye after sensing was plotted in Figure 3.4(b)–(e). Figure 3.4(b)–(c) shows that the color of CO_2 added sensing area (unit 2) has different RGB distribution compared with that of the reference unit (unit 1), while RGB distribution of HCl added sensing area (unit 3) remained highly similar to the reference unit, indicating that cresol red ion pair and pyranine ion pair are selective to CO_2 compared with HCl of the same pH on this paper platform. Figure 3.4 (e) shows that the RGB distribution in NaOH, $NaHCO_3$ and NH_3 added sensing areas (units 4, 5, and 6) were similar to each other but different from the reference unit, showing that methyl red was responsive to NaOH, $NaHCO_3$ and NH_3. In Figure 3.4(d) only NH_3 added sensing area (unit 6) showed distinguishable RGB distribution compared with the reference unit, indicating Zn-TPP is selective to NH_3. However, the color change of Zn-TPP upon adding NH_3 was not significant enough to be visualized. This can be explained in the study of Zn-TPP by Vaughan et al. (1996), which demonstrated that the wavelength shift of Zn-TPP for NH_3 sensing was small (10 nm).

Based on our prior work, pH sensitive dyes cresol red and pyranine, when combined with an organic quaternary cation as an ion-pairing agent, are selective to CO_2 when the pH of the back- ground solution is in the range of 4–4.5 [128]. Zn-TPP is proved to be highly selective to NH_3 compared to other strong or weak base [130]. Thus we chose cresol red ion pair, pyranine ion pair and Zn-TPP for selective sensing on CO_2 and NH_3 while methyl red as pH indicators for base.

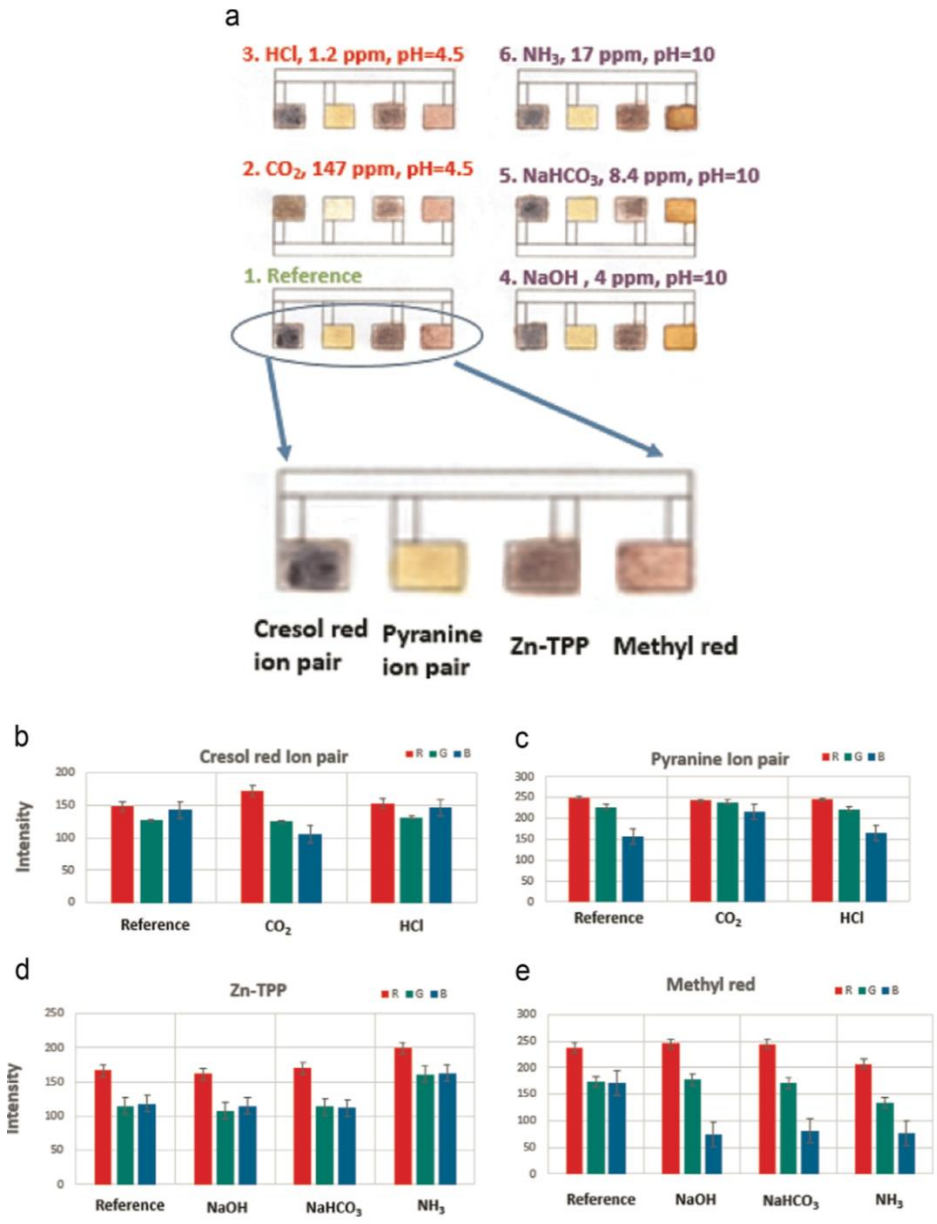

Figure 3.4: Selective sensing of CO_2 and NH_3 on dye-functionalized paper platform: (a) scanned image of post-sensing paper based platform. Four dyes, cresol red ion pair, pyranine ion pair, Zn-TPP, methyl red (from left to right) were deposited in each testing unit; (b) cresol red ion pair (CR-IP) color distribution after CO_2 and HCl sensing; (c) pyranine ion pair (P-IP) color distribution after CO_2 and HCl sensing; (d) Zn-TPP color distribution after NaOH, $NaHCO_3$ and NH_3 sensing; and (e) methyl red color distribution after NaOH, $NaHCO_3$ and NH_3 sensing. From (b) to (c), the color of unit 2 was distinguished from the reference unit, while color of unit 3 was highly similar to reference unit, showing that CR-IP and P-IP are selective to CO_2; (e) showed that in units 4, 5, 6, methyl red changed color after sensing NaOH, $NaHCO_3$ and NH_3, however in (d) only unit 6 showed distinguishable color distribution compared to the reference unit, indicating Zn-TPP is selective to NH_3.

3.6.2 Paper based platform for sensing CO_2 and NH_3 of different concentrations:

Figure 3.5(a) shows the scanned images of pre- and post-sensing paper platform for detecting dissolved CO_2 and NH_3 of different concentrations. The four blocks on the paper platform were functionalized with cresol red ion pair, pyranine ion pair, methyl red and phenolphthalein, respectively. In each block, the first row was left untouched after dye functionalization as reference. Dissolved CO_2 solutions of three concentrations (147 ppm, 14.7 ppm, and 1.47 ppm) were injected into three different rows of cresol ion pair and pyranine ion pair functionalized blocks; similarly, NH_3 solutions of three concentrations (1700 ppm, 17 ppm, and 0.17 ppm) were injected into three different rows in methyl red and phenolphthalein functionalized blocks. Figure 3.5(b) plotted the RGB color distribution of all the sensing areas in all blocks. In each dye block, the RGB color distribution varied with analyte concentration. It is found that the sensitivity of this platform was limited by the standard error of RGB read-out and not by the sensing dye themselves. If in the measurement, the change of RGB value is equal or below the value of standard error, this sample cannot be distinguished from the reference. When very low concentration of NH_3 (0.17 ppm) or CO_2 (1.47 ppm) was injected to the sensing areas, the RGB patterns were

approaching the reference RGB pattern and RGB readout difference was within the standard error, thus this concentration could not be well distinguished. This corresponds to the lower limit of detection for NH_3 is around 17 ppm, for CO_2 is around 14.7 ppm for this experiment. Figure 3.5 (c) plotted the changes of RGB verses the change of analyte concentration in different dye blocks. The values of R, G, B are the average of four repeated measurements. From Figure 3.5(c), it is observed that the change of RGB values exhibited difference for different dyes. For example, for CO_2 sensing, R, B of pyranine ion pair varied linearly with decreasing concentration, while for cresol red ion pair, R, G showed this linearity. Similar observation was obtained in methyl red and phenolphthalein blocks for NH_3 sensing.

For sensing NH_3 of different concentrations, the NH_3 selective dye Zn-TPP was substituted by phenolphthalein due to its relative insignificant color change to the present of NH_3 [130]. The plot of RGB change vs. analyte concentration in Figure 3.5 (c) can be used as a calibration chart when NH_3 or CO_2 solution of unknown concentration is detected. The difference in R, G, B for different dyes can help determine the analyte concentration more accurately. The accuracy of calibration chart can be further improved by repeated measuring NH_3 and CO_2 solution in broader concentration range.

3.6.3 PCA analysis result:

Principle Component Analysis was done in MATLAB on the sensing results in Figure 3.5(b), the obtained principle components PC1 and PC2 were plotted in Figure 3.6. In Figure 3.6, the points of principal components were aggregated into two separated clusters. The green circle cluster represents the responses from sensing CO_2 of different concentrations

and the blue rectangle cluster represents the responses of sensing NH_3 of different concentrations. Within green cluster, a decreasing trend was observed with decreasing CO_2 concentration, while within the blue cluster, an increasing trend was observed with decreasing NH_3 concentration. These two clusters are completely separated in the plot, which provides a clear discrimination between NH_3 and CO_2. This analysis method will further extend the capability of paper based sensing platform for sensing multiple analytes simultaneously.

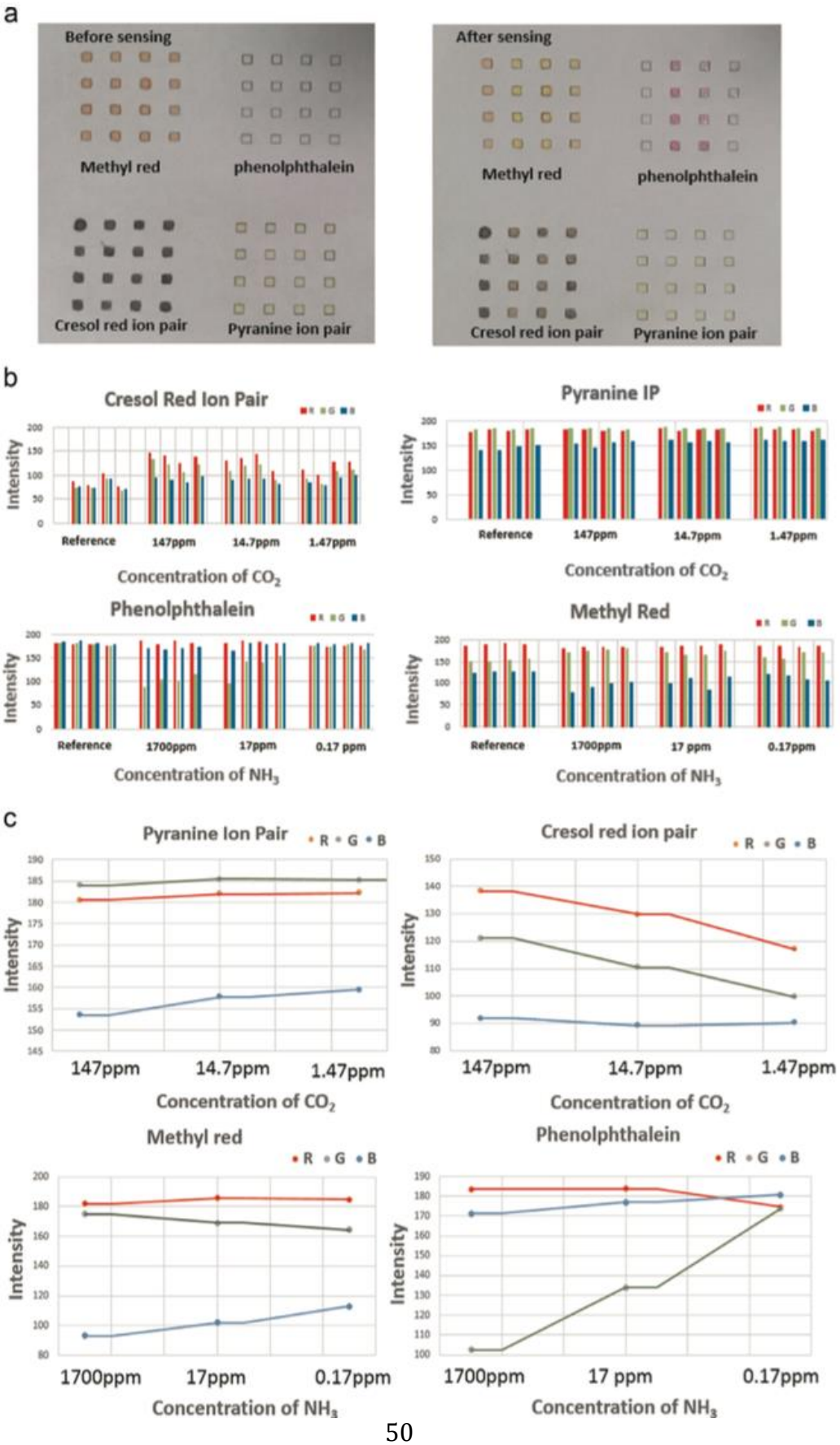
a
Before sensing
Methyl red
phenolphthalein
Cresol red ion pair
Pyranine ion pair
After sensing
Methyl red
phenolphthalein
Cresol red ion pair
Pyranine ion pair
b
Cresol Red Ion Pair
Intensity
Reference
147ppm
14.7ppm
1.47ppm
Concentration of CO2
Pyranine IP
Intensity
Reference
147ppm
14.7ppm
1.47ppm
Concentration of CO2
Phenolphthalein
Intensity
Reference
1700ppm
17ppm
0.17 ppm
Concentration of NH3
Methyl Red
Intensity
Reference
1700ppm
17 ppm
0.17ppm
Concentration of NH3
c
Pyranine Ion Pair
R G B
Intensity
147ppm
14.7ppm
1.47ppm
Concentration of CO2
Cresol red ion pair
R G B
Intensity
147ppm
14.7ppm
1.47ppm
Concentration of CO2
Methyl red
R G B
Intensity
1700ppm
17ppm
0.17ppm
Concentration of NH3
Phenolphthalein
R G B
Intensity
1700ppm
17 ppm
0.17ppm
Concentration of NH3

Figure 3.5: Sensing different concentrations of CO_2 (147 ppm, 14.7 ppm, 1.47 ppm) and NH_3 (1700 ppm, 17 ppm, 0.17 ppm): (a) image of four sensing blocks on paper platform; (b) color distribution (RGB) of sensing areas of all blocks; and (c) RGB vs. analyte concentration for four different dyes. For each analyte concentration measurement, four data points were collected and averaged.

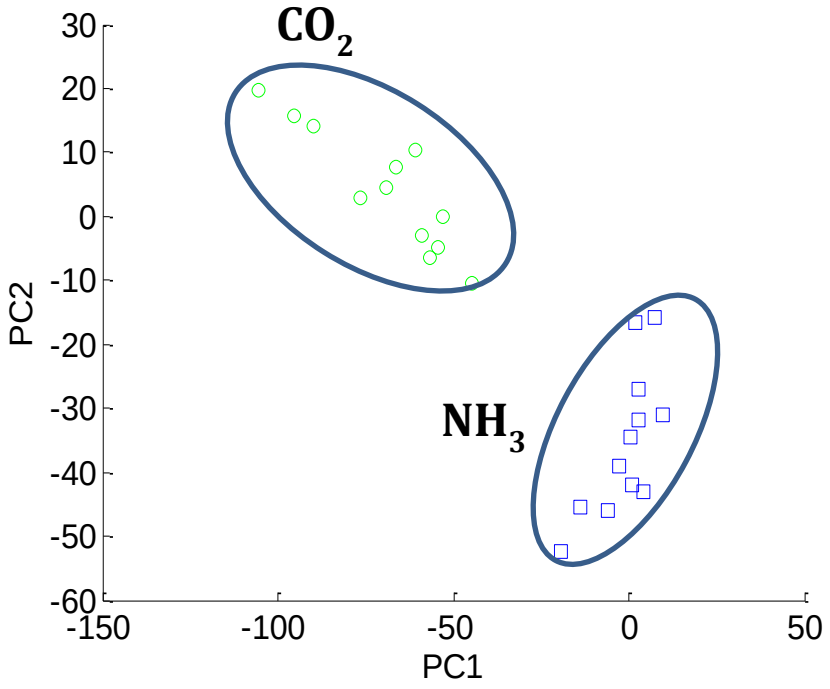

Figure 3.6: Principle component analysis (PCA) of CO_2 and NH_3 sensing results. From all the plots, it is found that the color change of each dye vary with different CO_2 and NH_3 concentration. Responses of CO_2 and NH_3 can be distinguished by PCA.

3.7 Summary

In this chapter, we showed a new way for patterning paper-based devices by using a hydrophobic silicone water repellent spray. This technique is easy, effective and environmentally friendly, and can be considered as one of the cost-effective techniques among others, which include wax printing and inkjet printing. The hydrophobic silicone can create a strong hydrophobic barrier on any hydrophilic substrate. It can be used to alter the hydrophobicity on one-dimensional substrate, such as thread, or any other non-uniform/deformed surface, which cannot be achieved by wax or inkjet printing. Due to its fast spreading on hydrophilic substrate, immediate heating is required to prevent over-spreading of silicone into undesired area.

In our experiment, we have functionalized this paper platform with CO_2 and NH_3 sensitive dyes and showed its performance in selective sensing of dissolved CO_2 and NH_3 and at different concentrations. The sensitivity and selectivity of this sensor platform, as well as the categories of detectable analytes can be further improved by including more chemoresponsive dyes without adding the complexity in fabrication. For optical readout, flatbed scanner is employed to record sensor images and RGB color information is used for data quantification. However, the sensitivity of this paper platform is limited by the RGB color readout from the scanned images processed in Matlab. Other color models, such as HSV (hue, saturation, value) or CMYK model can be used to improve the color discriminative capability. Moreover the sensitivity of the imager in the scanner also limits the sensitivity which could also be improved with a high quality scanning machine. Machine learning methods can also be applied to classify the responses from different analytes which will be basis of future work.

CHAPTER 4

Fiber based optical sensor for gastric gas sensing

Objective: The objective of this work is to develop a gas sensor for direct detection of dissolved ammonia and carbon dioxide in gastric acid that can eventually be integrated with a tethered capsule endoscope. Towards this goal, we present a gastric gas sensor based on conjoined dual optical fibers functionalized with sensitive optical dyes for sensing gases in both fluidic and gaseous environments.

In this Chapter, a gastric gas sensor based on conjoined dual optical fibers functionalized with sensitive optical dyes for sensing gases in both fluidic and gaseous environments is developed. The sensor aims to sense various concentrations of carbon dioxide (CO_2) and ammonia (NH_3), which are two significant biomarkers of H. pylori infection in the stomach. It is known that CO_2 and NH_3 are released during the hydrolysis of urea by H. pylori, a bacterium that may cause stomach cancer with relatively high probability. CO_2 and NH_3 sensitive optical dyes, cresol red ion pair and zinc tetraphenylporphyrin, are embedded in silica beads and then functionalized onto the thin PDMS-coated fiber tip. Each type of dye provides a unique spectral emission response when excited with light ranging from 450 to 700 nm. Two SMA connector legs of the as-functionalized sensor are connected to an external light source for illumination and a ultraviolet-visible-near infrared (UV-Vis-NIR) spectrometer for signal collection/readout. To perform the measurements, one fiber illuminates while the other fiber collects the back-scattered light and feeds it to the UV-Vis-

NIR spectrometer to measure the change in light spectrum as a function of CO_2 or NH_3 concentration. This method is easy and flexible and achieves ppm level sensitivity to targeted gas analytes. The proposed sensor can be integrated into a customized tethered capsule for adjunctive diagnosis of H. pylori infection to improve the accuracy of visual endoscopic inspection.

4.1 Introduction

H.pylori bacterium is known to be a likely cause of type B gastritis [131] and peptic ulcer [132] in the human stomach [133]. With H.pylori infection, the chances that the patients may develop stomach cancer are very high [134]. According to the study of Plummer et al., H.pylori infection-induced gastric cancer alone contributed to more than 5% of the total number of cancer cases in the world [135], [136]. Furthermore, the potential impact of H.pylori infection can be seen from the fact that close to half of the human population are carriers of H.pylori [137].

Various techniques are available to detect H.pylori infection, including invasive and non-invasive techiniques, depending on whether or not endoscopy is required [132]. Some commonly used invasive techniques include histological evaluation, polymerase chain reaction (PCR), and the rapid urease test (RUT), with test samples obtained during endoscopy. Histology collects gastric biopsy specimens from antrum and corpus and applies several stain techniques on these samples for H.pylori detection [138]. Culturing of H.pylori on fresh gastric biopsy specimen is used as a specific H.pylori detection method [139]. PCR is useful when the specimen is small with few H.pylori bacteria [140]. RUT is carried out by presenting urea in the H.pylori infected biopsy and by examining the byproduct of the sample

(CO_2 and NH_3) using pH indicator [141]. Non-invasive techniques include serology, urea breath test (UBT), and stool antigen test (SAT). Serology and SAT are all based on enzyme immunoassay principle [142], [143], while UBT detects the carbon dioxide produced by H.pylori hydrolyzed urea through one's breath [144]. None of the existing techniques, based on either biopsy of specimens obtained directly from the stomach, or from examination of the byproducts related to H.pylori infection, provide all the required features of convenience, rapid response and low cost in the same test platform. For example, histology needs a long examination procedure, PCR also takes long and is not effective at distinguishing between a living or dead bacteria, while RUT suffers from low sensitivity [132].

An alternative way to detect H.pylori infection is through direct examination of the amount of gas byproduct by H.pylori infection. A healthy human stomach contains around 6000 to 7000 ppm of CO_2 [145], and 20 to 50ppm of NH_3 on average [146], [147]. While in infected human stomach, H.pylori converts urea into CO_2 and NH_3, resulting in excessive amount of gas [148]. According to the study of Yang et al, the NH_3 level in H.pylori infected stomach can be as high as 200 ppm [147]. The amount of CO_2 produced by H.pylori is half of that of NH_3 according to the urea hydrolysis formula [149], and this amount of CO_2 is small compared with the background CO_2 in stomach. Thus, to measure CO_2 produced by H.pylori, it is important to void the background CO_2 in the stomach before measurement. For example, this can be achieved by performing a measurement of the rate of increase of CO_2 over time after administration of water in empty stomach.

In our work, we built a gastric gas sensor based on the functionalized optical fiber with optical dyes sensitive to CO_2 and NH_3, which is aimed to be integrated into the tethered

capsule endoscopy (TCE) for visual inspection of the inner lining of the esophagus and the stomach. The TCE was built using medical grade plastic capsule, which can be made into different sizes according to the physiology of patients [150]. The capsule was made precisely to be the same size as a standard capsule for ease of swallowing [150]. The imaging system incorporated six multimode optical fibers to collect the backscattered light. It has been evaluated for Barretts esophagus detection and early esophagus cancer diagnostics [151], [152]. Taking advantage of the illumination system of TCE, one of the imaging fibers can be replaced with the proposed sensing fiber. The modified TCE with gastric gas sensor can improve the accuracy of screening for the presence and the severity of H.pylori infection by combining gas sensor data with visual inspection images. The critical step is to ensure that the gastric sensor in contact with analytes when TCE is in the stomach. As a first step towards that goal, we have developed a stand-alone functionalized optical fiber- based gastric gas sensor that is compatible for future integration into TCE in terms of use of fiber for delivery and capture of light and for its size and flexibility. The functionalization is based on our prior work on saliva-based diagnostics for detection of CO_2 and NH_3 [124], [128]. This chapter describes the design, fabrication, test and characterization of a fiber-based gastric gas sensor for the screening of H.pylori infection.

4.2 Principle of Operation

The prototype of a stand-alone optical fiber-based gastric gas sensor compatible with TCE is shown in Figure 4.1. Taking advantage of the configuration and operating principle of this tethered capsule endoscope, this fiber based gastric gas sensor can be easily integrated into this tethered capsule. At the same time, it also collects sensing information from backscattered light. The sensor consists of two multimode fibers conjoined together as one

unit. Optical dyes loaded in beads are functionalized on the tip of the conjoined fiber. Illumination light is provided from one fiber while backscattered light is collected from the other. Both light source and optical data collection units are external. It is noteworthy to mention that in our previous study on saliva-based diagnostics, it was found that cresol red ion pair and Zn-TPP are selectively sensitive to CO_2 and NH_3, respectively [124], [128]. ZnTPP are metalloporphyrins with a metal center (Zinc in case of ZnTPP) coupled to porphyrins with the teraphenyl functional group. Porphyrins are intense chromophores. Coordination reaction with ligand amine molecules bound to Zn metal center in this dye manifests a color change on the chromophore. Ammonia is detected due to the coordination of NH_3 molecules to the Zn ion in this immobilized metalloporphyrin. Ammonia acts as a lewis base donating its free electron pair, making the use of ZnTPP for detection of ammonia as a most favorable colorimetric dye choice. Cresol red is a pH sensitive dye, which can respond to the changes in Brønsted acidity due to the interation between CO_2 and ion pair [128]. Thus, choosing these two dyes as sensing elements has significant advantage over the commonly used pH indicator dyes, which exhibit non- specific sensitivity to most acid and base.

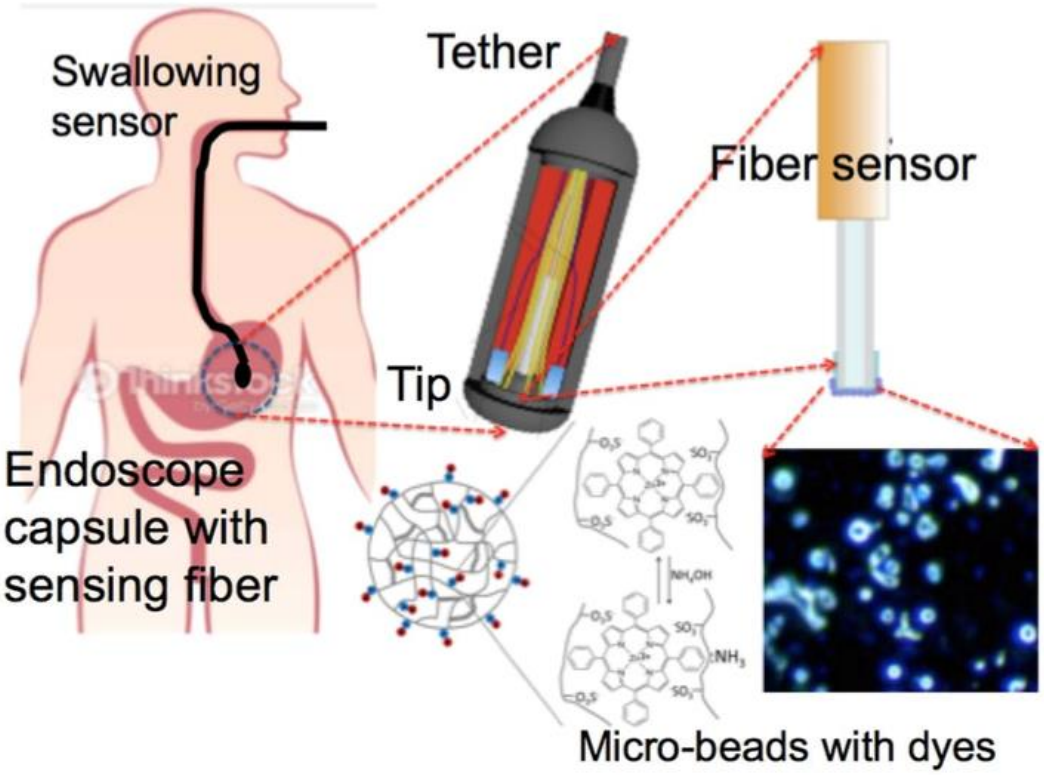

Figure 4.1:The potential application of functionalized optical fiber into tethered capsule endoscope to help detect H.pylori infection. The products of H.pylori metabolism are the elevated levels of gastric gases (i.e. CO_2 and NH_3).

4.3 Sensor fabrication

4.3.1 Preparation of optical dyes and analytes

The Zn-TPP solution was prepared by dissolving 25.6 mg of Zn-TPP powder (Sigma Aldrich) in 3 mL of toluene. Then the mixture of Zn-TPP and toluene was stirred on a stirrer for 2 hours to allow Zn-TPP powder to be fully dissolved in toluene [153]. To encapsulate Zn-TPP into resin microbeads (sphere with diamater of 30-50 um), the prepared Zn-TPP solution was poured into 375 mg cation exchange resin microbeads (Sigma-Aldrich). 5 mL deionized water was added into the mixture of Zn-TPP solution and resin beads. The

resulting mixture was again stirred on a stirrer for 5 hours at room temperature [128]. After that it was observed under microscope that the resin microbeads were filled with Zn-TPP dyes.

The procedure for preparing cresol red ion pair solution was described in detail in a previous work [153]. Two solutions, named solution A and solution B were prepared separately. Solution A was prepared by dissolving 24 mg of cresol red powder in 22.5 mL of 0.1 mol NaOH. Solution B was made by adding 3 mL of toluene into 37.39 mg tetraoctylammo- nium bromide (ToABr). The cresol red ion pair solution was obtained by extracting the organic phase of the mixture of solution A and solution B. Similar to the Zn-TPP encapsu- lation process, cresol red ion pair solution was poured into 560 mg anion exchange resin microbeads (Sigma-Aldrich). The mixture of these two was stirred on the stirrer for 5 hours at room temperature to ensure full encapsulation of dyes in microbeads [128].

Dissolved CO_2 solution was prepared by bubbling pure CO_2 gas into deionized water for 1 hour to obtain saturated CO_2 solution. To obtain dissolved CO_2 solution of differ- ent concentrations, the saturated CO_2 solution contained in four different bottles were diluted by different amount of deionized water. By measuring the pH of the four diluted carbon dioxide solution, the corresponding CO_2 concentrations were calculated. These were 2 ppm, 20 ppm, 200 ppm.

4.3.2 Sensor fabrication process

Two gas sensors, one for CO_2 and one for NH_3, were fabricated separately following

the same procedure. For fabricating one gas sensor, the two customized optical fibers (Thorlabs, FG200UCC, diameter: 200 um, length: 1 m) were used. Each fiber was encapsulated with a SMA (SubMiniature version A, Thorlabs, SMA905) connector at one end while the other end was flat cleaved without jacketing. Figure 4.2 shows all the necessary materials for sensor fabrication. Two single fibers (diameter: 200 um) with cladding were aligned in parallel and were combined together using silicone glue (Figure 4.2-ii). The tip of combined fibers was dipped into as-prepared PDMS mixture (Figure 4.2-iii). Care was taken to coat only a thin layer of PDMS on top of the tip. After that, this PDMS coated tip was dipped into cluster of solvent-free dye-contained beads (either Cresol red ion pair beads or Zn-TPP beads) several times until the beads were attached to the PDMS layer (Figure 4.2-iv). In this case, the PDMS layer serves as the glue to bind beads to the fiber tip. The as-coated beads were half-immersed in the PDMS layer and half-exposed to the air to ensure effective absorption of the dissolved or gaseous analytes in the experiment. The as-fabricated fiber sensor was left untouched for 24 hours under room temperature before use to allow the PDMS layer to cure fully. This step is necessary to completely immobilize the functionalized beads at the tip of the conjoined dual-fiber sensor. Thus, the as-fabricated fiber sensor will have one combined tip functionalized with dye-contained beads and two separate legs with SMA connectors.

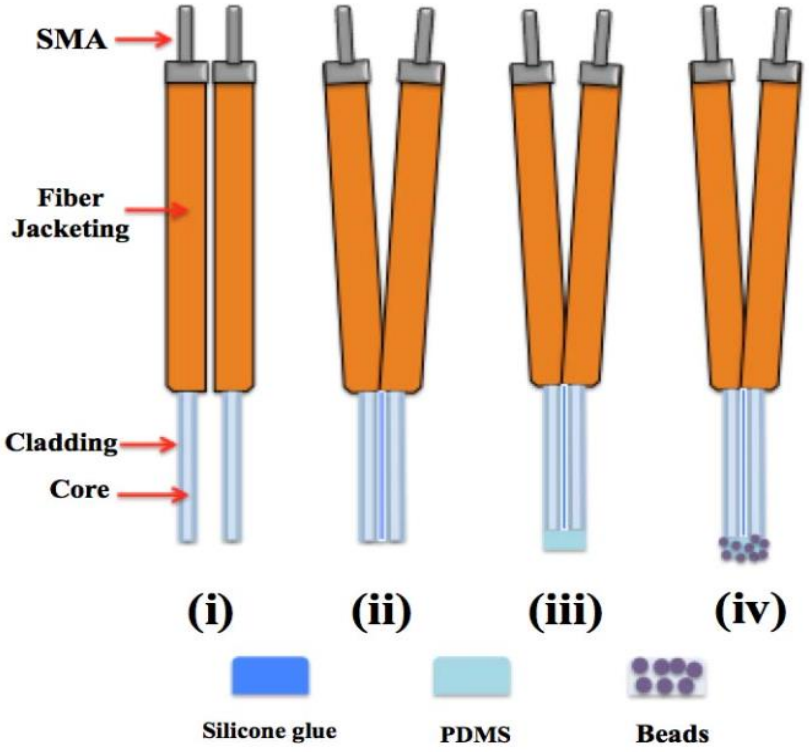

Figure 4.2: Sensor fabrication process: (i) two customized optical fiber with flat cleaved ends; (ii) the sensor is made by physically combining two single fibers together into one using sillicone glue; (iii) a thin layer of PDMS is then coated onto the combined end of bifurcated fiber; and (iv) the gas sensing beads with optical dyes are coated onto the thin PDMS layer; silicone glue, PDMS and micro-beads are shown below.

4.4 Experimental set up

Figure 4.3 shows the schematic of the experimental set up. The gas chamber used in the experiment has a volume of 250 mL, with one inlet and one outlet, which allows analyte to flow in and out simultaneously. The inlet and outlet can be closed to seal the chamber. This set up can be used for sensing both dissolved and gaseous CO_2 or NH_3. The sensing tip of the conjoined dual-fiber sensor was inserted into a gas chamber from the top, while the two SMA legs were brought outside. One leg of the sensor was connected to a white LED to

obtain excitation light for the sensor, while the other leg was connected to a Ultraviolet-Visible-Near Infrared (UV-Vis-NIR) spectrometer (Ocean Optics). The illumination light provided by one fiber was scattered by the optical dye-contained beads at the sensing tip, which was then fed to the spectrometer through the other fiber. The wavelengths collected are within the visible light spectrum, ranging from 450 nm to 700nm.

For sensing the dissolved CO_2 or NH_3, two sensors, one with cresol red ion pair functionalized sensing tip, and the other with Zn-TPP functionalized tip, were inserted into the gas chamber one at a time to detect CO_2 and NH_3 separately. The procedures of detecting CO_2 or NH_3 were similar. The chamber was pre-filled with 50 mL of deionized water and the sensing tip was immersed in the water without touching the bottom of the chamber. The solutions containing different concentrations of CO_2 or NH_3 starting from lower concen- tration, was pumped into the pre-filled deionized water in the chamber using micro-pump. The dissolved gas of different concentrations was transferred into the chamber through the inlet tube, gradually diffusing through the flow to the sensing tip, and flowing out of the chamber through the outlet tube. On average, it takes 15 minutes for the background de-ionized water to be saturated with the desired gas concentration. The sensor responses were recorded by spectrometer, from which the changes of different wavelengths ranging from 450 to 700 nm could be distinguished.

For sensing gaseous CO_2 or NH_3, the sensor tip is sus- pended in the middle of the chamber and the pulses of gas, either CO_2 or NH_3, were subsequently injected into the chamber through the inlet of the chamber. The inlet is connected to a gas flow meter to control the gas flow rate and the concentration of gas is controlled by the duration of gas

flow. The outlet of the chamber was left open to test the sensor responses to a subsequent gas pulses and later closed to sense the accumulated responses of analyte gas. The corresponding changes in the spectroscopic signature was recorded by the external spectrometer

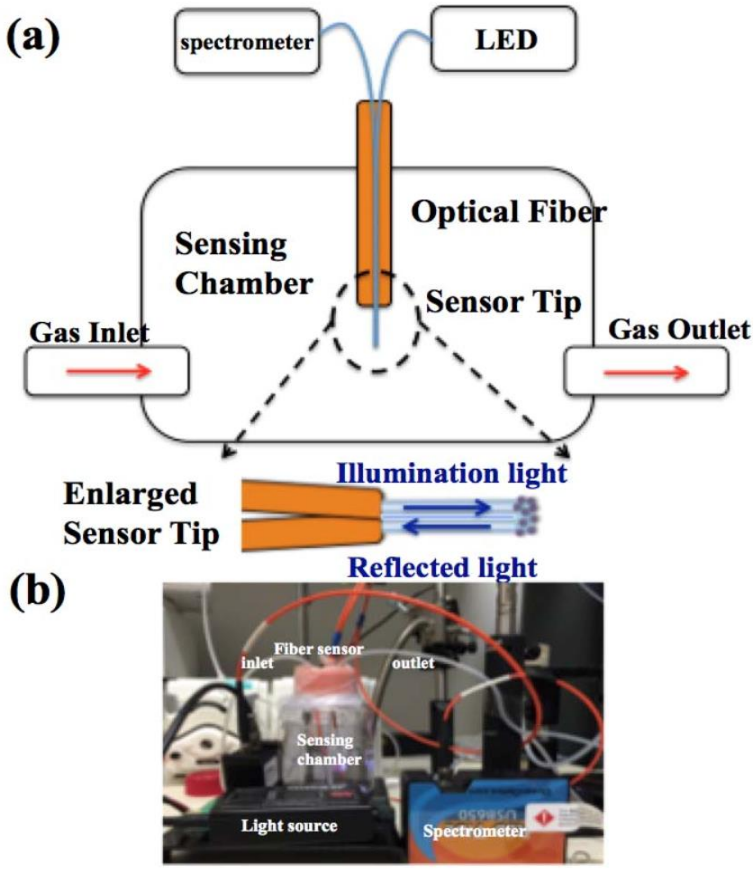

Figure 4.3: Experimental set up: (a) as functionalized fiber sensor is inserted into a sealed chamber with inlet and outlet for gas/flow; the two SMA connector legs of the fiber sensor are connected to spectrometer and light source, respectively; and (b) real image of experimental set up.

4.5 Sensor performance

In Figure 4.4, the full spectrum responses (450 nm to 700 nm) of cresol red ion pair or Zn-TPP functionalized sensors to the CO_2 or NH_3 in fluidic environment were plotted as the transmittance verses wavelengths. Figure 4.4(a) shows the response of cresol red ion pair to two different concentrations of CO_2 (20 ppm and 100 ppm), with the largest response observed in the range of 550 nm to 640 nm. Similarly, in Figure 4.4(b), the response of Zn-TPP to NH_3 (20 ppm and 40 ppm) is plotted. In both cases, the magnitude change of the whole spectrum results from the color change of optical dyes. In the case of sensing CO_2 and NH_3, cresol red ion pair changes color from purple to yellow, while Zn-TPP from green to brown, respectively. Each optical dye has its maximum responses at different wavelength range. The magnitude of responses depends on the concentrations of these analytes. The advantage of looking into the whole spectrum is to observe the overall effect of change in color and extracting the wavelength or a range of wavelengths, where most discerning responses can be obtained.

4.5.1 Sensing dissolved CO_2 and NH_3

Figure 4.5 shows the sensing performance of cresol red ion pair or Zn-TPP functionalized fiber sensors under fluidic environment. The Y axis in Figure 4.5 represents the percentage change of light transmission intensity when adding different concentrations of analyte, compared with the original spectrum. In Figure 4.5(a), the change of two wavelengths, 550 nm and 580 nm, is plotted to represent the typical responses of cresol red ion pair functionalized sensor to dissolved CO_2. It is shown that cresol red ion pair functionalized sensor can detect a wide range of concentration of dissolved CO_2 from relatively low concentration (2ppm) to relatively high concentration (2000 ppm). The inset

figure in Fig. 5(a) enlarges the sensor response to dissolved CO_2 from 2 ppm to 200 ppm. From Figure 4.5(a), it can be observed that when the concentration of dissolved CO_2 is below 200 ppm, the signal magnitude changes at two wavelengths (550 nm and 580 nm) are closely related. However, in high concentration environment (2000 ppm), the signal magnitude change at these two wavelengths varies. In Figure 4.5(b), the response of Zn-TPP functionalized sensor to dissolved NH_3 of different concentrations from 1 ppm to 100 ppm is represented by the signal magnitude change at the two wavelengths 620 nm and 640 nm. Similar to that of CO_2 sensing, these two wavelengths (620 nm and 640 nm) showed increasing signal magnitude with increasing NH_3 concentration. In Figure 4.5, the slope of sensor response was caused by the diffusion of analyte from inlet to the sensor tip and the time duration of this slope corresponds to the time needed for the background to reach desired analyte concentration. The sensing result in Figure 4.5 demonstrates the suitability of this gastric sensor by showing its capability in sensing wide range of CO_2 and NH_3.

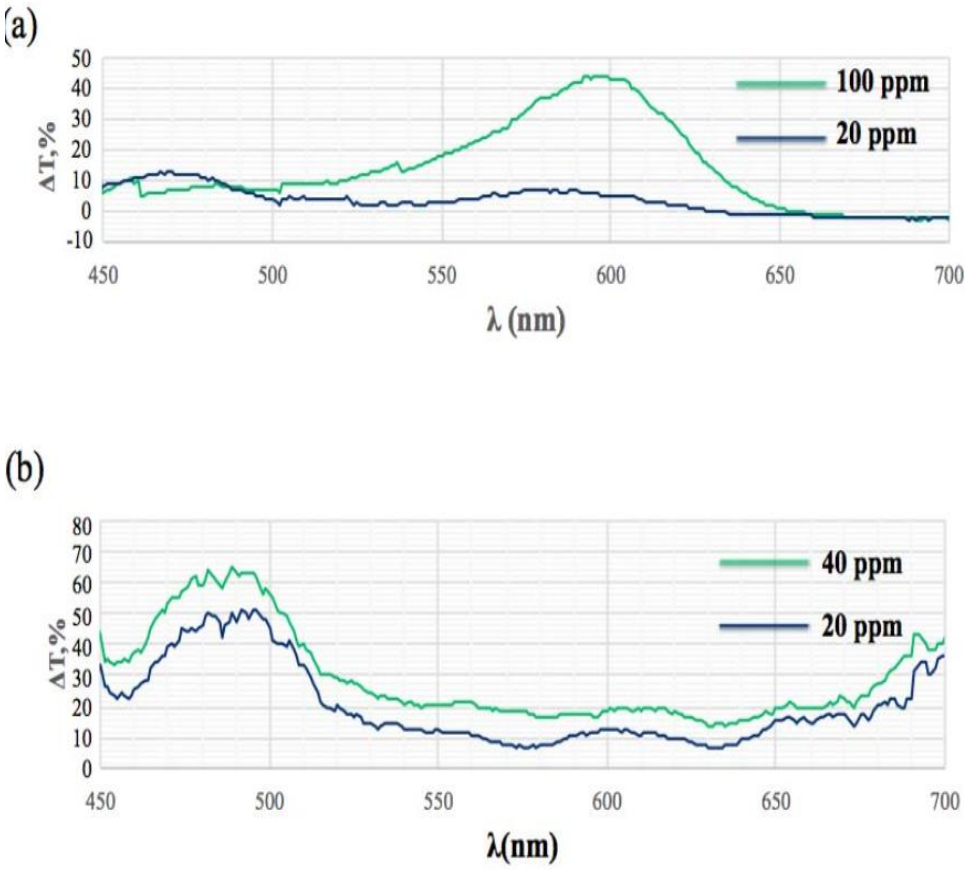

Figure 4.4. Normalized transmission spectra (450 nm to 700 nm) of the sensor exposed to different concentration of gastric gases: (a) CO_2 of concentrations 20 ppm and 100 ppm; and (b) NH_3 of concentrations 20 ppm and 40 ppm.

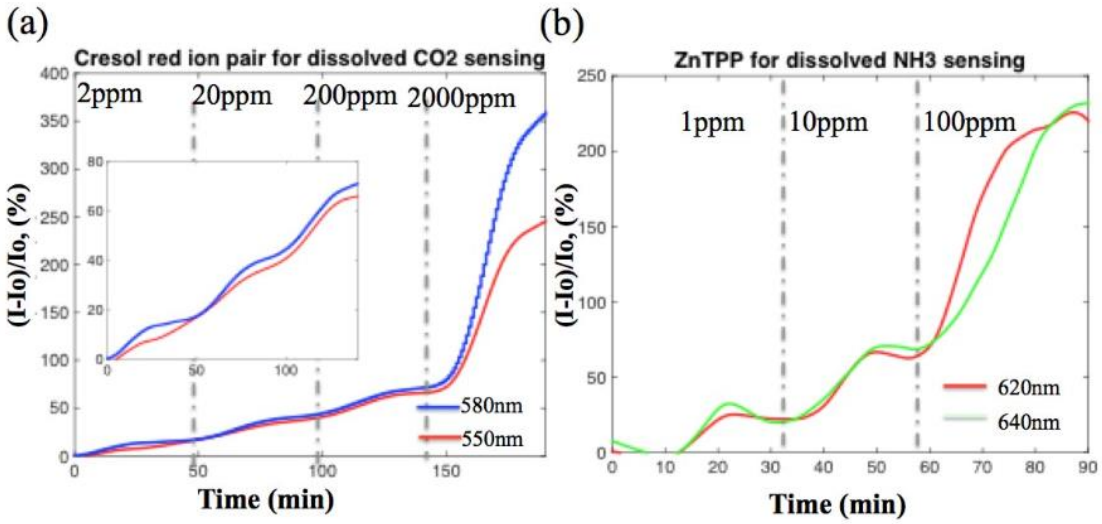

Figure 4.5: Normalized sensor responses when exposed to different concentration of gastric gases (dissolved CO_2 and NH_3): (a) CO_2 of concentrations 2 ppm, 20 ppm, 200 ppm, 2000 ppm, the inset figure shows the enlarged image of sensor response to 2 ppm, 20 ppm, 200 ppm CO_2; (b) NH_3 of concentrations 1 ppm, 10 ppm,100 ppm.

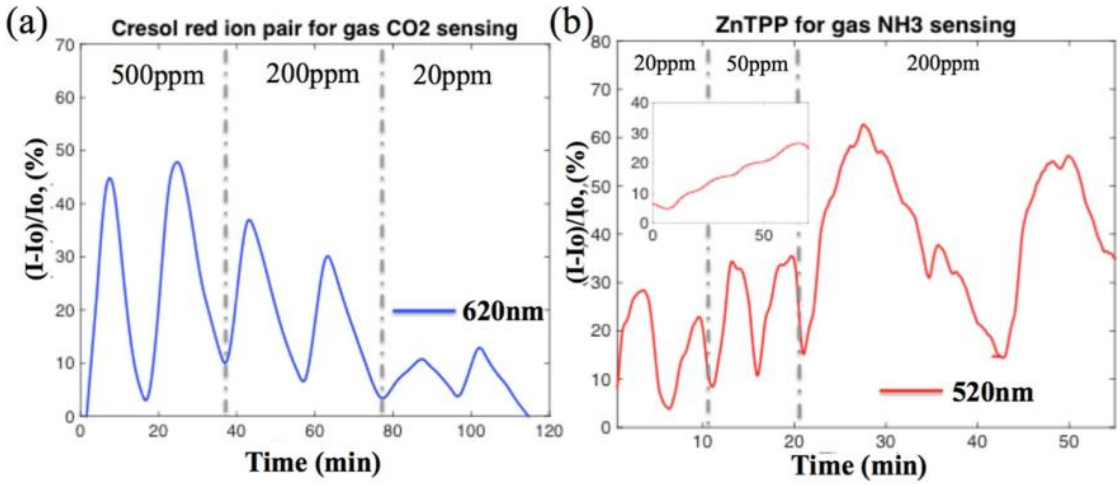

Figure 4.6: Normalized sensor responses when exposed to different concentrations of gastric gases (gaseous CO_2 and NH_3), each concentration is presented twice: (a) CO_2 of concentration 20 ppm, 200 ppm, 500 ppm; and (b) NH_3 of concentrations 20 ppm, 50 ppm, 200 ppm, the inserted figure shows the step response of NH_3 gas, with increasing of 4 ppm each step.

4.5.2 Sensing gaseous CO_2 and NH_3

While the conjoined dual-fiber based gastric gas sensor has been shown capable in sensing dissolved CO_2 and NH_3, per- forming detection of gaseous CO_2 and NH_3 further extends its functionality. Figure 4.6 shows the responses of cresol red ion pair or Zn-TPP functionalized fiber sensors to gaseous CO_2 or NH_3 of different concentrations. Each concentration is tested twice to ensure a repeatable response of the sensor. In Figure 4.6(a), the cresol red ion pair functionalized sensor responds to gaseous CO_2 of 20 ppm, 200 ppm and 500 ppm with 10%, 35% and 50% changes in signal magnitude at 620 nm. The same experiment was performed on Zn-TPP functionalized sensor in sensing NH_3. The sensor responded to gaseous NH_3 pulse of 20 ppm, 50 ppm and 200 ppm, as shown in Figure 4.6(b). The magnitude variation in the repeated test was due to the difficulty in controlling the amount of injected gas precisely. In the inset figure in Figure 4.6(b), the NH_3 gas is injected into the sealed chamber with the interval of 4 ppm per injection. With the addition of NH_3 injection, a step response in the spectrum is observed, which indicates that the sensor is able to distinguish gaseous NH_3 with ppm level accuracy.

The result in Figure 4.6 shows that this fiber-based gastric sensor can be applied in both fluidic and gaseous environment to perform gas sensing without any further modification in the sensor configuration. Furthermore, the sensor can distinguish CO_2 and NH_3 of various concentrations with ppm level sensitivity in both fluidic and gaseous environment. This is important in enabling sensing in both fluid-filled or empty stomach environment. Compared with the conventional methods, for example, breath test, which also measured vapor gaseous byproduct due to H.pylori infection, this fiber-based gastric sensor is aimed at assisting traditional endoscopy imaging approach by detecting the gas products directly in the stomach

instead of breath or saliva during the endoscopy procedure.

4.6 Summary

In this work, we showed a conjoined dual-fiber based optical sensor platform for gas sensing in both fluidic and gaseous environments. The sensor can detect various concentrations of NH_3 and CO_2 under back-scattered light condition at the ppm level. This will be the basis of future work. Finally, we believe that the proposed fiber sensor can not only be integrated into an endoscopy capsule, but can also be utilized stand-alone for detection of CO_2 and NH_3. By changing the types of optical dyes, this fiber based sensor platform can be used sense more types of gases, such as oxygen and volatile organic compounds. Regardless of all the merits of existing work, more improvement is needed to enhance the sensitivity of this sensor platform. A better signal to noise ratio can be achieved by increasing the intensity of excitation light. Moreover, for the fabrication, better control of PDMS layer thickness is needed to optimize the bead density at the tip of the fiber. Further more, different types of optical dyes encapsulated beads can be functionalized on the same fiber to simultaneously sense multiple analytes.

CHAPTER 5

Colorimetric barcode sensor for food quality monitoring

Objective: The objective of this work is to propose a low cost solution by repurposing the food's barcode as a colorimetric sensor array to monitor food condition. A smart phone camera is used to read color information from the sensor barcode for quantitative estimate of the food quality.

Quality of food from production to consumption is a major barometer for whether the food is consumed or discarded. Arbitrary end-of-life indicators of food quality based on expiration date are sub-optimal and have resulted in good food being discarded or unhealthy food being consumed, resulting in food poisoning and debilitating health consequences. Majority of techniques used for food quality monitoring are single point measurements done discretely on few samples at sparse times during the food supply chain by qualified food inspectors using expensive equipment. To avoid food wastage/loss and prevent food borne illness, a true revolution in food quality monitoring is essential. We believe that this is possible by empowering the consumer with sensors for monitoring food quality to make smart choices. In this work, we present a disposable paper-based optical sensor arranged as geometric barcode with smartphone read-out for monitoring the changes in the chemical composition of the package environment to monitor food spoilage. These chemical changes are a result of change in pH and the emitted volatile organic compounds (VOCs) from food

spoilage. The sensor fabrication is low-tech and easy to perform. Different cross-reactive vapor sensitive dyes are first encapsulated in resin micro-beads, and then functionalized onto filter paper. The sensor strips are packaged with the food at the source. A smart phone is used to monitor color change in the geometric barcode food sensor as an indirect but continuous metric of food freshness or spoilage.

5.1 Background

Generally, food quality is monitored during the food supply chain by qualified food inspectors using relatively expensive equipment. Some common techniques for food quality monitoring are gas chromatography [154], spectroscopy [155], electromagnetic interrogation [156], ultrasound interrogation [157] and chemical sensing using electronic nose [158]. However, regardless of the fine accuracy of these systems, they are neither cost effective nor user friendly for direct use by consumers to monitor the food quality at point of consumption. Consumers usually judge whether food is acceptable for consumption by looking at the expiration date, which is sub-optimal and has resulted in healthy food being discarded or unhealthy food being consumed [159]. If one could implement a low cost sensor platform that could objectively provide the consumer with the information on whether the food is healthy for consumption, it would be a significant step in avoiding global food wastage and in preventing food borne illness.

In recent years, several research groups have successfully employed colorimetric sensor arrays based on various optical dyes [160][161][162]. These sensor arrays have shown sensitivity to sub-ppm levels of target gases in their environment [53]. The most commonly used optical dyes for colorimetric sensors are metalloporphyrins, Brønsted acid/base dyes, solvatochromic dyes, and redox indicators [54]. They have been utilized for sensing volatile

organic compounds [39], environmental pollutants [163], and toxic industrial chemicals [45]. Interestingly, the volatile gases that the foods emanate can be used to estimate its freshness and quality. This has been the basis of many sensor platforms utilized for food sensing. Li et al. has incorporated a variety of optical dyes, including pH indicators, Lewis acid and natural dyes into inorganic support materials to monitor the gas products of meat spoilage [164]. Similar ideas have been used for monitoring the freshness of pork [165], fish [166] and chicken [167] under the package atmosphere. While these colorimetric sensor arrays have shown promise for food monitoring, they are still not amenable for direct consumer use due to the need for expensive and bulky accessory to sample and deliver food-related gases to sensors, and of the optical readout instrumentation. Moreover the cost of fabrication in making some of these sensors may be cost prohibitive for many food items. In this work, we demonstrate a low cost easy to use sensor platform using colorimetric sensor arrays with mobile phone camera based readout for direct consumer use at point of consumption.

There are plenty of advantages of using mobile phones for optical readout. First, in some of the less developed regions of the world, where there is little or no electricity, there are more mobile phones than landlines. Many of these phones have cameras with sufficient color and image resolution for scientific imaging. In fact, smart phone for medical diagnostics have already been proposed. For example, smart phone has been successfully used in a number of chemical and biological sensing applications [168] [169] [170]. Some examples include using smartphone as sensor read out of pattern change on a paper-based blood typing sensor [171] and of colorimetric detection of pH change in sweat and saliva [172]. Smartphone implemented fluorimeter has been successfully used for detecting specific nucleic acid sequence in a liquid sample [140]. It is shown that the color information

captured by smart phone can be represented using various RGB color models, such as HSL or CIE. Some smartphone application algorithm has also been developed to directly quantify color information in the smartphone interface [174]. It has been proven that the smartphone-based colorimetric detection scheme can achieve the same accuracy as a benchtop spectrometer [175]. The successful use of smartphone shows promise for realization of low cost sensor platforms leveraging existing consumer devices as a substitute for an otherwise expensive scientific instrumentation.

Combining the advantages of optical dyes for gas sensing and smartphone detection, we present a disposable paper-based colorimetric geometric barcode sensor for monitoring food quality. The sensor is fabricated by stamping dye-encapsulated silica beads that are pH and VOC responsive on a paper substrate in geometric shapes resembling a barcode. The as-fabricated sensor can be directly attached to the surface of the food (e.g. meat) or onto the inner lining of the food package to monitor its condition. The sensor then changes its color based on the volatiles emanating from the food, which is trapped inside the sealed package. For readout, any smart phone with a camera is used to capture the images of the sensing barcode, and a built in app which directly measures the color change in this sensing barcode using image processing to generate quantitative results. Compared to the existing work on food monitoring, our sensor platform has several advantages. First, the sensor fabrication process is low cost and highly reproducible; Second, compared to electrochemical sensing based approach, utilizing optical dyes as sensor provides high sensitivity and rapid response as shown in prior work on using such dyes in gas sensing [42][160]. Moreover optical sensing provides natural wireless means for readout. Our approach aims to incorporate colorimetric dye sensing arrays into the product barcode or QR code for simultaneously

obtaining food UPC code and condition/quality information. Some existing bio-barcode applications include immobilizing small DNA molecules onto gold nanoparticles to form a barcode for pathogen detection [176] or converting photoluminescence spectrum of nanoporous anodic alumina into barcode [177]. The more popular QR code is able to store more information and is highly compatible with smartphone readout. Compared with monochrome barcode, colorful QR code has the advantage of increasing the data rate and lowering the error rate [178], which provides the promise of making the colorful QR code using optical dyes. The convenience of using smartphone for scientific readout makes it amenable for use by consumers at home. Third, in terms of fabrication, we employ the resin encapsulation of the colorimetric optical dyes, which prevents food contamination from dye leakage. Finally, we can apply machine learning approaches on colorimetric data to provide accurate assessment of food quality. For proof of principle, we utilized the principle component analysis (PCA) on the quantitative data from packaged chicken meat where we can not only monitor spoilage status of the chicken each day, but also at an interval of every hour, making this a very sensitive platform for food condition monitoring.

5.2 Sensor fabrication

5.2.1 Preparation of colorimetric beads

Bromocresol purple, Bromothymol blue and cresol red were used for pH sensing. Nile red, Zn-TPP and Methyl red were used for sensing emanating gases from meat. The procedures of preparing Bromocresol purple, Bromothymol blue, cresol red, Methyl red and Nile red micro-beads solutions are similar: 25 mg of each dye powder was first dissolved in 5 mL of de-ionized water, and this mixture was stirred on the a magnetic stirrer for 20 min before being poured into 256 mg of anion exchange resin micro-beads (Sigma Aldrich). The

resulting mixture was stirred again on magnetic stirrer for 2 hours at room temperature to fill the resin micro-beads with optical dyes. The method of preparing Zn-TPP beads solution is described in detail in our previous work [124]. Briefly, 25.6 mg of Zn-TPP powder was first dissolved in 3 mL of toluene and stirred on a magnetic stirrer for 2 hours to ensure good dissolution. The dye solution was poured into 256 mg cation exchange resin microbeads. The resulting mixture was again stirred on a stirrer for 2 hours at room temperature to fill the microbeads with optical dyes. The as-prepared Zn-TPP micro-beads solution was left in the fume hood over-night for toluene to evaporate. 3 mL of de-ionized water is added into the dried Zn-TPP micro-beads

5.2.2 Stamping technique

The sensor fabrication process is described conceptually in Figure 5.1 As shown in Figure 5.1(a), the micro-beads containing various optical dyes were prepared based on a recipe discussed in the previous section. Each category of optical dye-loaded beads is stored in its own container and is ready for use. A polymer mold with triangle, square and circle grooves was made through laser cutting (Figure 5.1b). These shapes were chosen as a geometric substitute for QR code to show our capability to pattern complex geometry. The de-gassed PDMS was poured into the as-fabricated polymer mold and cured in the oven under 80 °C for 5 hours. After that, the cured stamp was peeled off the mold (Figure 5.1c). In Figure 5.1(d), three types of dye-contained micro-beads were drop-casted on to the triangle, square and circle patterns of the stamp using a micro-pipette (20 uL), respectively. The dye-loaded microbeads organized in the geometric pattern on the stamp is simply attached to the double-sided tape (Figure 5.1e), to transfer them in their geometric pattern onto the tape (Figure 5.1f). This micro-beads-attached tape was then attached to filter paper

(as protective covering and a barrier) to complete device fabrication. The image of as-fabricated device is shown in Figure 5.1(h).

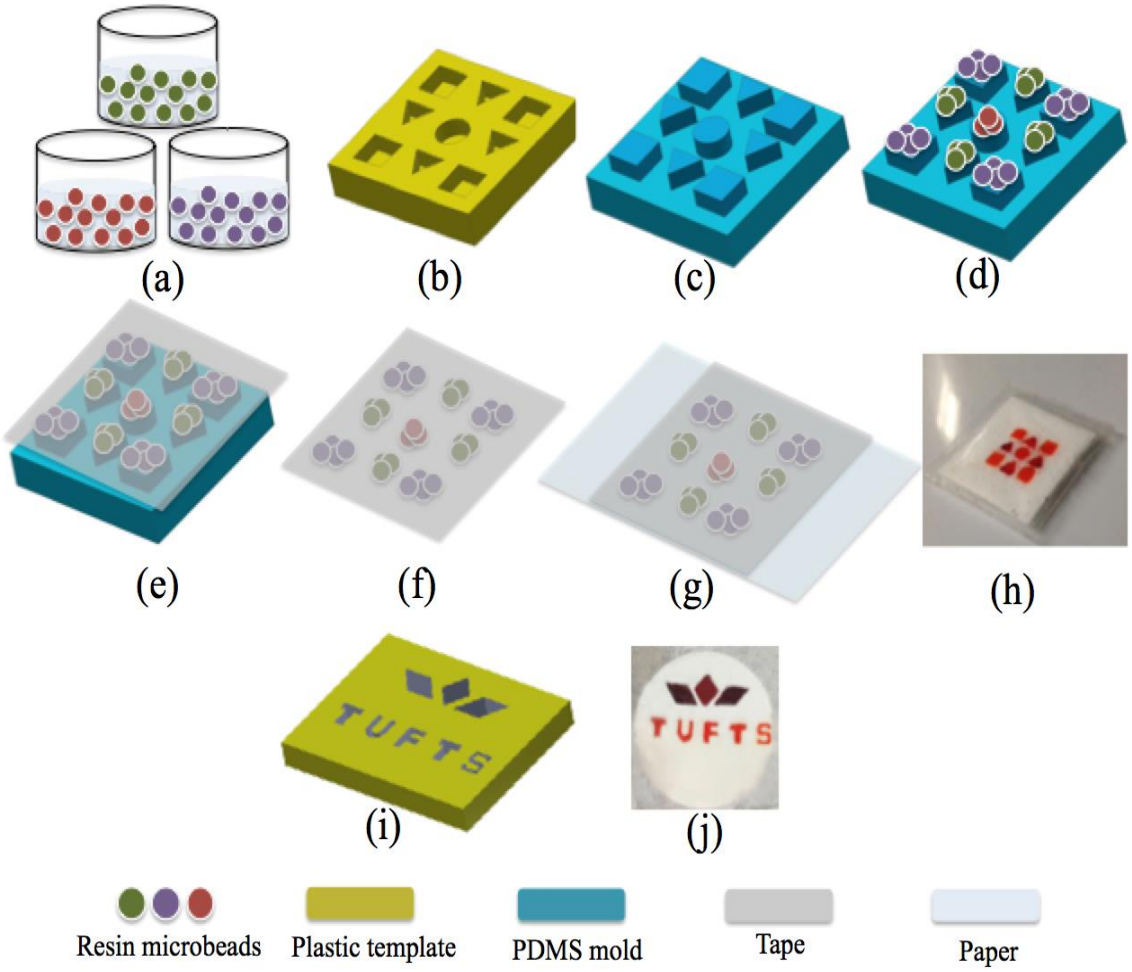

Figure 5.1: Device fabrication process: (a) dye-contained resin micro-beads, various dyes can be encapsulated based on specific application, each optical dye shown here with different color is loaded individually in different reservoirs; (b) plastic template made by laser cutter; (c) PDMS mold made using template shown in (b); (d) sensing beads are drop-casted onto the PDMS mold; (f) a piece of double-sided tape which serves as a sensor substrate is attached to the PDMS mold; (f) the tape with beads a repeeled off from the PDMS mold; (g) the tape with beads attached to a piece of filter paper; (h) image of as-fabricated device; (i) another plastic template made through same procedure for another pattern spelling TUFTS ; (j) image of as-fabricated beads pattern on paper using the template in (i).

5.3 Data detection and processing

The images of geometric barcode sensors are taken by smartphone camera (Apple iPhone was used in this study). Ambient illumination is used for imaging. These colorimetric images are imported into MATLAB for image processing to extract the R, G, B channel intensities of different sensing dyes at different times. An app that performs color extraction directly on the phone or in the cloud could also be employed and will be explored in the future [179](Oncescu et al., 2014). As described previously, the triangle, square and circle patterns correspond to different sensing dyes. The obtained R, G, B values for each dye on the sensor are the average over the sensing areas (squares, triangles or circle) of that dye. To compensate for the non-uniformity in the background lighting, a calibration step is performed by monitoring the R, G, B channel intensity of the background region (where no optical dyes are present) and subtracting this background variation from the captured images of the sensing region. This step is performed individually for each image capture to account for the varying background illumination. To discriminate the sensor responses to different degrees of food spoilage, principle component analysis (PCA) is applied to the colorimetric data arranged as a vector of all the three channels of R, G, B intensities at the square, triangle and circle areas at different times, with three repetitions of the same measurement. For the proposed study, due to the choice of the dyes, we were able to discriminate sensor response using just the red (R) channel information.

5.4 Sensor characterization

Geometric barcode food sensor functionalized with. Bromocresol purple (rectangle), Bromothymol blue (triangle) and cresol red (circle) micro-beads, are made using the procedure described in the previous section. The pH sensing range of Bromocresol purple, Bromothymol blue and cresol red are pH 5.2-6.8, pH 6.0-7.6, pH 7.2-8.8, respectively. To study its color variation characteristic versus pH, the sensor was immersed in different pH solutions with pH value from 5 to 9. In each pH solution, the image of the sensor was taken by iPhone camera after 30 min of immersion to ensure stable color at that pH. The images of geometric barcode sensor under pH 5 to pH 9 are shown in Figure 5.2(a); the colors of the sensing areas on the sensor gradually change as the pH increases. It is found that at each pH, the rectangle, circle and triangle areas showed different colors, which together form a unique color pattern at each pH. The color changing rates at rectangle, circle and triangle areas correspond to the sensitivity of different dyes at different pH. For instance, the R, G, B channel intensities of the rectangle sensing area change faster from pH 5 to 7 than from pH 8 to 9. This fact matches well with the sensitive pH region for the Bromocresol Purple dye. Same trend can be observed on the circle and triangle sensing areas, where the most apparent color change happens at the pH sensitive range of cresol red and Bromothymol blue. Principal component analysis (PCA) was used as a simple machine learning algorithm to demonstrate classification based on R, G and B component for each optical dye. Figure

5.2(b) showed the PCA analysis on the collected color information of Bromocresol purple, Bromothymol blue and cresol red at different pH. The PCA results clearly distinguished the sensor responses of different samples at different pH. Combining the color images and PCA analysis, GBFS-1 can visually and quantitatively distinguish different pH through a smartphone-based detection methods.

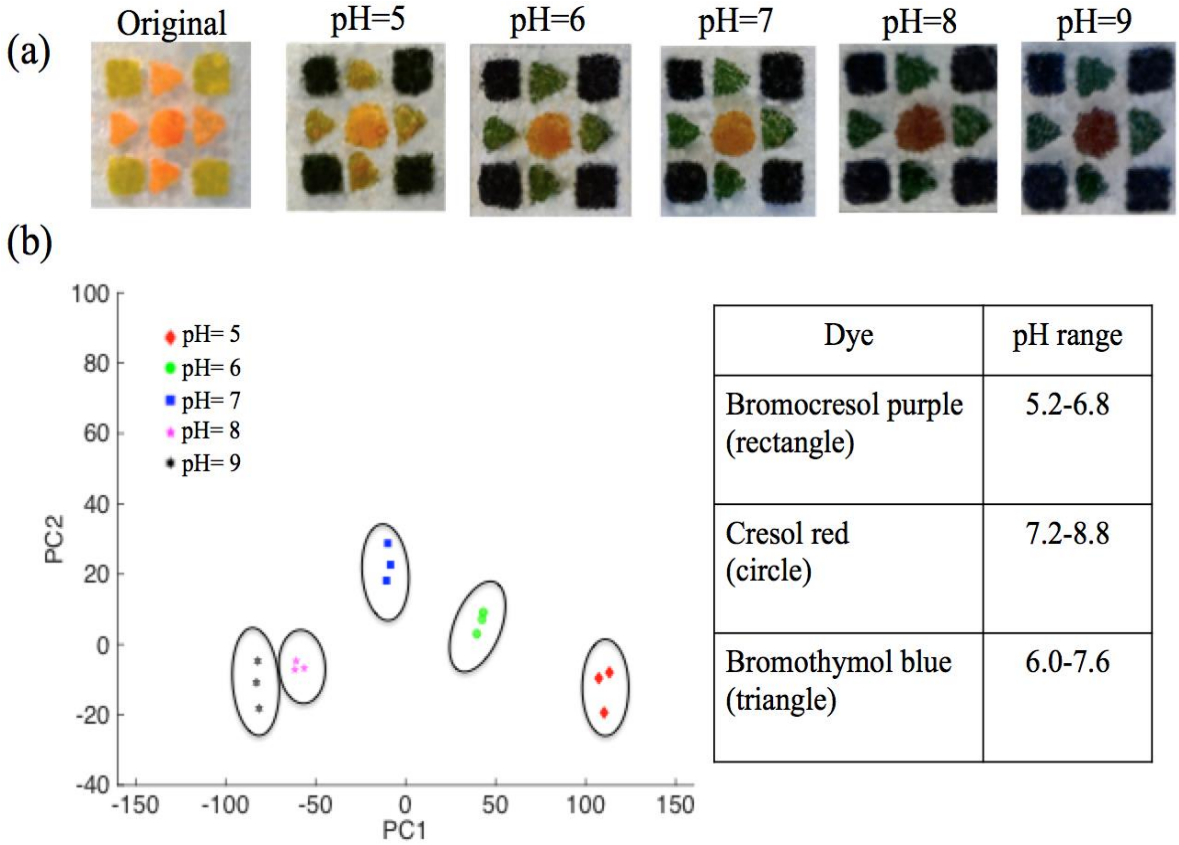

Dye	pH range
Bromocresol purple (rectangle)	5.2-6.8
Cresol red (circle)	7.2-8.8
Bromothymol blue (triangle)	6.0-7.6

Figure 5.2: pH sensing: (a) Geometric barcode sensor with Bromocresol purple (rectangle), Bromothymol blue (triangle) and cresol red (circle) was immersed in petri-dishes with different pH solutions in sequence (from pH 5 to pH 9) and images of GBFS-1 in different pH solutions were taken by iPhone camera for visualizing changes of color in all sensing areas from pH 5 to pH 9; (b) PCA analysis on Bromocresol purple (rectangle), Bromothymol blue (triangle) and cresol red (circle) sensing results.

5.5 Chicken spoilage sensing

5.5.1 Principle of operation

Figure 5.3 describes the procedure of using smart phone diagnostic sensing system to detect the spoilage status of the chicken as an example. The as-fabricated barcode sensor can be placed on the surface of the raw chicken meat or on the inner lining of the package. To monitor the spoilage status of that packaged chicken, a smart phone is employed to take images of the barcode sensor. The photos of the barcode sensors are sent to MATLAB for image processing. Red (R), Green (G) and Blue (B) component of each pixel in the image is extracted to quantify color change. The extracted R, G, B values of the specific dyes on barcode sensors can be compared objectively with pre-obtained R, G, B characterization curves of all dyes to estimate the freshness of this chicken. Such images can be taken by anyone during the food supply chain from the food inspector, the grocer and the consumer until the food is unpacked and consumed. The result can serve as an important reference to decide if this chicken is suitable for consumption or should be discarded. It can also help to estimate the shelf life of the food based on existing knowledge base of food quality degradation with time under similar storage conditions.

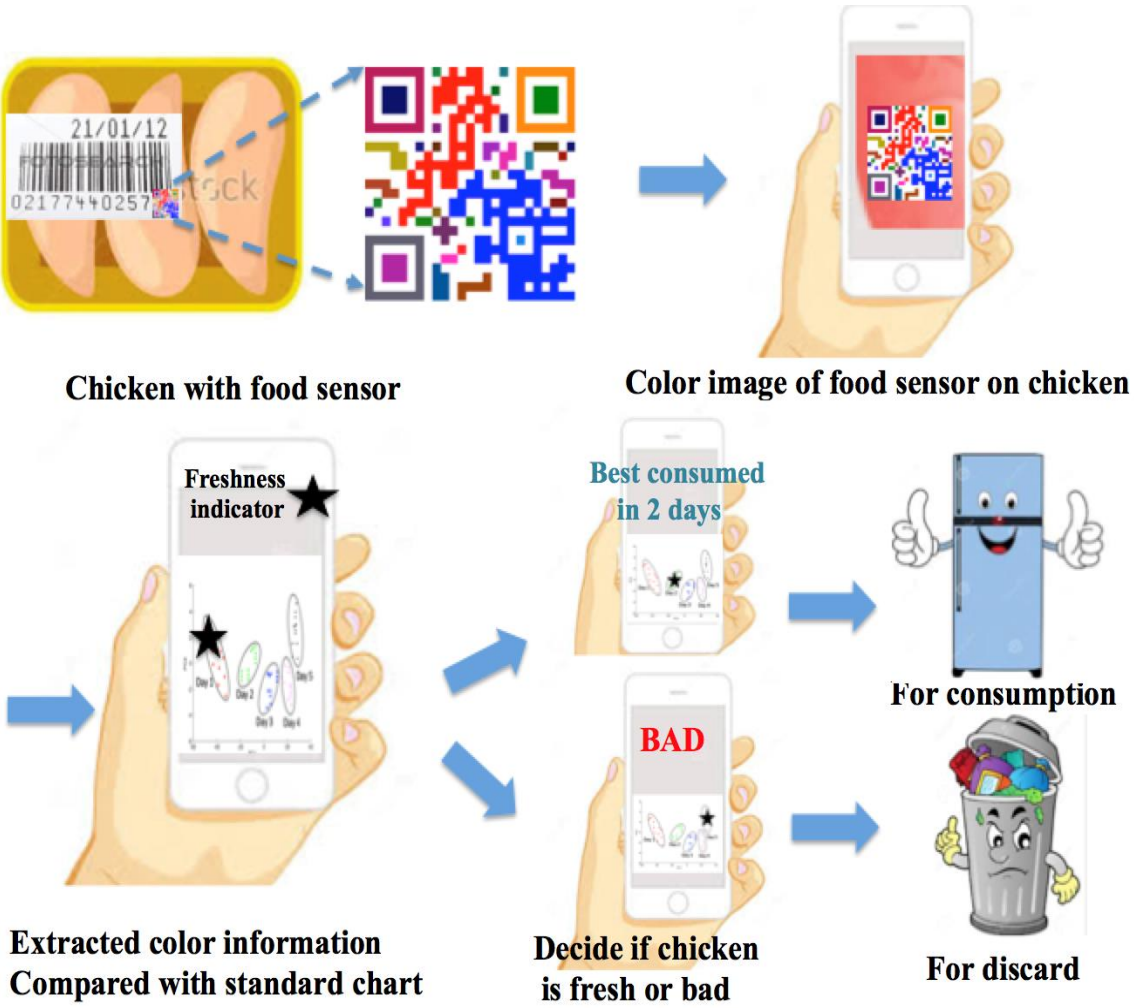

Figure 5.3: Schematic of device application as food quality sensor. The sensor can be attached to the surface of the meat or placed onto the inside lining of the package. The status of the meat product can be monitored using smartphone by taking a photo of the sensor. The color information is extracted from the photo and compared with the standard chart to decide the quality of meat.

5.5.2 Spoilage sensing with varying temperature

For proof of demonstration, a simple geometric barcode as shown in Figure 5.1 was implemented in lieu of a QR code. Barcode sensors functionalized with Nile red (rectangle), Zn-TPP (triangle) and Methyl red (circle) microbeads are used to monitor raw chicken meat spoilage status. Nile red and Zn-TPP are sensitive to broad cross-section of VOCs, including ethanol, methanol, toluene, etc [180](Barnard et al. 1991) [42](Rakow et al. 2000). Zn-TPP is

also sensitive to ammonia [153](Chen et al. 2015), which is a typical chemical byproduct sensed during chicken spoilage among other VOCs [181](Balamatsia et al. 2007). Methyl red is a pH indicator dye with sensing range from pH 4.4- 6.2, which covers the natural pH change range from meat spoilage [182](Vidal-Carou et al. 1990). The as-fabricated barcode sensor has a total sensing area of 1cm by 1cm, as shown in Figure 5.4a-i. Barcode sensor was placed on the surface of a piece of fresh chicken meat such that the filter paper side is in contact with the meat, and then packaged with a plastic wrap (Figure 5.4a-ii). This prevents a direct contact of the beads with the meat while providing permeability to gases emanating from the chicken. Conversely, one could also attach the barcode sensor to the inner lining of the plastic wrapping. The images of barcode sensor on fresh (Figure 5.4a-iii) and spoiled (Figure 5.4a-iv) chicken were taken for comparing the color change inside the rectangle, circle and triangle sensing areas. The evaluation of this sensor involves recreating varying conditions for food spoilage. One such condition is based on temperature. It is well known that meat needs refrigeration to prolong its shelf life and will degrade or decompose rapidly at room and higher temperatures. We used the sensor's ability to monitor spoilage in this case from different temperature fluctuations.

The experiment consisted of placing barcode sensors on 9 different pieces of chicken meat to form sampling groups. For comparison, those samples are divided into three groups kept under different temperature conditions. The 1st group of samples are kept under room temperature (20 °C) and the 2nd group of samples are kept in the refrigerator (5 °C), while the 3rd group of samples are cycled alternately between refrigerator and room temperature at the interval of 24 hours. During 5 days observation, the images of all groups of samples were taken four times a day, with two hours interval in between the reading. The R channel

intensities of all the sensing areas on all the sensors under different temperature conditions are extracted since it shows the most sensitivity. However for other food groups, information from all the channels (R, G and B) may be needed for finer discrimination. For quantitative analysis, PCA analysis is applied on the R channel intensity of all the sensing areas to differentiate responses under different conditions and different days, as shown in Figure 5.4 (b) to (g). In Figure 5.4(b), the responses of barcode sensors under different temperature conditions were categorized into three groups. The sensor responses to 5 °C and 20 °C can be clearly distinguished, while the responses to 5 °C /20 °C fell into both groups. The results indicated that the sensor could easily distinguish chicken status according to the varying spoilage rate of chicken under different temperatures. Meanwhile, the sensor's responses to 5 °C /20 °C verified that it could monitor spoilage even under complex temperature modulation of the meat. Figure 5.4 (c) to (e) represent the daily response of barcode sensor on chicken samples under 20 °C, 5 °C and 5 °C /20 °C. Under all temperature conditions, it is observed that the spoilage status of the chicken samples experienced a significant daily change, which can be used to predict the age, which corresponds directly to the freshness of the chicken meat. To further explore the sensor's sensitivity within a day, in Figure 5.4(f), the sensor's hourly responses under 20 °C were distinguished using markers of different colors and shapes. In the case of 20 °C, the difference in hourly response is large earlier in the duration (day 1, day 2) due to the faster spoilage rate. As chicken spoils further, the sensor response becomes saturated and it is harder to differentiate the responses from day 3, 4 and 5 in our example.

5.5.3 Freshness sensing

Another experiment was performed by keeping the chicken samples in the freezer (-5°C) for 2 weeks. It is known that meat retains its freshness when frozen. The images of barcode sensor were taken on the 1st, 4th, 7th, 10th and the 13th day. The extracted R channels intensities are analyzed and presented in Figure 5.4 (g). We observe that the sensors' responses at the end of the 4th, 7th,10th and 13th day fell in the same data group as the first day response, indicating that the spoilage status of these chicken samples during two weeks' observation matches the fact that the chicken is in fact unspoiled during the two weeks it was in the freezer and is of acceptable quality for consumption. As a food sensor, we show that barcode sensor can clearly indicate both fresh and spoiled status on chicken, which could then be traced back to underlying cause of chicken spoilage, which in our case was based on temperature modulation. Other causes of meat spoilage could be monitored as well such as leakage or air exposure, or contamination with bacteria, since these are expected to alter the chemical composition of the gases they naturally emanate.

As shown here, the colorimetric sensor array can predict the freshness and also track daily and hourly changes in the food spoilage. While the work here was limited to chicken, it can be easily extended to other meats. The spoilage rate and profile of different meats can be

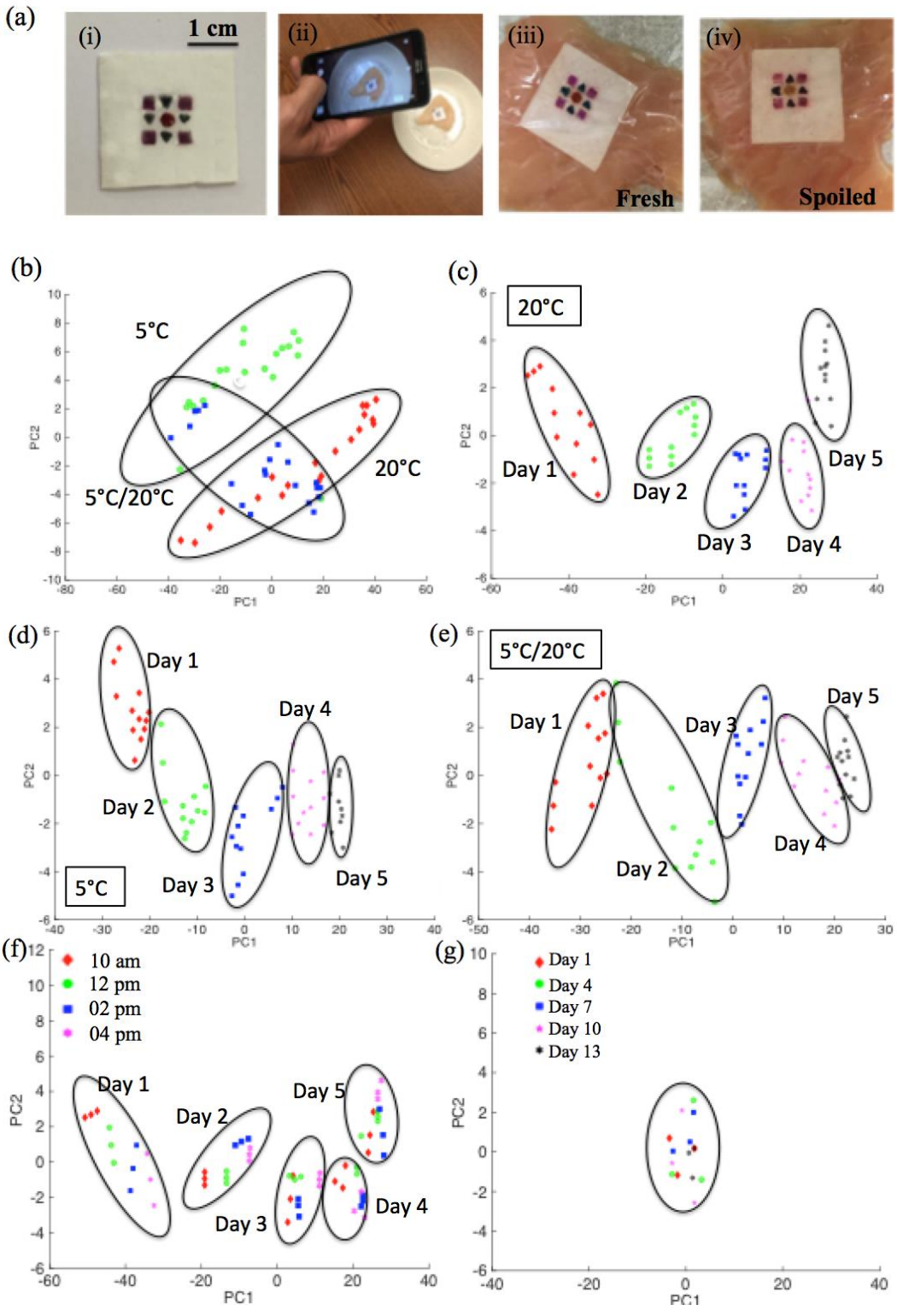

Figure 5.4: Geometric barcode sensor for monitoring chicken spoilage under different temperature conditions. (a): (i) image of as-fabricated sensor with Nile Red (rectangle), Methyl Red (circle) and

Zn-TPP (triangle); (ii) image of smartphone-based detection; (iii)-(iv) sensor placed on fresh and spoiled chicken at room temperature; (b) the sensing results on three groups of chicken samples (S1, S2 , S3), with S1 kept under 20 °C and S2 under 5 °C, while S3 under temperature alternating between 20 °C and 5 °C. PCA analysis is used to distinguish the sensing results under different conditions; (c)-(e) the daily responses of the sensor on S1, S2 , S3 under 20 °C, 5 °C, and 20 °C / 5 °C. Principal Component Analysis (PCA) results clearly distinguish the daily response of chicken sample under different temperatures; (f) the hourly change of S1 under 20 °C; (g) sensor performance on fresh chicken. Chicken samples with the sensor were maintained fresh in the freezer (-5 °C), the images were taken every 3 days for 2 weeks. Through PCA analysis, refrigerated chicken provided results that fell into same class, which corresponds to the fact that the chicken is unspoiled and good for consumption.

cataloged in a central database or made available in the cloud. Once a rich data set is generated, one could use that to estimate the remaining shelf life of the given meat based on the current colorimetric readout and comparison to the standard chart for archived over many users for a given meat. Such an estimate of the end of life indication will be more useful and accurate compared to the arbitrary "best used by" date marker provided with the packaged food today. By using paper and plastic tape as a substrate, barcode sensor also possesses the merits of being low-cost for use with both common and expensive foods. Smartphone-based readout empowers the consumers with ease of use directly at home or at the grocer without the need for expensive sensor hardware.

5.6 Summary

In this work, a food diagnostic platform using low cost sensors with smart phone readout was presented. The barcode of the product is repurposed using optical dyes to serve as an optical sensor for monitoring gases emanating from the food inside the package environment as an indirect indicator of its condition. The barcode sensor strips were fabricated by functionalizing different cross-reactive pH and VOCs sensitive dyes encapsulated-resin microbeads onto filter paper. For demonstration, chicken meat spoilage was simulated by

varying its temperature and monitored using the proposed barcode sensor. Continuous monitoring of food freshness is realized by using a smart phone to acquire images that are then quantified for color change as a quantitative measure.

The sensor has the advantages of biodegradable, disposable and extremely low-cost with minimal infrastructure overhead. As a continuation of this work, this sensor platform can be used for sensing other categories of food, including poultry, seafood and fruits. The choices of the optical dyes can be expanded and the results more rigorously analyzed for different food types to achieve objective metrics for food freshness and spoilage.

CHAPTER 6

Paper based optoelectronic sensor for sensing volatile gases

Objective: The hypothesis of this work is to show that a combination of optical sensing and chemiresistive sensing can increase the range of gases to be detected while enhancing the accuracy of detection.

In this chapter, a paper-based optoelectronic sensor is presented for sensing a number of volatile gases in air environment. Compared to sensors discussed earlier, the optoelectronic sensor consists of a combination of chemiresistive and optical sensor arrays. The chemiresistive sensors are based on nanomaterials and the optical sensor arrays are based on chemoresponsive dyes as discussed in prior chapters. The sensor is designed, fabricated and tested under air environment with different volatile gases and its mixtures of varying concentrations. The detected electrical and optical responses together form a unique signature for each gas or its mixtures, which effectively enhances the discriminative power of the sensing platform for a richer set of gas analytes. This optoelectronic sensor is easily fabricated with a "Paint-on-paper" technique, with flexibility in tuning the size of the sensor and the number of sensing elements. Machine learning method is applied to clearly classify the sensor responses to different analytes and its mixtures.

6.1 Motivation

Air quality monitoring plays a crucial role in environment monitoring. Various gas sensing techniques have been applied for air quality monitoring, including optical technique (e.g. absorption spectroscopy) [183], electrical technique (electronic nose)[104], gas chromatography (GC) [114] and acoustic technique [115]. With the increasing need of enabling common population to perform air quality monitoring in daily life, it is important to develop a new type of gas sensors, which have the merits of easy fabrication, simple operation, cost effective and environmental friendly. These sensors aim to be used by untrained personnel to run a fast test and get an immediate response. Most of the currently available gas sensing techniques, however accurate, requires additional equipment, either bulky or costly, to perform the measurement, and expertise is required to handle the sensor. To overcome this inconvenience, tremendous efforts are spent on improving the sensing principle and structure of gas sensors. For sensor fabrication, a variety of materials, such as plastic, polymer and paper, are employed as a substitute of traditional sensor substrates [184][20], among which paper substrate has caught a lot of attention due to its ubiquity, cheapness and eco-friendliness [153].

So far, paper based sensors have been applied in a number of applications, including biomedical diagnostics (e.g. glucose sensing, blood testing) [185][186], chemical sensing (e.g. metal ion detection) [187], and mechanical sensing (e.g. strain sensor) [188]. Moreover, the hydrophilic nature of paper allows the functionalization of a variety of materials onto paper substrate, including conductive inks, which paves the way for building electrical element on paper [189]. So far, single sensing element based chemiresistive sensors have been built on paper substrate for gas sensing [190]. One successful example of paper based

gas chemiresistor is realized by using carbon nanotube (CNT) pencil to directly draw CNT on the interdigitated gold electrodes pre-deposited on the paper substrate [191]. This sensor has been successfully used for ammonia sensing.

In this work, we have functionalized paper substrate with a variety of chemoresponsive dyes and conductive nanomaterials as chemiresistors to form an optoelectronic sensor arrays for gas sensing. Several common volatile gases (e.g. methanol, ammonia, toluene), as well as the mixture of different gases, have been tested with this paper-based optoelectronic sensing platform. For each gas, the collective responses from the optical and electrical sensing elements together form a unique signature to enhance the discriminative power of the sensor. Machine learning method have been applied to classify the responses to different gas analytes with great accuracy.

6.2 Sensor fabrication and experimental set up

6.2.1 Sensor fabrication

The fabrication of paper-based optoelectronic sensor arrays is realized through a "pen-on-paper" technique. The details are described as follows:

(a) Preparation of sensing elements: six chemoresponsive dyes, namely Reichardt's dye, bromocresol purple, methyl red, bromothylmol blue, brilliant yellow, Manganese tetraphenylporphorin (Mn-TPP), 25 mg of each, are dissolved in ethanol respectively. These mixtures are span on the centrifuge to form six uniform dye inks. CNT, PEDOT:PSS, ionic liquid solution are used as received. An 8B pencil is served as the source of graphite (Figure 6.1 (d));

(b) Patterning of paper substrate: the paper selected is Whatman Chromatography paper. The sensor layout is pre-designed in Solidworks and then transferred onto paper substrate through wax printing. The wax printed paper is placed on a hot plate at 85 C to allow uniform penetration of wax through the whole thickness of paper substrate (Figure 6.1 (a));

(c) Functionalization of patterned paper substrate: the as-prepared sensing elements are painted onto the designated areas using cotton swab or by refillable pen. The electrical contacts are made by painting conductive silver ink onto the contact areas (Figure 6.1 (a)). The image of as-fabricated sensor is shown in Figure 6.1 (b);

(d) Encapsulation of as-fabricated sensor: the as-funcationalized sensor is encapsulated in a sealed acrylic chamber to allow simultaneously performing electrical and optical measurement. The acrylic chambers has inlet and outlet which allows the gas to flow through the chamber.

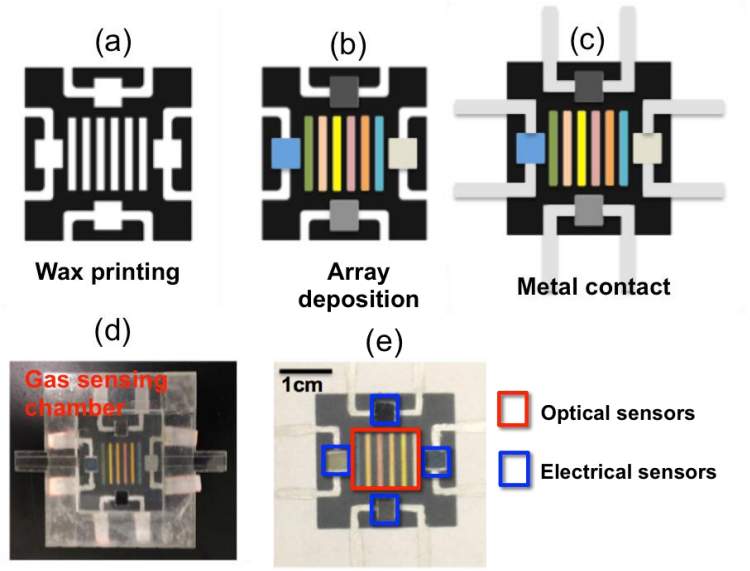

Figure 6.1: Fabrication of paper based optoelectronic sensors: (a) Patterning and functionalization; (b) image of as-fabricated sensor; (c) Sensor encapsulated in a sealed chamber with inlet and outlet; (d) list of all sensing elements.

6.2.2 Experimental set up

Figure 6.2 shows the schematic of test set up. The targeted gas analytes, including methanol, ammonia, toluene, acetone and ethanol, are prepared through bubbling air into each liquid analyte using a bubbler (4mL). A gas mixing system is created using two acrylic gas flow meters to control the flow rates of the targeted gas (0.1-1 SCFH) and air (1-10 SCFH) respectively. The targeted gas and air of different flow rates are mixed to obtain different analyte concentration (7.5%, 15%, 50%). The gas mixture is then passing through the sensing chamber shown in Figure 6.1 (c). To measure the sensor responses at each gas concentration, the targeted gas is flowing through the chamber continuously for 20 min to get a stable response. For recovery between two measurements, 100% air is flown through the chamber for 30 min.

In the experiment, the optical responses are collected through taking the images of optical sensor arrays using a USB microscope camera. The camera is fixed above the sensing chamber and maintains a relatively uniform illumination for all the images. The electrical responses can be obtained by Labview controlled DAQ card. For characterization purpose, the conductance of each chemiresistor in the electrical sensor arrays is measured by digital multimeter. To obtain quantitative values of optical signals, the R, G, B channel intensities of each chemoresponsive dye are extracted from the images of optical sensor arrays. Each obtained R, G, B intensity value is the average of a region in each color bar in the image. The electrical responses are presented by the amount of conductance change (%)of each chemiresistor. The optical and electrical responses together form a complete set of sensor responses to each gas analyte.

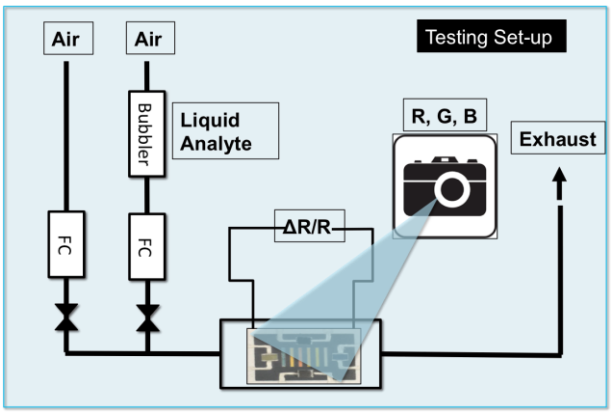

Figure 6.2: Experiment set up.

6.3 Gas sensing experiments and results

The sensor is tested in a sealed chamber with an inlet and outlet, as shown in Figure 6.1 (c). The targeted gas species include methanol, ammonia, toluene, acetone and ethanol, as well as the mixture of them. These targeted gases are mixed with air at different percentage and passed through the sealed chamber through the inlet. The sensor responses are recorded by measuring the conductance change of electrical elements and taking the images of optical elements.

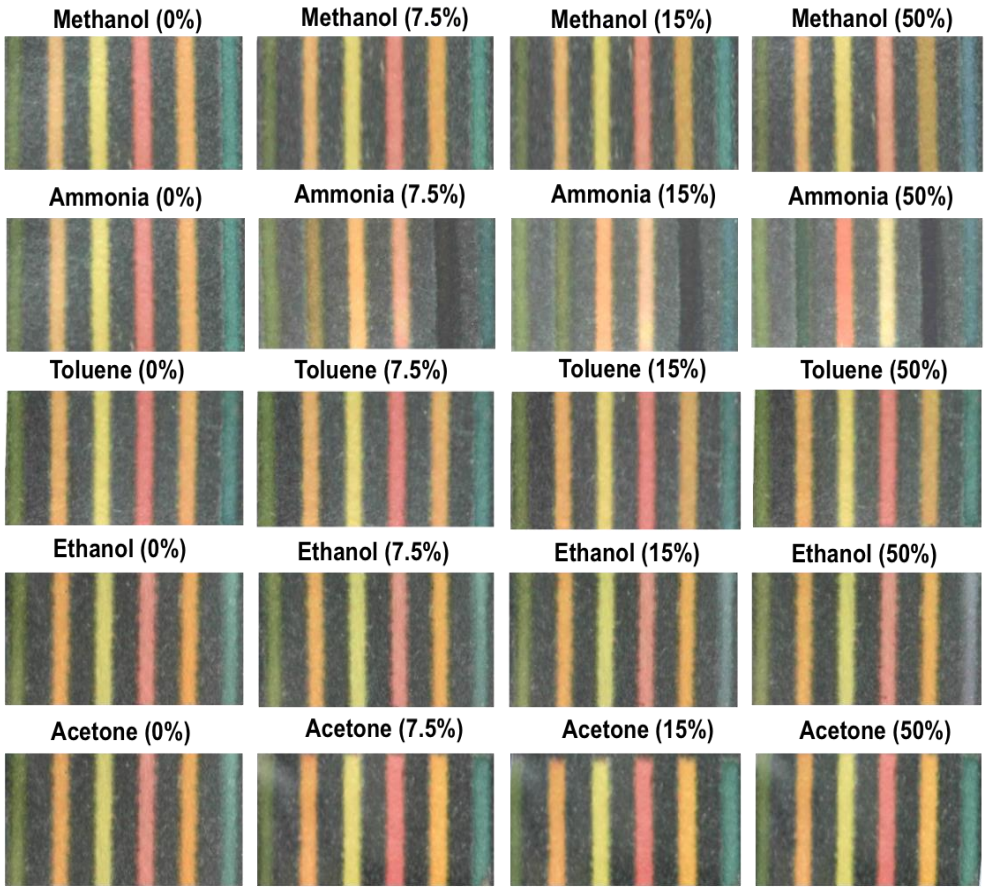

Figure 6.3: Optical responses of paper-based sensor platform to 5 different gas analytes, namely methanol, ammonia, toluene, ethanol and acetone, at 3 different concentrations .

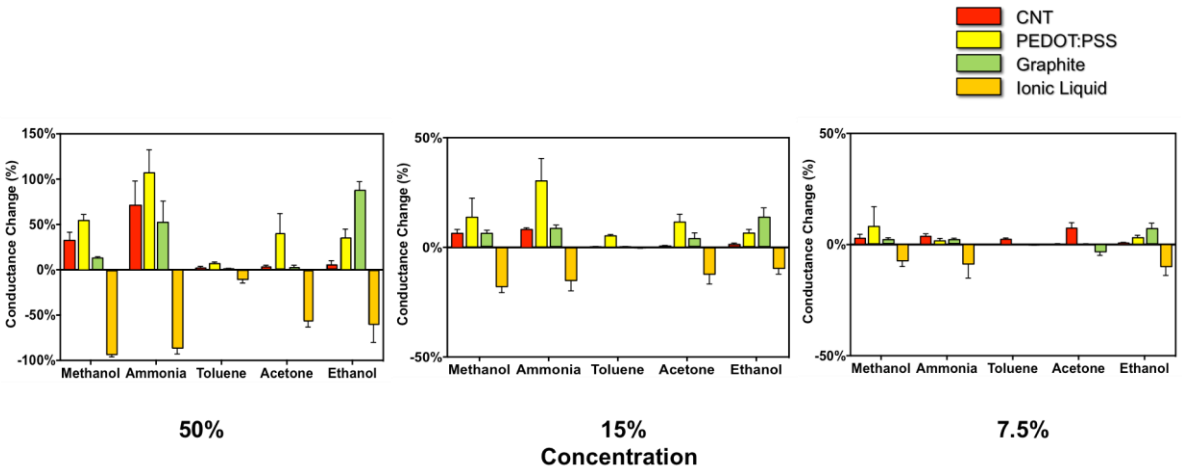

Figure 6.4: Electrical responses of paper-based sensor platform to 5 different gas analytes, namely methanol, ammonia, toluene, ethanol and acetone, at 3 different concentrations.

6.3.1 Sensing volatile gases

The optoelectronic sensor platform is used to monitor five volatile gases, namely methanol, ammonia, toluene, acetone and ethanol. The sensor is exposed to the targeted gas at three different concentrations (50%, 15%, 7.5%). The concentration of each targeted gas is tuned by varying the flow rate ratio between air and targeted gas. In Figure 6.3, the sensors' optical responses to different targeted gases are visualized. It is observed that the color change of these optical sensor arrays varied with different gases, resulting in different color patterns. This is because the selected chemo-responsive dyes have varying sensitivity towards different gases. Based on this property, a unique color pattern is formed for each gas, which acts as the optical signature for the specific gas. For each gas analyte, a gradual color change of optical dyes is observed from low concentration to high concentration, indicating the capability of optical sensor arrays in distinguishing gas of different concentrations.

In Figure 6.4, the responses of electrical sensor arrays to targeted gases of different concentrations (methanol, ammonia, toluene, acetone and ethanol) are summarized. It is found that the electrical sensor arrays have different sensitivities towards different gases. For example, these electrical sensors are highly sensitive to ammonia, while having low sensitivity to toluene; the sensor's responses to acetone reflect the varying sensitivity of the selected sensing elements towards the same gas analyte. Compared with optical responses, it is more difficult to distinguish targeted gases using electrical sensor arrays alone due to the similarity in the resulting response pattern. Therefore, by combining the optical responses and electrical responses, a more comprehensive response signature can be acquired to differentiate between different gases.

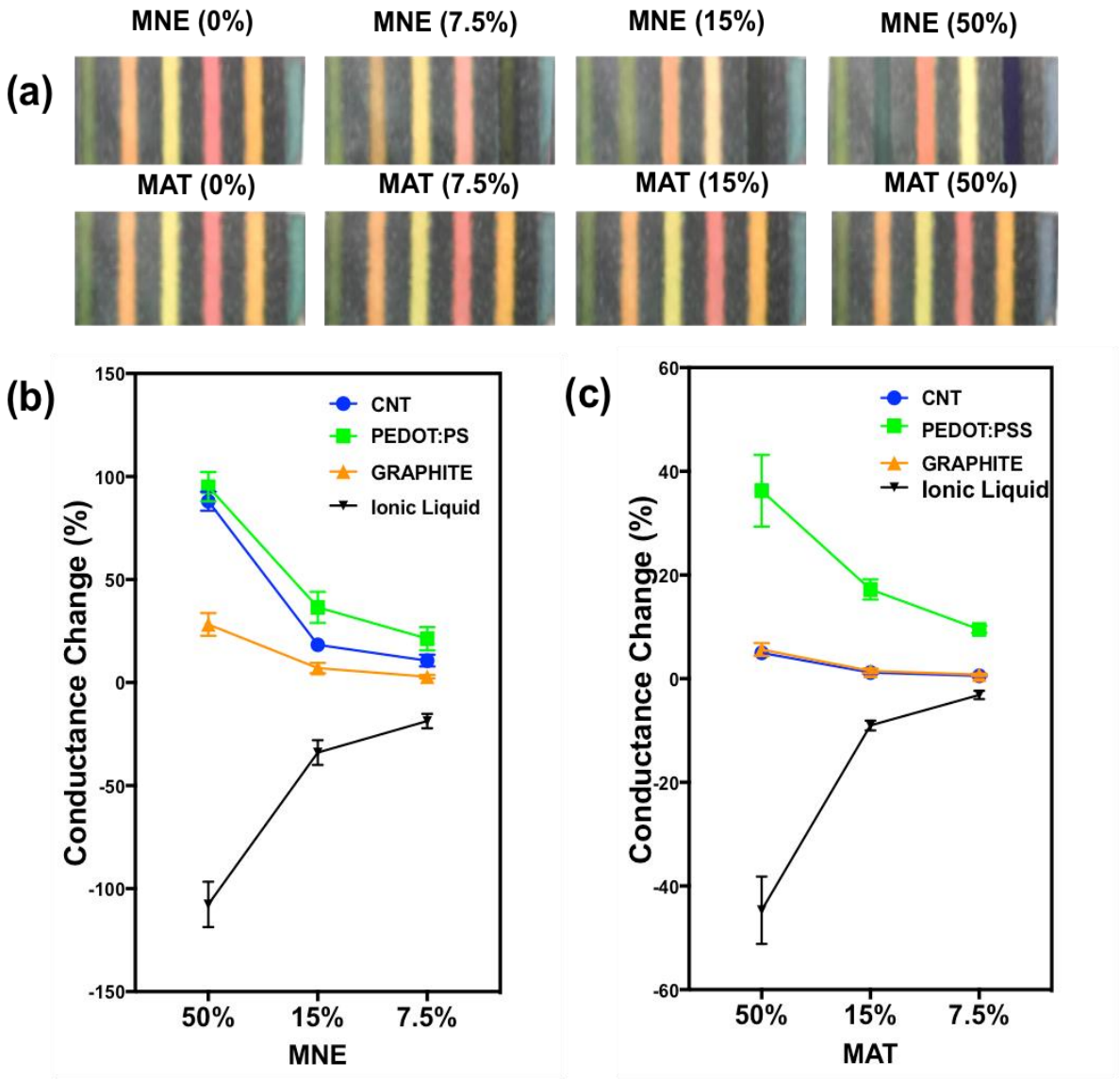

Figure 6.5: Optical and electrical responses of paper-based sensor platform to 2 different gas mixtures, namely MNE (methanol, ammonia, ethanol) and MAT (methanol, acetone, toluene); (a) color images of optical sensor arrays to MNE and MAT at 3 different concentrations; (b) electrical responses of electrical sensor arrays to MNE; (c)) electrical responses of electrical sensor arrays to MAT.

6.3.2 Sensing of gas mixtures

The optoelectronic sensor arrays have exhibited good performance in sensing and distinguishing the selected gases. To demonstrate the sensor's capability in sensing complex gas analytes, two gas mixtures, MAT (methanol, acetone and toluene) and MNE (methanol, ammonia and ethanol) are prepared for testing. Similarly, these two gas mixtures are flown through the gas chamber with varying concentrations. The optical and electrical responses of these sensor arrays are recorded, as shown in Figure 6.5. Figure 6.6 summarizes the sensor responses to all the targeted gases and two gas mixtures. Each column represents the response pattern to a specific gas analyte. By combining the optical and electrical responses, a more discriminative signature is obtained for each gas. For instance, the optical responses of ethanol and MAT are highly similar, but the electrical responses clearly show the difference; for acetone and MAT, the electrical responses are almost identical while the optical responses are different. Similar observation can be found when comparing the sensor responses to toluene and MAT. All these observations demonstrate an enhancement in sensor's discriminative capability towards different gas analytes, compared with the situation of using electrical sensors or optical sensors alone.

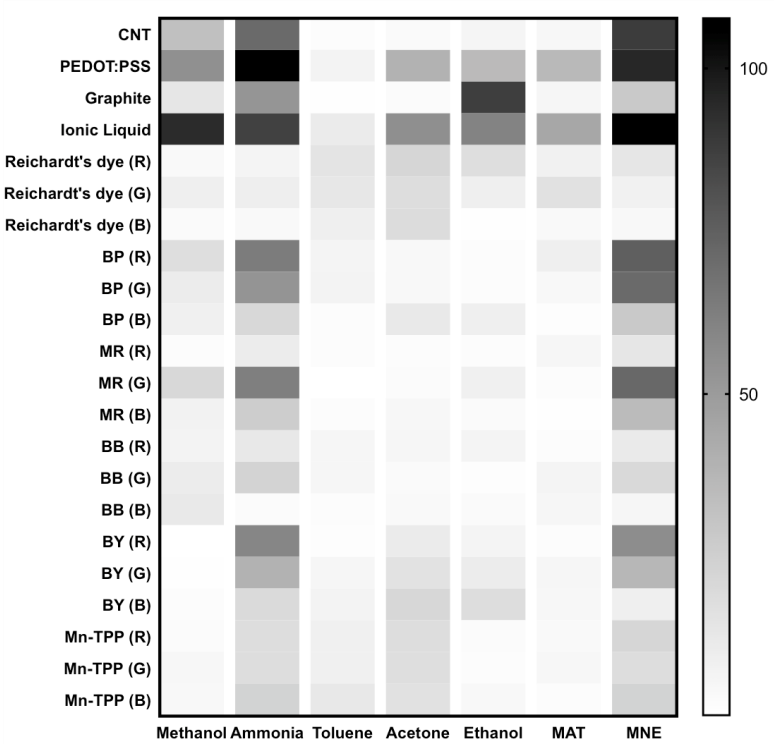

Figure 6.6: the overall responses of optoelectronic sensor arrays towards different gases and gas mixtures. The gray scale represents the absolute amount of change of each sensing element in percentage form (%). BP=bromocresol purple, MR=methyl red, BB=bromothymol blue, BY=brilliant yellow, Mn-TPP= Manganese tetraphenylporphorin.

6.3.3 Classification of sensor responses

Support vector machine (SVM) classifier with linear Kernel function is used to classify the sensor responses to seven different gases and mixtures. As shown in Figure 6.6, one complete set of sensor responses in one measurement is comprised of the R, G, B channel intensities of all optical dyes and the electrical responses (conductance change in %), totally 22 parameters.

To perform SVM classification, eight measurements for each class of gas are selected and trained by SVM classifier. The obtained model for each class is used to test the untrained responses (9 points). Classification is performed on three categories of data: combination of optical and electrical responses, only optical responses and only electrical responses. The

classification results for three categories of data are shown in Table 6.1. It is found that even though the electrical sensor arrays are responding to all gas analytes with different sensitivities, electrical responses alone are not sufficient to distinguish different gases, given the significant number of mismatch points and much higher error rate. Optical sensor arrays alone performed much better than electrical sensors in gas discrimination, with significant lower number of mismatch points and error rate. By combining both optical and electrical responses, higher possibility of error free classification is observed, which shows the improvement of sensor's discriminative power.

Table 6.1: Support vector machine (SVM) classification of sensor responses. There are three categories of classification: classification based on the combination of optical and electrical responses (O+E); classification of optical responses only; classification of electrical responses only.

Number of accurately classified points								Error Rate
Data set	Methanol	Ammonia	Toluene	Acetone	Ethanol	MAT	MNE	
O+E	9/9	9/9	9/9	9/9	9/9	9/9	9/9	0%
Optical	9/9	9/9	9/9	8/9	9/9	9/9	9/9	1.58%
Electrical	9/9	3/9	9/9	9/9	9/9	9/9	5/9	15.87%

6.4 Conclusion

In this work, a paper-based optoelectronic sensor platform with optical and electrical sensor arrays are presented for sensing a number of volatile gases and its mixtures. This sensor platform can simultaneously generate optical and electrical responses when exposed to gas analytes. The collective responses from optical and electrical sensor arrays form a unique signature for each gas analyte. The proposed optoelectronic sensor platform profits from the gas sensitive nature of chemo-responsive dyes and conductive nanomaterials. By

incorporating different categories of sensing materials, selective sensing of each selected gas is achieved. The sensor is built on paper substrate, which effectively simplifies the fabrication process and reduces the fabrication cost. The application of this gas sensor is not limited to the selected gases described here, but can also be extended to many other volatile organic compounds.

For future improvement, the choices of optical dyes and conductive sensing materials can be expanded to extend its application to other gases. The stability of some electrical sensing elements, such as ionic liquid, needs to be improved to achieve better accuracy in the measurement. Better image processing technique and color analyzing models are needed to enhance the sensitivity of optical read-out.

CHAPTER 7

Colorimetric sensing with dye encapsulated microbeads

Objective: The objective of this work is to show the integration of dye-contained microbeads into different sensing platform (PDMS, hydrogel) and its application in health-care related fields.

In the previous chapters, we have discussed the applications of chemo-responsive dyes for colorimetric sensing of dissolved and gaseous analytes. In some of these applications, the chemoresponsive dyes are encapsulated into the ion exchange silica microbeads before being functionalized onto the substrates. The ion exchange silica microbeads are connected to chemoresponsive dyes through ionic bonding. These beads serve as a micro size hydrophobic container for chemoresponsive dyes and effectively prevent dye leakage. In addition, the encapsulation of chemoresponsive dyes into ion-exchange beads has made it easier to transfer the dyes from one substrate to another without significant loss. Based on these merits, it is very promising to apply these dye contained silica microbeads in a variety of applications. In this chapter, we will briefly discuss some work of using these dye contained silica microbeads in a health-care related application.

7.1 Motivation

With increasing market demand of chemical sensors in various applications, such as medical diagnostics and environmental monitoring, there are more requirements on the

stability of sensing elements [1]. The sensor should be built with sensing elements, which are robust enough for real time measurement under different environments without significant degradation on its performance [192][193]. The sensor response should be reversible so that the operator doesn't need to change the sensing elements after one time use.

Many existing sensing technologies have strict restrictions on the sensing conditions and have limited its adaptability when suffering any change in the sensing environment [62]. For example, most of the metal oxide based electronic noses used for gas sensing have some requirement for the sensing environment [62]. A number of parameters, including temperature, pressure, humidity level, need to be simultaneously recorded as an important reference for the final result [194]. Usually, these environmental parameters are strictly controlled to guarantee that the sensing results are reproducible under the same environmental conditions. This vulnerability to environmental change has hindered the potential application of these sensors in a more complicated environment. Moreover, a lot of commercialized health care products, such as urine test strips and pregnancy test strips, are for one-time use and have to be disposed immediately upon use. These sensors are specifically made for one targeted analyte and its functionality cannot be transferred for other applications.

Given the sensitivity and convenience of the currently available techniques, there is still a need to improve the stability of sensing elements to enhance the sensor's compatibility in a varying sensing environment. In our works, we have employed the dye contained silica microbeads as the key sensing elements for different sensor platforms. The proposed sensors are used in health care related fields, such as saliva diagnostics and wound monitoring.

7.2 Colorimetric sensing beads in health care applications

In this section, examples of using dye contained silica microbeads in saliva diagnostics and wound healing are discussed. These dye contained silica microbeads are embedded into different sensing platform with no degradation of its sensing performance. In one example, the dye contained silica microbeads are incorporated with a microfluidic platform to examine the flow of aqueous anaylte. Another example describes a hydrogel fiber with dye-contained silica microbeads used for wound monitoring.

7.2.1 Microfluidic colorimetric sensing platform for saliva diagnostics

In this work, a microfluidic colorimetric sensing platform is proposed for sensing ammonia in aqueous phase at ppm level. Ammonia is an important biomarker in human saliva, the concentration of which can quickly reflect the health status of a person. For example, when there is Helicobacter pylori infection in stomach, the amount of ammonia presented in gastric juice, breath and saliva increases. Comparably, it is easier to examine saliva than gastric juice due to the simplicity in sample collection and preparation. Therefore, a microfluidic sensing platform is built for the purpose of detecting ammonia concentration in saliva.

This microfluidic colorimetric sensing platform is comprised of a microfluidic chamber, arrays of dye-contained microbeads, and optical spectrometer for signal read-out. As shown in Figure 7.1, the microfluidic chamber is made of Polydimethylsiloxane (PDMS), with arrays of micro-wells built at the bottom of chamber to hold the dye-contained sensing beads (Figure 7.1 (b)). The selected chemoresponsive dye is metalloporphyrins. As discussed in Chapter 2, metalloporphyrins contains metal ions and responds to analytes capable of Lewis acid/base interation. Ammonia is considered as a Lewis base, which can donate free electron

pair in solution. Therefore, metalloporphyrins are deemed as a favorable choice for sensing ammonia in aqueous phase. The metalloporphyrins selected here is zinc tetraphenylporphyrin (ZnTPP) dye, which is encapsulated in cation ion exchange microbeads. By utilizing microbeads, ZnTPP dye can be effectively immobilized within the arrays of micro-wells without being washed away by the flow of solutions. The image of the filled micro-we;; arrays is shown in Figure 7.1 (c). Different solutions (DI water, ammonia solution, saliva) are mixed and flowing through the microfluidic chamber through the control of micropumps (Figure 7.1 (a)). The optical responses are generated by illuminating the microfluidic chamber with an external LED source and collect the transmitted light transmitted using a USB spectrometer.

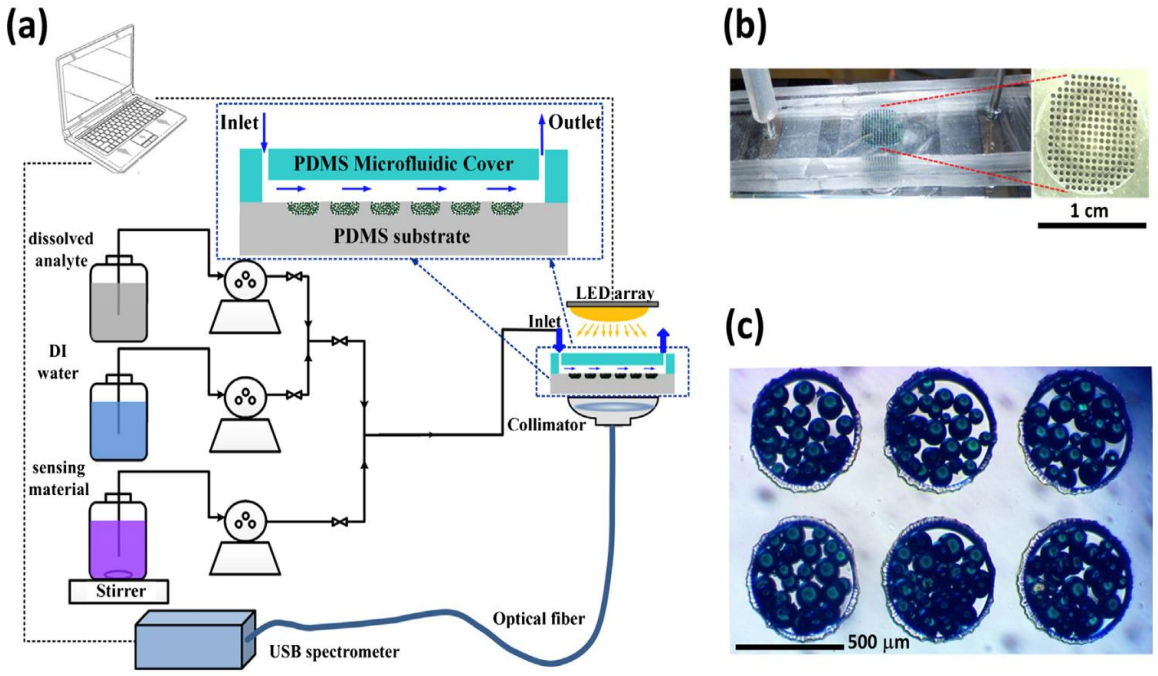

Figure 7.1:(a)Schematic representation of the optical setup and flow system;(b)arrays of Zn(TPP)-encapsulated in microbeads embedded in the microfluidic chamber;(c)micrograph of Zn(TPP)-contained microbeads trapped inside microwells.

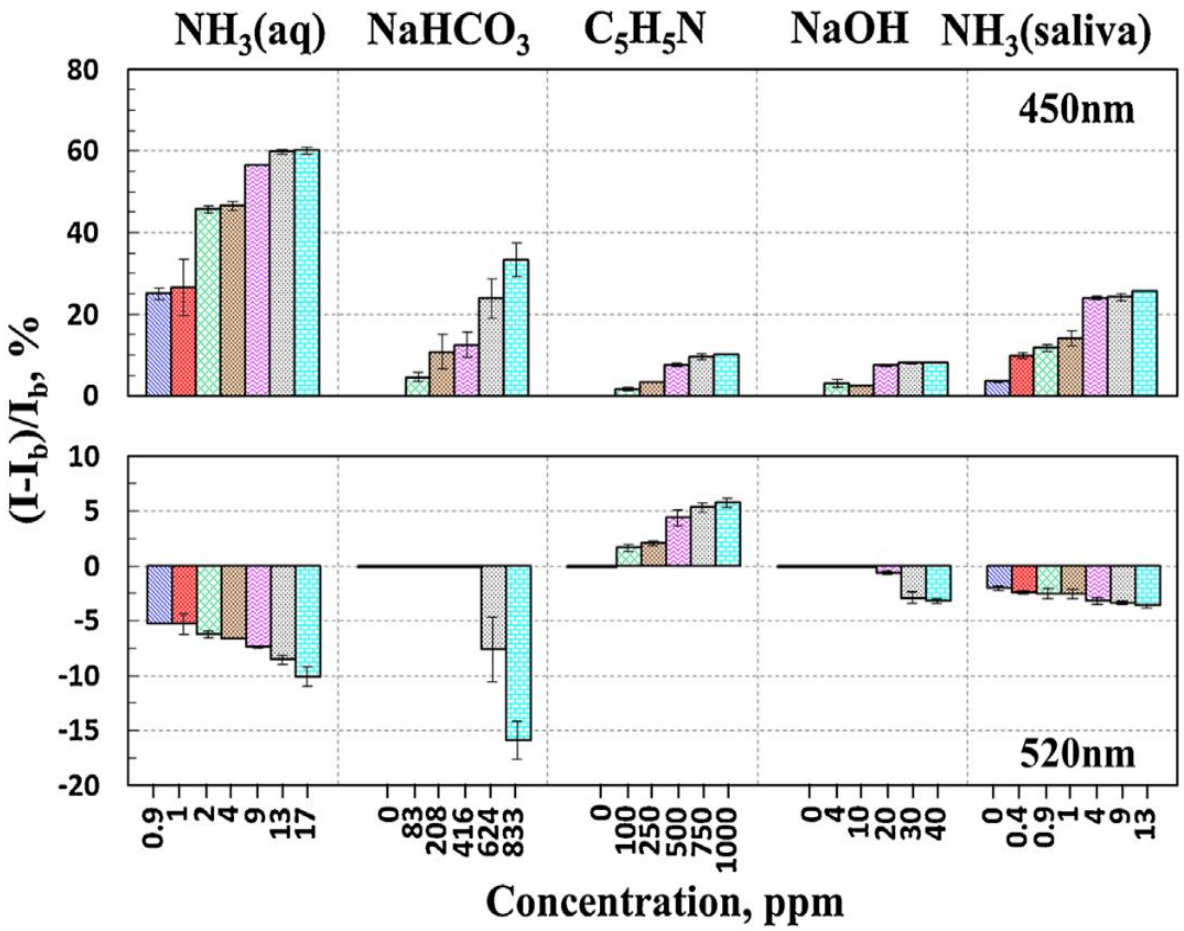

Figure 7.2: Microfluidic sensing platform for sensing ammonia in deionized water, NaHCO3 solution, C5H5N solution, NaOH solution, ammonia in saliva.[124]

In the experiment, the microfluidic colorimetric sensing platform has been tested with different analytes, including dissolved ammonia in deionized (DI) water and dissolved ammonia in saliva, as well as several other bases (NaHCO3, C5H5N, NaOH) in DI water. The sensing results are summarized in Figure 7.2. By comparing the sensor responses to different analytes at two wavelengths in visible spectrum, it is observed that the sensor is highly responsive to aqueous ammonia compared with other basic solutions (NaHCO3,

C5H5N, NaOH), even though those basic solutions are in a much higher concentration. Meanwhile, it is also observed that the sensor's responses to ammonia in saliva exhibit a similar trend as that of ammonia in DI water. These results indicate that ZnTPP microbeads are more sensitive and selective aqueous ammonia compared with other bases, and this sensitivity to ammonia is preserved when it is sensing the ammonia in saliva.

There are several advantages of using this microfluidic colorimetric sensing platform for diagnostics. First, the microfluidic sensing chamber is completely sealed, eliminating the influence from the surrounding environment; second, this sensor platform provide an easy way to mix different solutions, allowing creation of complex analyte; moreover, the microfluidic sensing platform allows functionalization of more than one type of sensing beads; finally, the application of this microfluidic sensing platform is not limited to saliva diagnostics and can be further extended to any application that requires a real time examination of targeted analyte in aqueous phase. The choices of chemoresponsive dyes can be broadened to fulfill of requirement of sensing different analytes.

7.2.2 Hydrogel colorimetric fiber for epidermal pH monitoring

In the previous work, the chemoresponsive dye is impregnated in ion exchange microbeads to prevent being washed away by the flow. These dye-contained microbeads can also be incorporated into the polymer structure for other application. In this work, hydrogel microfibers containing colorimetric microbeads are fabricated for monitoring the pH of skin. These hydrogel microfibers are fabricated by microfluidic spinning method to obtain different sizes. The selected sensing element is a pH indicator (brilliant yellow) encapsulated in anion ion exchange microbeads.

As shown in Figure 7.3, the as-fabricated hydrogel colorimetric fiber are closely aligned and immersed in different pH buffer solutions. The color change of these aligned fibers in these pH buffer solutions is captured by a smart phone camera [195]. These fibers can be made with different diameters and their performances are compared to select the optimal size

Figure 7.3 (a) shows the variation in the color of the hydrogel colorimetric fibers at pH □□6 (yellow) and pH □□8 (red). For characterization, the hydrogel colorimetric fibers were immersed in different pH solutions (pH □□6, 6.5, 7, 7.5, 8, and 9) at room temperature, and photos were taken after 30 min using smart phone camera. To quantify the sensing results, RGB (red, green, blue) channel intensities were extracted from the images of fibers at different pH. Figure 7.3 (b) shows the RGB channel intensities extracted from 800 um microfibers at different pH (ranging from 6.5 to 9). In Figure 7.3 (c), a fitted curve showing the relation between R channel intensity and the actual pH is generated as a reference for future measurement. The results showed continuous RGB intensity change when transferring pH-sensing fibers from one pH solution to another. Figure 7.3 (d) shows the response time of fibers with different diameters. By comparison, the 800 μm fiber showed the fastest response time. We used the extracted RGB intensities as references to generate a formula relating the pH to R channel intensity, which can be used to extract pH value in a real measurement.

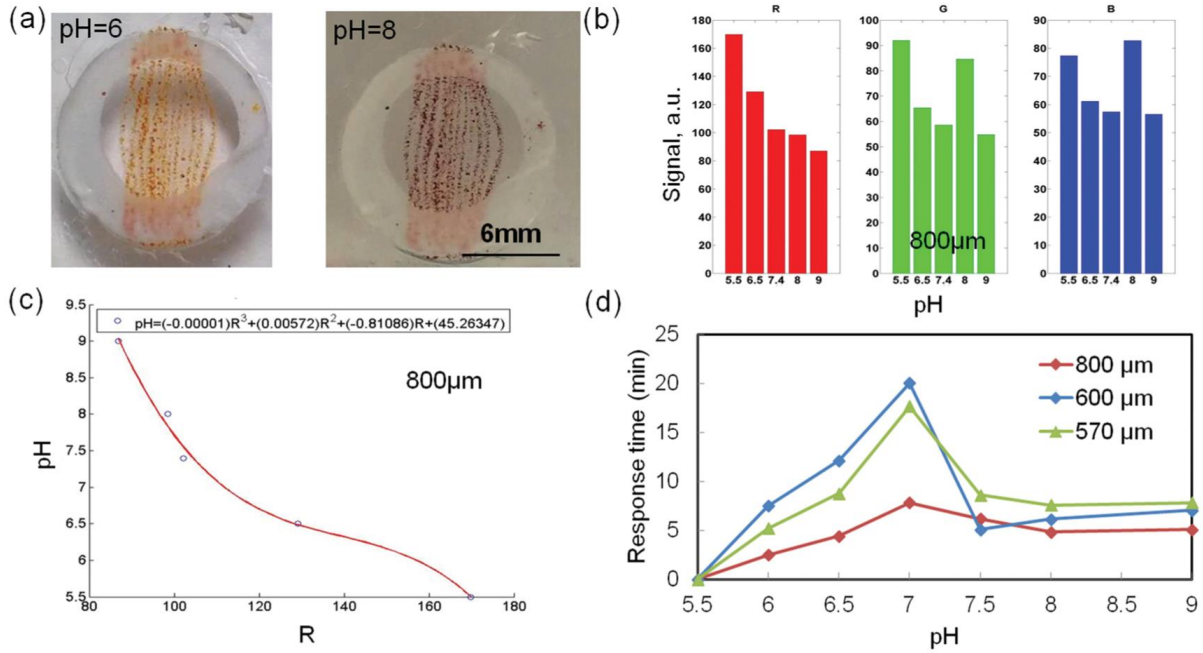

Figure 7.3. Hydrogel colorimetric fiber arrays for pH sensing. (a) Arrays of aligned hydrogel fibers composed of brilliant yellow microbeads at different pH environments (pH=6 and pH=9); (b) Extracted R, G, B information from the image of fiber arrays; (c) Extracted pH formula from the RGB signal in (b); (d) Response time of fibers with different diameters. [195]

In Figure 7.4, the hydrogel colorimetric fibers were attached to a transparent medical tape to create a wearable sensor patch. These sensor patches were placed on a piece of explanted pig skin sprayed with different pH solutions (pH = 5.2, 6.2, 7.2, and 8.2). The photos were taken using a smart phone after 30 min, when the fiber colors were stable. By applying the same procedure of image processing and referring to the fitting curve, the extracted pH values were 5.69, 6.26, 7.38, and 8.13, which were in accord with the actual pH of the pig skin samples (5.2, 6.2, 7.2, and 8.2, respectively) within reasonable error range.

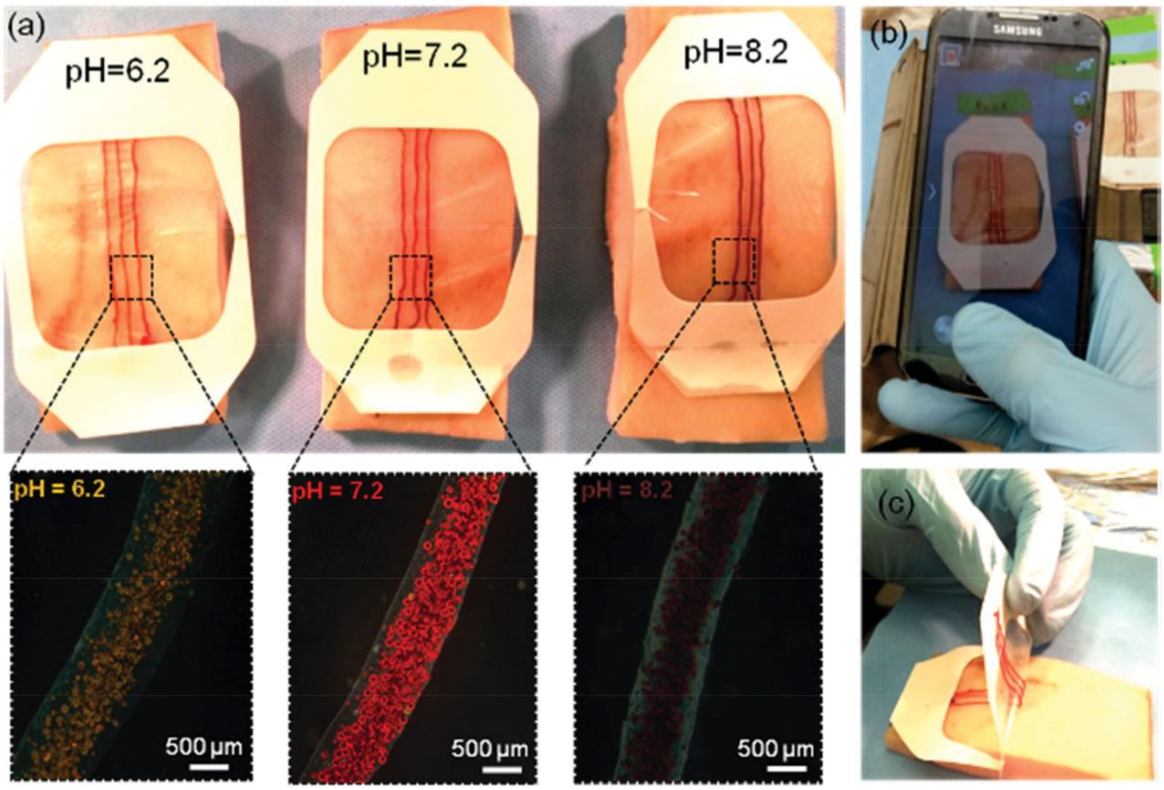

Figure 7.4 Hydrogel colorimetric fibers attached to medical tape to form a wound dressing. (a) As-fabricated wound dressing placed on pig skin to detect the skin pH. Microscope images of hydrogel colorimetric fiber are taken at different pH (b) Smart phone based image capturing; (c) The flexibility of as-fabricated hydrogel colorimetric fibers. [195]

From the experiment, it is shown that these hydrogel colorimetric fibers are flexible and pH responsive. The use of silica mircobeads for dye encapsulation has successfully prevented any dye leakage and allowed the fibers to conformably contact with skin. The fibers can be easily assembled the on a transparent medical tape to form a pH-responsive wound dressing. Images of the pH-sensing fibers during real-time pH measurement were captured with a smart phone camera for on-site readout. Using the same fabrication technique, different types of chemoresponsive dyes can be functionalized into the hydrogel matrix to monitor other parameters during wound dressing, for instance, oxygen concentration, CO2 concentration, etc.

7.3 Summary

In this chapter, we discussed two representative works of using colorimetric sensing beads as the basic sensing elements to build different sensing platform for health care related applications. A microfluidic sensing platform made of PDMS is presented for detecting ammonia concentration in saliva, which has shown high sensitivity (ppm) and good selectivity (among other bases). This sensing platform is adaptable to varying sensing condition and is applicable to detect many other analyte in aqueous phase. The hydrogel colorimetric fiber incorporates dye containing silica microbeads and can be used directly on the skin to monitor the pH of wound. The size of the fiber can be easily tuned during fabrication. For future work, it is very promising to integrate these dye-contained microbeads into different polymer matrix to create flexible, sensitive and robust optical sensors. For these dye-contained microbeads to funcion, it is important to guarantee the direct contact of the analytes and the microbeads during the measurement. Any hydrophilic and gas permeable materials will be the ideal supporting media for these sensing beads.

CHAPTER 8

Conclusions and Future work

8.1 Conclusions

This dissertation discussed several low-cost optoelectronic sensor platforms for gas detection in diverse environments. We have explored the device fabrication process and the performance of sensors under different situations. The aim is to combine the advantages of clean room free fabrication, low-cost substrate material and highly sensitive detection capability of optical dyes, to build a cost effective and highly reproducible platform to realize gas sensing in diverse environments. One of the commonly used substrates in our work is paper, a ubiquitous and inexpensive material. In one work, a paper-based microfluidic platform functionalized with an array of chemo-responsive dyes is built for sensing dissolved ammonia and carbon dioxide. The hydrophobic patterning of paper substrate is realized by applying silicone spray. In another work, a disposable food sensor is made on paper substrate with colorimetric microbeads arrays arranged as geometric barcode to monitor the food spoilage. The sensor is fabricated through a stamping process, which is quite easy and highly reproducible. This barcode sensor is safe to be placed directly on the sample surface without the concern of dye leakage into the food. While paper substrate can be easily functionalized with various chemo-responsive dyes, it can also hold a variety of conductive nano-materials. A paper based optoelectronic platform with optical and electrical sensor arrays for gas sensing is proposed, which combines the sensitivity of chemo-responsive dyes and gas responsive nanomaterials (e.g. CNT, PEDOT:PSS). By combining the optical and electrical

read-outs, a unique cross-reactive response signature can be generated for each gas analyte. The enhancement of sensor's gas discriminative power has been utilized by performing support vector machine (SVM) based classification. The results of classification indicates that the combination of optical and electrical sensor responses generate a much lower error of detection compared to using optical or electrical sensing elements alone.

In addition, different sensors using dye-contained colorimetric microbeads as the key-sensing element are also investigated. We presented an optical fiber based sensor functionalized with colorimetric beads for the detection of gastric gas, which can be integrated into the endoscope system for simultaneously imaging the inner lining of stomach and detecting the gas products. Further more, a microfluidic sensing platform incorporating colorimetric beads is presented for detecting different concentrations of ammonia in saliva, which has shown high sensitivity (ppm) and good selectivity. In another example, a colorimetric beads embedded hydrogel fiber is used directly on the skin to monitor the pH of wound.

All the works discussed here cover the process of sensor design, fabrication and testing and data analysis. All the fabrication techniques described in this dissertation are cost effective and highly reproducible. These works lay the foundation of low cost mass produced gas sensors for applications in environment, food and health.

8.2 Future work

Regardless of the existing progress in exploring cost-effective gas sensors, more effort is still needed to improve to create a more effective sensing platform. We will briefly discuss some aspects of the future works here.

- The choices of substrate materials for building colorimetric sensor arrays can be extended to other low cost materials, for example, thread [196]. Thread naturally preserves an one dimensional (1D) structure. The capillary force allows solution to flow through the thread without any external driving force. It is easier to deposit several sensing elements on one single thread, which can further simplify the fabrication process.
- The choices of chemoresponsive dyes are not limited to those mentioned in this dissertation. The functionality of the sensor platform can be easily tuned by changing the type of optical dyes. Fluorescent dyes can also be incorporated into the sensor platform. These colorimetric sensor platforms can also be applied to detect a variety of gas species and their mixtures.
- Smartphone based optical detection has more advantages in the aspects of portability and user comfort level. However, to reduce the variation due to the difference in smartphone hardware, it is necessary to calibrate the cameras of different smartphone to enhance the accuracy of extracted color information from images taken by smart phone. This will require incorporating smart image processing algorithms into the platform.
- The performance of the sensor platform in this dissertation can be improved by reducing the variation between as-fabricated sensors and enhancing the signal to

noise ratio during measurement. The degree of variation between sensors relies on the uniformity of dye solutions. Techniques like sonication and magnetic stirring can be used to improve the uniformity of dye solution. Signal to noise ratio can be improved by maintaining uniform background illumination and applying better image processing algorithm.

- It is promising to build colorimetric sensor arrays on CMOS as an integrated system for gas sensing and direct signal read-out. The integrated system can effectively solve the interconnect problem and realize miniaturization of the sensor platform. It will also minimize the variations between different sensors and enhance the sensor performance.

PUBLICATIONS

Journal publications

- **Y. Chen**, Y. Zilberman, P. Mostafalu and S. Sonkusale, "Paper based platform for colorimeteric sensing of dissolved NH_3 and CO_2", Biosensors and Bioelectronics, 2014
- Y. Zilberman, **Y. Chen** and S. Sonkusale, "Dissolved ammonia sensing in complex mixtures using metalloporphyrin-based optoelectronic sensor and hyperspectral detection", Sensors and Actuators B: Chemical, 2014
- **Yu Chen**, Yael Zilberman, Shideh Kabiri, W. Jong Yoon, John-John Cabibihan, Sameer Sonkusale, "A flexible gastric gas sensor based on functionalized optical fiber", IEEE Sensors Journal, 2016
- Ali Tamayol, Mohsen Akbari, Yael Zilberman, Mattia Comotto, Emal Lesha, Ludovic Serex, Sara Bagherifard, **Yu Chen**, Guoqing Fu, Shideh Kabiri Ameri, Weitong Ruan, Eric L. Miller, Mehmet R. Dokmeci, Sameer Sonkusale, Ali Khademhosseni, "Flexible pH-Sensing Hydrogel Fibers for Epidermal Applications", Advanced Healthcare Materials, 2016
- Nuno M Oliveira, Yu Shrike Zhang, Jie Ju, Ai-Zheng Chen, **Yu Chen**, Sameer R Sonkusale, Mehmet Dokmeci, Rui L Reis, João F Mano, Ali Khademhosseini, "Hydrophobic hydrogel: towards construction of floating (bio) microdevices", Chemistry of Materials, 2016
- **Yu Chen**, Guoqing Fu, Yael Zilberman, Weitong Ruan, Shideh Kabiri Ameri, Yu Shrike Zhang, Eric Miller, Sameer Sonkusale, "Low cost smartphone diagnostics for food ", Food Control, 2017

- **Yu Chen,** Sameer Sonkusale, “Paper-based combined optical and electronic nose platform for robust detection of volatile gases” (in preparation)

Conferences and meetings

- **Yu Chen**, Y. Zilberman, P. Mostafalu and S. Sonkusale, “Colorimetric Sensing of Dissolved Gases on Paper Based Microfluidic Platform”, Material Research Society (MRS) Fall Meeting 2014
- **Y. Chen**, Y. Zilberman, S. Sonkusale, “Paper based platform for colorimetric sensing of ammonia and CO_2”, World Congress on Biosensors, (Biosensors) May 2014
- Pengxiang Hu**, Yu Chen,** Sameer Sonkusale, “Low cost spectrometer accessory for cell phone based optical sensor”, IEEE Virtual Conference on Applications of Commercial Sensors (VCACS), 2015
- **Yu Chen**, Shideh Kabiri Ameri and S. Sonkusale, “Highly stretchable low-cost strain sensor for human motion sensing”, The 38th Annual International Conference of the IEEE Engineering in Medicine and Biology Society (EMBC) 2016
- **Yu Chen**, Guoqing Fu, Yael Zilberman, Weitong Ruan, Shideh Kabiri Ameri, Eric Miller, Sameer Sonkusale, “ Disposable colorimetric geometric barcode sensor for food quality monitoring”, Transducers, 2017

REFERENCES

[1] N. Yamazoe, “Toward innovations of gas sensor technology,” *Sens. Actuators B Chem.*, vol. 108, no. 1–2, pp. 2–14, Jul. 2005.

[2] J. Jang and J. Bae, “Carbon nanofiber/polypyrrole nanocable as toxic gas sensor,” *Sens. Actuators B Chem.*, vol. 122, no. 1, pp. 7–13, Mar. 2007.

[3] E. Llobet, J. Brezmes, X. Vilanova, J. E. Sueiras, and X. Correig, “Qualitative and quantitative analysis of volatile organic compounds using transient and steady-state responses of a thick-film tin oxide gas sensor array,” *Sens. Actuators B Chem.*, vol. 41, no. 1, pp. 13–21, Jun. 1997.

[4] M. Phillips *et al.*, “Volatile organic compounds in breath as markers of lung cancer: a cross-sectional study,” *The Lancet*, vol. 353, no. 9168, pp. 1930–1933, Jun. 1999.

[5] M. Shirasu and K. Touhara, “The scent of disease: volatile organic compounds of the human body related to disease and disorder,” *J. Biochem. (Tokyo)*, vol. 150, no. 3, pp. 257–266, Sep. 2011.

[6] C. Di Natale *et al.*, “An electronic nose for food analysis,” *Sens. Actuators B Chem.*, vol. 44, no. 1–3, pp. 521–526, Oct. 1997.

[7] S. Ampuero and J. O. Bosset, “The electronic nose applied to dairy products: a review,” *Sens. Actuators B Chem.*, vol. 94, no. 1, pp. 1–12, Aug. 2003.

[8] S. Panigrahi, S. Balasubramanian, H. Gu, C. M. Logue, and M. Marchello, “Design and development of a metal oxide based electronic nose for spoilage classification of beef,” *Sens. Actuators B Chem.*, vol. 119, no. 1, pp. 2–14, Nov. 2006.

[9] A. Marsal, G. Dezanneau, A. Cornet, and J. R. Morante, “A new CO2 gas sensing material,” *Sens. Actuators B Chem.*, vol. 95, no. 1–3, pp. 266–270, Oct. 2003.

[10] E. R. Leite, I. T. Weber, E. Longo, and J. A. Varela, “A New Method to Control Particle Size and Particle Size Distribution of SnO2 Nanoparticles for Gas Sensor Applications,” *Adv. Mater.*, vol. 12, no. 13, pp. 965–968, Jun. 2000.

[11] G. Lu, L. E. Ocola, and J. Chen, “Room-Temperature Gas Sensing Based on Electron Transfer between Discrete Tin Oxide Nanocrystals and Multiwalled Carbon Nanotubes,” *Adv. Mater.*, vol. 21, no. 24, pp. 2487–2491, Jun. 2009.

[12] B. Timmer, W. Olthuis, and A. van den Berg, “Ammonia sensors and their applications—a review,” *Sens. Actuators B Chem.*, vol. 107, no. 2, pp. 666–677, Jun. 2005.

[13] N. E. Barbri *et al.*, “An electronic nose system based on a micro-machined gas sensor array to assess the freshness of sardines,” *Sens. Actuators B Chem.*, vol. 141, no. 2, pp. 538–543, Sep. 2009.

[14] S. J. Vella *et al.*, “Measuring Markers of Liver Function Using a Micro-Patterned Paper Device Designed for Blood from a Fingerstick,” *Anal. Chem.*, vol. 84, no. 6, pp. 2883–2891, Mar. 2012.

[15] V. Demarne and A. Grisel, “An integrated low-power thin-film CO gas sensor on silicon,” *Sens. Actuators*, vol. 13, no. 4, pp. 301–313, Apr. 1988.

[16] J. Wöllenstein *et al.*, “Cobalt oxide based gas sensors on silicon substrate for operation at low temperatures,” *Sens. Actuators B Chem.*, vol. 93, no. 1–3, pp. 442–448, Aug. 2003.

[17] J. M. Baik, M. Zielke, M. H. Kim, K. L. Turner, A. M. Wodtke, and M. Moskovits, "Tin-Oxide-Nanowire-Based Electronic Nose Using Heterogeneous Catalysis as a Functionalization Strategy," *ACS Nano*, vol. 4, no. 6, pp. 3117–3122, Jun. 2010.
[18] J. Hu, K. Xu, Y. Jia, Y. Lv, Y. Li, and X. Hou, "Oxidation of Ethyl Ether on Borate Glass: Chemiluminescence, Mechanism, and Development of a Sensitive Gas Sensor," *Anal. Chem.*, vol. 80, no. 21, pp. 7964–7969, Nov. 2008.
[19] A. Oprea, J. Courbat, N. Bârsan, D. Briand, N. F. de Rooij, and U. Weimar, "Temperature, humidity and gas sensors integrated on plastic foil for low power applications," *Sens. Actuators B Chem.*, vol. 140, no. 1, pp. 227–232, Jun. 2009.
[20] F. Zee and J. W. Judy, "Micromachined polymer-based chemical gas sensor array," *Sens. Actuators B Chem.*, vol. 72, no. 2, pp. 120–128, Jan. 2001.
[21] M. Singh, H. M. Haverinen, P. Dhagat, and G. E. Jabbour, "Inkjet Printing—Process and Its Applications," *Adv. Mater.*, vol. 22, no. 6, pp. 673–685, Feb. 2010.
[22] J. Suehiro *et al.*, "Schottky-type response of carbon nanotube NO2 gas sensor fabricated onto aluminum electrodes by dielectrophoresis," *Sens. Actuators B Chem.*, vol. 114, no. 2, pp. 943–949, Apr. 2006.
[23] Z. Gu, Y. Xu, and K. Gao, "Optical fiber long-period grating with solgel coating for gas sensor," *Opt. Lett.*, vol. 31, no. 16, pp. 2405–2407, Aug. 2006.
[24] O. S. Wolfbeis, "Fiber-Optic Chemical Sensors and Biosensors," *Anal. Chem.*, vol. 80, no. 12, pp. 4269–4283, Jun. 2008.
[25] C. McDonagh, C. S. Burke, and B. D. MacCraith, "Optical Chemical Sensors," *Chem. Rev.*, vol. 108, no. 2, pp. 400–422, Feb. 2008.
[26] W. Dungchai, O. Chailapakul, and C. S. Henry, "Electrochemical Detection for Paper-Based Microfluidics," *Anal. Chem.*, vol. 81, no. 14, pp. 5821–5826, Jul. 2009.
[27] J. Lankelma, Z. Nie, E. Carrilho, and G. M. Whitesides, "Paper-Based Analytical Device for Electrochemical Flow-Injection Analysis of Glucose in Urine," *Anal. Chem.*, vol. 84, no. 9, pp. 4147–4152, May 2012.
[28] E. Carrilho, A. W. Martinez, and G. M. Whitesides, "Understanding Wax Printing: A Simple Micropatterning Process for Paper-Based Microfluidics," *Anal. Chem.*, vol. 81, no. 16, pp. 7091–7095, Aug. 2009.
[29] S. M. Z. Hossain, R. E. Luckham, M. J. McFadden, and J. D. Brennan, "Reagentless Bidirectional Lateral Flow Bioactive Paper Sensors for Detection of Pesticides in Beverage and Food Samples," *Anal. Chem.*, vol. 81, no. 21, pp. 9055–9064, Nov. 2009.
[30] J. L. Delaney, C. F. Hogan, J. Tian, and W. Shen, "Electrogenerated Chemiluminescence Detection in Paper-Based Microfluidic Sensors," *Anal. Chem.*, vol. 83, no. 4, pp. 1300–1306, Feb. 2011.
[31] W. Zhao, M. M. Ali, S. D. Aguirre, M. A. Brook, and Y. Li, "Paper-Based Bioassays Using Gold Nanoparticle Colorimetric Probes," *Anal. Chem.*, vol. 80, no. 22, pp. 8431–8437, Nov. 2008.
[32] N. Yamazoe and K. Shimanoe, "New perspectives of gas sensor technology," *Sens. Actuators B Chem.*, vol. 138, no. 1, pp. 100–107, Apr. 2009.
[33] A. B. Littlewood, *Gas Chromatography: Principles, Techniques, and Applications*. Elsevier, 2013.
[34] C. de Julián Fernández *et al.*, "Surface plasmon resonance optical gas sensing of nanostructured ZnO films," *Sens. Actuators B Chem.*, vol. 130, no. 1, pp. 531–537, Mar. 2008.

[35] H. Wohltjen, “Mechanism of operation and design considerations for surface acoustic wave device vapour sensors,” *Sens. Actuators*, vol. 5, no. 4, pp. 307–325, Jul. 1984.
[36] A. V. Shevade, M. A. Ryan, M. L. Homer, A. M. Manfreda, H. Zhou, and K. S. Manatt, “Molecular modeling of polymer composite–analyte interactions in electronic nose sensors,” *Sens. Actuators B Chem.*, vol. 93, no. 1–3, pp. 84–91, Aug. 2003.
[37] K. Saetia *et al.*, “Spray-Layer-by-Layer Carbon Nanotube/Electrospun Fiber Electrodes for Flexible Chemiresistive Sensor Applications,” *Adv. Funct. Mater.*, vol. 24, no. 4, pp. 492–502, Jan. 2014.
[38] K. S. Suslick, “An Optoelectronic Nose:‘Seeing’ Smells by Means of Colorimetric Sensor Arrays,” *MRS Bull.*, vol. 29, no. 10, pp. 720–725, Oct. 2004.
[39] M. C. Janzen, J. B. Ponder, D. P. Bailey, C. K. Ingison, and K. S. Suslick, “Colorimetric Sensor Arrays for Volatile Organic Compounds,” *Anal. Chem.*, vol. 78, no. 11, pp. 3591–3600, Jun. 2006.
[40] J. W. Kemling and K. S. Suslick, “Nanoscale porosity in pigments for chemical sensing,” *Nanoscale*, vol. 3, no. 5, pp. 1971–1973, 2011.
[41] K. S. Suslick *et al.*, “Seeing smells: development of an optoelectronic nose,” *Quím. Nova*, vol. 30, no. 3, pp. 677–681, Jun. 2007.
[42] N. A. Rakow and K. S. Suslick, “A colorimetric sensor array for odour visualization,” *Nature*, vol. 406, no. 6797, pp. 710–713, Aug. 2000.
[43] J. R. Askim, M. Mahmoudi, and K. S. Suslick, “Optical sensor arrays for chemical sensing: the optoelectronic nose,” *Chem. Soc. Rev.*, vol. 42, no. 22, pp. 8649–8682, 2013.
[44] L. Ding, Z. Zhang, X. Li, and J. Su, “Highly sensitive determination of low-level water content in organic solvents using novel solvatochromic dyes based on thioxanthone,” *Chem. Commun.*, vol. 49, no. 66, pp. 7319–7321, 2013.
[45] L. Feng, C. J. Musto, J. W. Kemling, S. H. Lim, W. Zhong, and K. S. Suslick, “Colorimetric Sensor Array for Determination and Identification of Toxic Industrial Chemicals,” *Anal. Chem.*, vol. 82, no. 22, pp. 9433–9440, Nov. 2010.
[46] N. A. Rakow, A. Sen, M. C. Janzen, J. B. Ponder, and K. S. Suslick, “Molecular Recognition and Discrimination of Amines with a Colorimetric Array,” *Angew. Chem. Int. Ed.*, vol. 44, no. 29, pp. 4528–4532, Jul. 2005.
[47] J. Kesselmeier and M. Staudt, “Biogenic Volatile Organic Compounds (VOC): An Overview on Emission, Physiology and Ecology,” *J. Atmospheric Chem.*, vol. 33, no. 1, pp. 23–88, May 1999.
[48] X. Xu *et al.*, “Comprehensive two-dimensional gas chromatography (GC × GC) measurements of volatile organic compounds in the atmosphere,” *Atmos Chem Phys*, vol. 3, no. 3, pp. 665–682, Jun. 2003.
[49] A. K. Srivastava, “Detection of volatile organic compounds (VOCs) using SnO2 gas-sensor array and artificial neural network,” *Sens. Actuators B Chem.*, vol. 96, no. 1–2, pp. 24–37, Nov. 2003.
[50] P. J. Mazzone *et al.*, “Exhaled Breath Analysis with a Colorimetric Sensor Array for the Identification and Characterization of Lung Cancer,” *J. Thorac. Oncol. Off. Publ. Int. Assoc. Study Lung Cancer*, vol. 7, no. 1, pp. 137–142, Jan. 2012.
[51] Z. Li, M. Jang, J. R. Askim, and K. S. Suslick, “Identification of accelerants, fuels and post-combustion residues using a colorimetric sensor array,” *Analyst*, vol. 140, no. 17, pp. 5929–5935, 2015.

[52] S. H. Lim, L. Feng, J. W. Kemling, C. J. Musto, and K. S. Suslick, "An optoelectronic nose for the detection of toxic gases," *Nat. Chem.*, vol. 1, no. 7, pp. 562–567, Oct. 2009.
[53] L. Feng, C. J. Musto, J. W. Kemling, S. H. Lim, and K. S. Suslick, "A colorimetric sensor array for identification of toxic gases below permissible exposure limits," *Chem. Commun.*, vol. 46, no. 12, p. 2037, 2010.
[54] S. H. Lim, J. W. Kemling, L. Feng, and K. S. Suslick, "A colorimetric sensor array of porous pigments," *Analyst*, vol. 134, no. 12, pp. 2453–2457, 2009.
[55] C. Zhang and K. S. Suslick, "Colorimetric Sensor Array for Soft Drink Analysis," *J. Agric. Food Chem.*, vol. 55, no. 2, pp. 237–242, Jan. 2007.
[56] C. J. Musto, S. H. Lim, and K. S. Suslick, "Colorimetric Detection and Identification of Natural and Artificial Sweeteners," *Anal. Chem.*, vol. 81, no. 15, pp. 6526–6533, Aug. 2009.
[57] B. A. Suslick, L. Feng, and K. S. Suslick, "Discrimination of Complex Mixtures by a Colorimetric Sensor Array: Coffee Aromas," *Anal. Chem.*, vol. 82, no. 5, pp. 2067–2073, Mar. 2010.
[58] N. Nath and A. Chilkoti, "A Colorimetric Gold Nanoparticle Sensor To Interrogate Biomolecular Interactions in Real Time on a Surface," *Anal. Chem.*, vol. 74, no. 3, pp. 504–509, Feb. 2002.
[59] I. Avrutsky, K. Chaganti, I. Salakhutdinov, and G. Auner, "Concept of a miniature optical spectrometer using integrated optical and micro-optical components," *Appl. Opt.*, vol. 45, no. 30, pp. 7811–7817, Oct. 2006.
[60] N. Lopez-Ruiz *et al.*, "Smartphone-Based Simultaneous pH and Nitrite Colorimetric Determination for Paper Microfluidic Devices," *Anal. Chem.*, vol. 86, no. 19, pp. 9554–9562, Oct. 2014.
[61] J. H. Bang, S. H. Lim, E. Park, and K. S. Suslick, "Chemically Responsive Nanoporous Pigments: Colorimetric Sensor Arrays and the Identification of Aliphatic Amines," *Langmuir ACS J. Surf. Colloids*, vol. 24, no. 22, pp. 13168–13172, Nov. 2008.
[62] J. W. Gardner and P. N. Bartlett, "A brief history of electronic noses," *Sens. Actuators B Chem.*, vol. 18, no. 1, pp. 210–211, Mar. 1994.
[63] A. A. Tomchenko, G. P. Harmer, B. T. Marquis, and J. W. Allen, "Semiconducting metal oxide sensor array for the selective detection of combustion gases," *Sens. Actuators B Chem.*, vol. 93, no. 1–3, pp. 126–134, Aug. 2003.
[64] F. Röck, N. Barsan, and U. Weimar, "Electronic Nose: Current Status and Future Trends," *Chem. Rev.*, vol. 108, no. 2, pp. 705–725, Feb. 2008.
[65] R. K. Paul, S. Badhulika, N. M. Saucedo, and A. Mulchandani, "Graphene nanomesh as highly sensitive chemiresistor gas sensor," *Anal. Chem.*, vol. 84, no. 19, pp. 8171–8178, Oct. 2012.
[66] M. Penza, R. Rossi, M. Alvisi, G. Cassano, and E. Serra, "Functional characterization of carbon nanotube networked films functionalized with tuned loading of Au nanoclusters for gas sensing applications," *Sens. Actuators B Chem.*, vol. 140, no. 1, pp. 176–184, Jun. 2009.
[67] C. L. Aravinda, S. Cosnier, W. Chen, N. V. Myung, and A. Mulchandani, "Label-free detection of cupric ions and histidine-tagged proteins using single poly(pyrrole)-NTA chelator conducting polymer nanotube chemiresistive sensor," *Biosens. Bioelectron.*, vol. 24, no. 5, pp. 1451–1455, Jan. 2009.

[68] D. K. Aswal and S. K. Gupta, *Science and Technology of Chemiresistor Gas Sensors*. Nova Publishers, 2007.
[69] N. Ramgir *et al.*, "Metal oxide nanowires for chemiresistive gas sensors: Issues, challenges and prospects," *Colloids Surf. Physicochem. Eng. Asp.*, vol. 439, pp. 101–116, Dec. 2013.
[70] E. Comini *et al.*, "Metal oxide nanoscience and nanotechnology for chemical sensors," *Sens. Actuators B Chem.*, vol. 179, pp. 3–20, Mar. 2013.
[71] E. Llobet, "Gas sensors using carbon nanomaterials: A review," *Sens. Actuators B Chem.*, vol. 179, pp. 32–45, Mar. 2013.
[72] J. Janata and M. Josowicz, "Conducting polymers in electronic chemical sensors," *Nat. Mater.*, vol. 2, no. 1, pp. 19–24, Jan. 2003.
[73] H. G. Moon *et al.*, "Chemiresistive Electronic Nose toward Detection of Biomarkers in Exhaled Breath," *ACS Appl. Mater. Interfaces*, vol. 8, no. 32, pp. 20969–20976, Aug. 2016.
[74] S. MacNaughton, S. Ammu, S. K. Manohar, and S. Sonkusale, "High-Throughput Heterogeneous Integration of Diverse Nanomaterials on a Single Chip for Sensing Applications," *PLOS ONE*, vol. 9, no. 10, p. e111377, Oct. 2014.
[75] E. Westenbrink *et al.*, "Development and application of a new electronic nose instrument for the detection of colorectal cancer," *Biosens. Bioelectron.*, vol. 67, pp. 733–738, May 2015.
[76] W. Yang, P. Wan, M. Jia, J. Hu, Y. Guan, and L. Feng, "A novel electronic nose based on porous In2O3 microtubes sensor array for the discrimination of VOCs," *Biosens. Bioelectron.*, vol. 64, pp. 547–553, Feb. 2015.
[77] S. Hwang *et al.*, "A near single crystalline TiO 2 nanohelix array: enhanced gas sensing performance and its application as a monolithically integrated electronic nose," *Analyst*, vol. 138, no. 2, pp. 443–450, 2013.
[78] B. D. Lampson, Y. J. Han, A. Khalilian, J. K. Greene, D. C. Degenhardt, and J. O. Hallstrom, "Development of a portable electronic nose for detection of pests and plant damage," *Comput. Electron. Agric.*, vol. 108, pp. 87–94, Oct. 2014.
[79] P.-G. Su and Y.-T. Peng, "Fabrication of a room-temperature H2S gas sensor based on PPy/WO3 nanocomposite films by in-situ photopolymerization," *Sens. Actuators B Chem.*, vol. 193, pp. 637–643, Mar. 2014.
[80] V. Talwar, O. Singh, and R. C. Singh, "ZnO assisted polyaniline nanofibers and its application as ammonia gas sensor," *Sens. Actuators B Chem.*, vol. 191, pp. 276–282, Feb. 2014.
[81] J. Qi, X. Xu, X. Liu, and K. T. Lau, "Fabrication of textile based conductometric polyaniline gas sensor," *Sens. Actuators B Chem.*, vol. 202, pp. 732–740, Oct. 2014.
[82] Y. Yang, S. Li, W. Yang, W. Yuan, J. Xu, and Y. Jiang, "In Situ Polymerization Deposition of Porous Conducting Polymer on Reduced Graphene Oxide for Gas Sensor," *ACS Appl. Mater. Interfaces*, vol. 6, no. 16, pp. 13807–13814, Aug. 2014.
[83] E. Espid and F. Taghipour, "Development of highly sensitive ZnO/In2O3 composite gas sensor activated by UV-LED," *Sens. Actuators B Chem.*, vol. 241, pp. 828–839, Mar. 2017.
[84] D. Zhang, A. Liu, H. Chang, and B. Xia, "Room-temperature high-performance acetone gas sensor based on hydrothermal synthesized SnO 2 -reduced graphene oxide hybrid composite," *RSC Adv.*, vol. 5, no. 4, pp. 3016–3022, 2015.

[85] X. Yang *et al.*, "Fabrication of highly sensitive gas sensor based on Au functionalized WO3 composite nanofibers by electrospinning," *Sens. Actuators B Chem.*, vol. 220, pp. 1112–1119, Dec. 2015.
[86] J. Liu *et al.*, "Highly sensitive and low detection limit of ethanol gas sensor based on hollow ZnO/SnO2 spheres composite material," *Sens. Actuators B Chem.*, vol. 245, pp. 551–559, Jun. 2017.
[87] G. Peng *et al.*, "Diagnosing lung cancer in exhaled breath using gold nanoparticles," *Nat. Nanotechnol.*, vol. 4, no. 10, pp. 669–673, Oct. 2009.
[88] B. Wang, J. C. Cancilla, J. S. Torrecilla, and H. Haick, "Artificial Sensing Intelligence with Silicon Nanowires for Ultraselective Detection in the Gas Phase," *Nano Lett.*, vol. 14, no. 2, pp. 933–938, Feb. 2014.
[89] G. Peng *et al.*, "Detection of lung, breast, colorectal, and prostate cancers from exhaled breath using a single array of nanosensors," *Br. J. Cancer*, vol. 103, no. 4, pp. 542–551, Aug. 2010.
[90] F. Patolsky, G. Zheng, and C. M. Lieber, "Fabrication of silicon nanowire devices for ultrasensitive, label-free, real-time detection of biological and chemical species," *Nat. Protoc.*, vol. 1, no. 4, pp. 1711–1724, Nov. 2006.
[91] Y. Paska, T. Stelzner, S. Christiansen, and H. Haick, "Enhanced Sensing of Nonpolar Volatile Organic Compounds by Silicon Nanowire Field Effect Transistors," *ACS Nano*, vol. 5, no. 7, pp. 5620–5626, Jul. 2011.
[92] C. Di Natale *et al.*, "Electronic nose and electronic tongue integration for improved classification of clinical and food samples," *Sens. Actuators B Chem.*, vol. 64, no. 1–3, pp. 15–21, Jun. 2000.
[93] W. Ping, T. Yi, X. Haibao, and S. Farong, "A novel method for diabetes diagnosis based on electronic nose1," *Biosens. Bioelectron.*, vol. 12, no. 9–10, pp. 1031–1036, Nov. 1997.
[94] R. E. Baby, M. Cabezas, and E. N. Walsöe de Reca, "Electronic nose: a useful tool for monitoring environmental contamination," *Sens. Actuators B Chem.*, vol. 69, no. 3, pp. 214–218, Oct. 2000.
[95] H. V. Shurmer and J. W. Gardner, "Odour discrimination with an electronic nose," *Sens. Actuators B Chem.*, vol. 8, no. 1, pp. 1–11, Apr. 1992.
[96] C. Wongchoosuk, A. Wisitsoraat, A. Tuantranont, and T. Kerdcharoen, "Portable electronic nose based on carbon nanotube-SnO2 gas sensors and its application for detection of methanol contamination in whiskeys," *Sens. Actuators B Chem.*, vol. 147, no. 2, pp. 392–399, Jun. 2010.
[97] V. V. Sysoev, B. K. Button, K. Wepsiec, S. Dmitriev, and A. Kolmakov, "Toward the Nanoscopic 'Electronic Nose': Hydrogen vs Carbon Monoxide Discrimination with an Array of Individual Metal Oxide Nano- and Mesowire Sensors," *Nano Lett.*, vol. 6, no. 8, pp. 1584–1588, Aug. 2006.
[98] J. Tamaki, C. Naruo, Y. Yamamoto, and M. Matsuoka, "Sensing properties to dilute chlorine gas of indium oxide based thin film sensors prepared by electron beam evaporation," *Sens. Actuators B Chem.*, vol. 83, no. 1–3, pp. 190–194, Mar. 2002.
[99] J. Suehiro, G. Zhou, H. Imakiire, W. Ding, and M. Hara, "Controlled fabrication of carbon nanotube NO2 gas sensor using dielectrophoretic impedance measurement," *Sens. Actuators B Chem.*, vol. 108, no. 1–2, pp. 398–403, Jul. 2005.

[100] S. H. Ko, H. Pan, C. P. Grigoropoulos, C. K. Luscombe, J. M. J. Fréchet, and D. Poulikakos, "All-inkjet-printed flexible electronics fabrication on a polymer substrate by low-temperature high-resolution selective laser sintering of metal nanoparticles," *Nanotechnology*, vol. 18, no. 34, p. 345202, 2007.
[101] M. K. LaGasse, J. M. Rankin, J. R. Askim, and K. S. Suslick, "Colorimetric sensor arrays: Interplay of geometry, substrate and immobilization," *Sens. Actuators B Chem.*, vol. 197, pp. 116–122, Jul. 2014.
[102] A. Sen, J. D. Albarella, J. R. Carey, P. Kim, and W. B. McNamara III, "Low-cost colorimetric sensor for the quantitative detection of gaseous hydrogen sulfide," *Sens. Actuators B Chem.*, vol. 134, no. 1, pp. 234–237, Aug. 2008.
[103] Y. Wu, N. Na, S. Zhang, X. Wang, D. Liu, and X. Zhang, "Discrimination and Identification of Flavors with Catalytic Nanomaterial-Based Optical Chemosensor Array," *Anal. Chem.*, vol. 81, no. 3, pp. 961–966, Feb. 2009.
[104] S. Deshmukh, R. Bandyopadhyay, N. Bhattacharyya, R. A. Pandey, and A. Jana, "Application of electronic nose for industrial odors and gaseous emissions measurement and monitoring – An overview," *Talanta*, vol. 144, pp. 329–340, Nov. 2015.
[105] A. Berliner *et al.*, "A patterned colorimetric sensor array for rapid detection of TNT at ppt level," *RSC Adv.*, vol. 4, no. 21, pp. 10672–10675, 2014.
[106] B. P. J. de Lacy Costello, R. J. Ewen, N. Guernion, and N. M. Ratcliffe, "Highly sensitive mixed oxide sensors for the detection of ethanol," *Sens. Actuators B Chem.*, vol. 87, no. 1, pp. 207–210, Nov. 2002.
[107] O. Seok Kwon, S. Joo Park, H. Yoon, and J. Jang, "Highly sensitive and selective chemiresistive sensors based on multidimensional polypyrrole nanotubes," *Chem. Commun.*, vol. 48, no. 85, pp. 10526–10528, 2012.
[108] F. Wang, H. Gu, and T. M. Swager, "Carbon Nanotube/Polythiophene Chemiresistive Sensors for Chemical Warfare Agents," *J. Am. Chem. Soc.*, vol. 130, no. 16, pp. 5392–5393, Apr. 2008.
[109] J. R. Carey *et al.*, "Rapid Identification of Bacteria with a Disposable Colorimetric Sensing Array," *J. Am. Chem. Soc.*, vol. 133, no. 19, pp. 7571–7576, May 2011.
[110] M.-Y. Jia, Q.-S. Wu, H. Li, Y. Zhang, Y.-F. Guan, and L. Feng, "The calibration of cellphone camera-based colorimetric sensor array and its application in the determination of glucose in urine," *Biosens. Bioelectron.*, vol. 74, pp. 1029–1037, Dec. 2015.
[111] P. Kim *et al.*, "Towards the development of a portable device for the monitoring of gaseous toxic industrial chemicals based on a chemical sensor array," *Sens. Actuators B Chem.*, vol. 134, no. 1, pp. 307–312, Aug. 2008.
[112] A. D. Wilson and M. Baietto, "Applications and Advances in Electronic-Nose Technologies," *Sensors*, vol. 9, no. 7, pp. 5099–5148, Jun. 2009.
[113] S. H. Lim, C. J. Musto, E. Park, W. Zhong, and K. S. Suslick, "A Colorimetric Sensor Array for Detection and Identification of Sugars," *Org. Lett.*, vol. 10, no. 20, pp. 4405–4408, Oct. 2008.
[114] J. Kopka, "Gas Chromatography Mass Spectrometry," in *Plant Metabolomics*, P. D. K. Saito, P. D. R. A. Dixon, and P. D. L. Willmitzer, Eds. Springer Berlin Heidelberg, 2006, pp. 3–20.
[115] W. Xuan *et al.*, "Fast Response and High Sensitivity ZnO/glass Surface Acoustic Wave Humidity Sensors Using Graphene Oxide Sensing Layer," *Sci. Rep.*, vol. 4, p. 7206, Nov. 2014.

[116] G. K. Kannan, A. T. Nimal, U. Mittal, R. D. S. Yadava, and J. C. Kapoor, "Adsorption studies of carbowax coated surface acoustic wave (SAW) sensor for 2,4-dinitro toluene (DNT) vapour detection," *Sens. Actuators B Chem.*, vol. 101, no. 3, pp. 328–334, Jul. 2004.
[117] D. D. Liana, B. Raguse, J. J. Gooding, and E. Chow, "Recent Advances in Paper-Based Sensors," *Sensors*, vol. 12, no. 9, pp. 11505–11526, Aug. 2012.
[118] S. M. Z. Hossain *et al.*, "Development of a Bioactive Paper Sensor for Detection of Neurotoxins Using Piezoelectric Inkjet Printing of Sol−Gel-Derived Bioinks," *Anal. Chem.*, vol. 81, no. 13, pp. 5474–5483, Jul. 2009.
[119] X. Li, J. Tian, T. Nguyen, and W. Shen, "Paper-Based Microfluidic Devices by Plasma Treatment," *Anal. Chem.*, vol. 80, no. 23, pp. 9131–9134, Dec. 2008.
[120] A. W. Martinez, S. T. Phillips, G. M. Whitesides, and E. Carrilho, "Diagnostics for the Developing World: Microfluidic Paper-Based Analytical Devices," *Anal. Chem.*, vol. 82, no. 1, pp. 3–10, Jan. 2010.
[121] A. W. Martinez, S. T. Phillips, and G. M. Whitesides, "Three-dimensional microfluidic devices fabricated in layered paper and tape," *Proc. Natl. Acad. Sci.*, vol. 105, no. 50, pp. 19606–19611, Dec. 2008.
[122] K. Abe, K. Suzuki, and D. Citterio, "Inkjet-Printed Microfluidic Multianalyte Chemical Sensing Paper," *Anal. Chem.*, vol. 80, no. 18, pp. 6928–6934, Sep. 2008.
[123] G. Chitnis, Z. Ding, C.-L. Chang, C. A. Savran, and B. Ziaie, "Laser-treated hydrophobic paper: an inexpensive microfluidic platform," *Lab. Chip*, vol. 11, no. 6, pp. 1161–1165, Feb. 2011.
[124] Y. Zilberman, Y. Chen, and S. R. Sonkusale, "Dissolved ammonia sensing in complex mixtures using metalloporphyrin-based optoelectronic sensor and spectroscopic detection," *Sens. Actuators B Chem.*, vol. 202, pp. 976–983, Oct. 2014.
[125] H. Wang *et al.*, "Integrated Circuits Based on Bilayer MoS2 Transistors," *Nano Lett.*, vol. 12, no. 9, pp. 4674–4680, Sep. 2012.
[126] S. Tao, L. Xu, and J. C. Fanguy, "Optical fiber ammonia sensing probes using reagent immobilized porous silica coating as transducers," *Sens. Actuators B Chem.*, vol. 115, no. 1, pp. 158–163, May 2006.
[127] A. W. Martinez, S. T. Phillips, E. Carrilho, S. W. Thomas, H. Sindi, and G. M. Whitesides, "Simple Telemedicine for Developing Regions: Camera Phones and Paper-Based Microfluidic Devices for Real-Time, Off-Site Diagnosis," *Anal. Chem.*, vol. 80, no. 10, pp. 3699–3707, May 2008.
[128] Y. Zilberman and S. R. Sonkusale, "Microfluidic optoelectronic sensor for salivary diagnostics of stomach cancer," *Biosens. Bioelectron.*, vol. 67, pp. 465–471, May 2015.
[129] B. Moore, "Principal component analysis in linear systems: Controllability, observability, and model reduction," *IEEE Trans. Autom. Control*, vol. 26, no. 1, pp. 17–32, Feb. 1981.
[130] A. A. Vaughan, M. G. Baron, and R. Narayanaswamy, "Optical ammonia sensing films based on an immobilized metalloporphyrin," *Anal. Commun.*, vol. 33, no. 11, pp. 393–396, Jan. 1996.
[131] T. Dn and B. Mj, "The epidemiology of Helicobacter pylori infection.," *Epidemiol. Rev.*, vol. 13, pp. 42–59, Dec. 1990.

[132] L. Monteiro *et al.*, "Diagnosis of Helicobacter pylori Infection: Noninvasive Methods Compared to Invasive Methods and Evaluation of two New Tests," *Am. J. Gastroenterol.*, vol. 96, no. 2, pp. 353–358, Feb. 2001.
[133] J.-F. Tomb *et al.*, "The complete genome sequence of the gastric pathogen Helicobacter pylori," *Nature*, vol. 388, no. 6642, pp. 539–547, Aug. 1997.
[134] Wong B, Lam S, Wong W, and et al, "Helicobacter pylori eradication to prevent gastric cancer in a high-risk region of china: A randomized controlled trial," *JAMA*, vol. 291, no. 2, pp. 187–194, Jan. 2004.
[135] M. Plummer, S. Franceschi, J. Vignat, D. Forman, and C. de Martel, "Global burden of gastric cancer attributable to Helicobacter pylori," *Int. J. Cancer J. Int. Cancer*, vol. 136, no. 2, pp. 487–490, Jan. 2015.
[136] L. A. Torre, F. Bray, R. L. Siegel, J. Ferlay, J. Lortet-Tieulent, and A. Jemal, "Global cancer statistics, 2012," *CA. Cancer J. Clin.*, vol. 65, no. 2, pp. 87–108, Mar. 2015.
[137] E. Garza-González, G. I. Perez-Perez, H. J. Maldonado-Garza, and F. J. Bosques-Padilla, "A review of Helicobacter pylori diagnosis, treatment, and methods to detect eradication," *World J. Gastroenterol. WJG*, vol. 20, no. 6, pp. 1438–1449, Feb. 2014.
[138] H. M. T. El-Zimaity and D. Y. Graham, "Evaluation of gastric mucosal biopsy site and number for identification of Helicobacter pylori or intestinal metaplasia: Role of the sydney system," *Hum. Pathol.*, vol. 30, no. 1, pp. 72–77, Jan. 1999.
[139] S. I. Mendoza-Ibarra, G. I. Perez-Perez, F. J. Bosques-Padilla, M. Urquidi-Rivera, Z. Rodríguez-Esquivel, and E. Garza-González, "Utility of diagnostic tests for detection of Helicobacter pylori in children in northeastern Mexico," *Pediatr. Int. Off. J. Jpn. Pediatr. Soc.*, vol. 49, no. 6, pp. 869–874, Dec. 2007.
[140] R. J. Owen, "Molecular testing for antibiotic resistance in Helicobacter pylori," *Gut*, vol. 50, no. 3, pp. 285–289, Mar. 2002.
[141] S. W. Moon *et al.*, "United Rapid Urease Test Is Superior than Separate Test in Detecting Helicobacter pylori at the Gastric Antrum and Body Specimens," *Clin. Endosc.*, vol. 45, no. 4, pp. 392–396, Nov. 2012.
[142] P. Harris *et al.*, "Relevance of adjusted cut-off values in commercial serological immunoassays for Helicobacter pylori infection in children," *Dig. Dis. Sci.*, vol. 50, no. 11, pp. 2103–2109, Nov. 2005.
[143] J. P. Gisbert and J. M. Pajares, "Review article: 13C-urea breath test in the diagnosis of Helicobacter pylori infection -- a critical review," *Aliment. Pharmacol. Ther.*, vol. 20, no. 10, pp. 1001–1017, Nov. 2004.
[144] P. Malfertheiner *et al.*, "Current European concepts in the management of Helicobacter pylori infection--the Maastricht Consensus Report. The European Helicobacter Pylori Study Group (EHPSG)," *Eur. J. Gastroenterol. Hepatol.*, vol. 9, no. 1, pp. 1–2, Jan. 1997.
[145] M. H. Stevens, R. C. Thirlby, and M. Feldman, "Mechanism for high PCO2 in gastric juice: roles of bicarbonate secretion and CO2 diffusion," *Am. J. Physiol.*, vol. 253, no. 4 Pt 1, pp. G527-530, Oct. 1987.
[146] W. H. Summerskill, T. Aoyagi, and W. B. Evans, "Ammonia in the upper gastrointestinal tract of man: quantitations and relationships.," *Gut*, vol. 7, no. 5, pp. 497–501, Oct. 1966.

[147] D. H. Yang, H. S. Bom, Y. E. Joo, S. K. Choi, J. S. Rew, and C. M. Yoon, "Gastric juice ammonia vs CLO test for diagnosis of Helicobacter pylori infection," *Dig. Dis. Sci.*, vol. 40, no. 5, pp. 1083–1086, May 1995.
[148] S. Schreiber *et al.*, "The spatial orientation of Helicobacter pylori in the gastric mucus," *Proc. Natl. Acad. Sci. U. S. A.*, vol. 101, no. 14, pp. 5024–5029, Apr. 2004.
[149] R. Vilaichone and V. Mahachai, "Functional Dyspepsia and Helicobacter pylori Infection," in *Dyspepsia - Advances in Understanding and Management*, M. Curley, Ed. InTech, 2013.
[150] E. J. Seibel *et al.*, "Tethered Capsule Endoscopy, A Low-Cost and High-Performance Alternative Technology for the Screening of Esophageal Cancer and Barrett's Esophagus," *IEEE Trans. Biomed. Eng.*, vol. 55, no. 3, pp. 1032–1042, Mar. 2008.
[151] E. J. Seibel, M. Kimmey, and R. S. Johnston, "Tethered capsule endoscope for Barrett's Esophagus screening," US7530948 B2, 12-May-2009.
[152] C. M. Lee, C. J. Engelbrecht, T. D. Soper, F. Helmchen, and E. J. Seibel, "Scanning fiber endoscopy with highly flexible, 1 mm catheterscopes for wide-field, full-color imaging," *J. Biophotonics*, vol. 3, no. 5–6, pp. 385–407, Jun. 2010.
[153] Y. Chen, Y. Zilberman, P. Mostafalu, and S. R. Sonkusale, "Paper based platform for colorimetric sensing of dissolved NH3 and CO2," *Biosens. Bioelectron.*, vol. 67, pp. 477–484, May 2015.
[154] G. Monti *et al.*, "Monitoring Food Quality by Microfluidic Electrophoresis, Gas Chromatography, and Mass Spectrometry Techniques: Effects of Aquaculture on the Sea Bass (Dicentrarchus labrax)," *Anal. Chem.*, vol. 77, no. 8, pp. 2587–2594, Apr. 2005.
[155] R. Karoui, G. Downey, and C. Blecker, "Mid-Infrared Spectroscopy Coupled with Chemometrics: A Tool for the Analysis of Intact Food Systems and the Exploration of Their Molecular Structure−Quality Relationships − A Review," *Chem. Rev.*, vol. 110, no. 10, pp. 6144–6168, Oct. 2010.
[156] H. Tao *et al.*, "Silk-Based Conformal, Adhesive, Edible Food Sensors," *Adv. Mater.*, vol. 24, no. 8, pp. 1067–1072, Feb. 2012.
[157] T. S. Awad, H. A. Moharram, O. E. Shaltout, D. Asker, and M. M. Youssef, "Applications of ultrasound in analysis, processing and quality control of food: A review," *Food Res. Int.*, vol. 48, no. 2, pp. 410–427, Oct. 2012.
[158] A. Loutfi, S. Coradeschi, G. K. Mani, P. Shankar, and J. B. B. Rayappan, "Electronic noses for food quality: A review," *J. Food Eng.*, vol. 144, pp. 103–111, Jan. 2015.
[159] N. L. W. Wilson, B. Rickard, R. Saputo, and S.-T. Ho, "Food Waste: The Role of Date Labels, Package Size, and Product Category," Social Science Research Network, Rochester, NY, SSRN Scholarly Paper ID 2700692, Dec. 2015.
[160] H. Lin, M. Jang, and K. S. Suslick, "Preoxidation for Colorimetric Sensor Array Detection of VOCs," *J. Am. Chem. Soc.*, vol. 133, no. 42, pp. 16786–16789, Oct. 2011.
[161] T. Soga, Y. Jimbo, K. Suzuki, and D. Citterio, "Inkjet-Printed Paper-Based Colorimetric Sensor Array for the Discrimination of Volatile Primary Amines," *Anal. Chem.*, vol. 85, no. 19, pp. 8973–8978, Oct. 2013.
[162] A. Buryak and K. Severin, "A Chemosensor Array for the Colorimetric Identification of 20 Natural Amino Acids," *J. Am. Chem. Soc.*, vol. 127, no. 11, pp. 3700–3701, Mar. 2005.

[163] H. N. Kim, W. X. Ren, J. S. Kim, and J. Yoon, “Fluorescent and colorimetric sensors for detection of lead, cadmium, and mercury ions,” *Chem. Soc. Rev.*, vol. 41, no. 8, pp. 3210–3244, Mar. 2012.
[164] Z. Li and K. S. Suslick, “Portable Optoelectronic Nose for Monitoring Meat Freshness,” *ACS Sens.*, vol. 1, no. 11, pp. 1330–1335, Nov. 2016.
[165] X. Huang *et al.*, “Determination of pork spoilage by colorimetric gas sensor array based on natural pigments,” *Food Chem.*, vol. 145, pp. 549–554, Feb. 2014.
[166] M. K. Morsy *et al.*, “Development and validation of a colorimetric sensor array for fish spoilage monitoring,” *Food Control*, vol. 60, pp. 346–352, Feb. 2016.
[167] U. Khulal, J. Zhao, W. Hu, and Q. Chen, “Comparison of different chemometric methods in quantifying total volatile basic-nitrogen (TVB-N) content in chicken meat using a fabricated colorimetric sensor array,” *RSC Adv.*, vol. 6, no. 6, pp. 4663–4672, 2016.
[168] A. Ozcan, “Mobile phones democratize and cultivate next-generation imaging, diagnostics and measurement tools,” *Lab. Chip*, vol. 14, no. 17, pp. 3187–3194, 2014.
[169] Q. Wei *et al.*, “Fluorescent Imaging of Single Nanoparticles and Viruses on a Smart Phone,” *ACS Nano*, vol. 7, no. 10, pp. 9147–9155, Oct. 2013.
[170] H. Zhu *et al.*, “Cost-effective and rapid blood analysis on a cell-phone,” *Lab. Chip*, vol. 13, no. 7, pp. 1282–1288, 2013.
[171] L. Guan, J. Tian, R. Cao, M. Li, Z. Cai, and W. Shen, “Barcode-Like Paper Sensor for Smartphone Diagnostics: An Application of Blood Typing,” *Anal. Chem.*, vol. 86, no. 22, pp. 11362–11367, Nov. 2014.
[172] V. Oncescu, D. O’Dell, and D. Erickson, “Smartphone based health accessory for colorimetric detection of biomarkers in sweat and saliva,” *Lab. Chip*, vol. 13, no. 16, pp. 3232–3238, 2013.
[173] H. Yu, Y. Tan, and B. T. Cunningham, “Smartphone Fluorescence Spectroscopy,” *Anal. Chem.*, vol. 86, no. 17, pp. 8805–8813, Sep. 2014.
[174] A. K. Yetisen, J. L. Martinez-Hurtado, A. Garcia-Melendrez, F. da Cruz Vasconcellos, and C. R. Lowe, “A smartphone algorithm with inter-phone repeatability for the analysis of colorimetric tests,” *Sens. Actuators B Chem.*, vol. 196, pp. 156–160, Jun. 2014.
[175] L. Shen, J. A. Hagen, and I. Papautsky, “Point-of-care colorimetric detection with a smartphone,” *Lab. Chip*, vol. 12, no. 21, pp. 4240–4243, 2012.
[176] D. Zhang, M. C. Huarng, and E. C. Alocilja, “A multiplex nanoparticle-based bio-barcoded DNA sensor for the simultaneous detection of multiple pathogens,” *Biosens. Bioelectron.*, vol. 26, no. 4, pp. 1736–1742, Dec. 2010.
[177] A. Santos *et al.*, “Nanoporous Anodic Alumina Barcodes: Toward Smart Optical Biosensors,” *Adv. Mater.*, vol. 24, no. 8, pp. 1050–1054, Feb. 2012.
[178] M. Ramya and M. Jayasheela, “Improved Color QR Codes for Real Time Applications with High Embedding Capacity,” *Int. J. Comput. Appl. N. Y.*, vol. 91, no. 8, 2014.
[179] V. Oncescu, M. Mancuso, and D. Erickson, “Cholesterol testing on a smartphone,” *Lab Chip*, vol. 14, no. 4, pp. 759–763, Jan. 2014.
[180] S. M. Barnard and D. R. Walt, “Fiber-optic organic vapor sensor,” *Environ. Sci. Technol.*, vol. 25, no. 7, pp. 1301–1304, Jul. 1991.

[181] C. C. Balamatsia, A. Patsias, M. G. Kontominas, and I. N. Savvaidis, "Possible role of volatile amines as quality-indicating metabolites in modified atmosphere-packaged chicken fillets: Correlation with microbiological and sensory attributes," *Food Chem.*, vol. 104, no. 4, pp. 1622–1628, 2007.
[182] M. C. Vidal-Carou, M. L. Izquierdo-Pulido, M. C. Martín-Morro, and Mariné-Font, "Histamine and tyramine in meat products: Relationship with meat spoilage," *Food Chem.*, vol. 37, no. 4, pp. 239–249, Jan. 1990.
[183] D. W. V. der Weide, J. Murakowski, and F. Keilmann, "Gas-absorption spectroscopy with electronic terahertz techniques," *IEEE Trans. Microw. Theory Tech.*, vol. 48, no. 4, pp. 740–743, Apr. 2000.
[184] Y. S. Kim, "Microheater-integrated single gas sensor array chip fabricated on flexible polyimide substrate," *Sens. Actuators B Chem.*, vol. 114, no. 1, pp. 410–417, Mar. 2006.
[185] T. Songjaroen, W. Dungchai, O. Chailapakul, C. S. Henry, and W. Laiwattanapaisal, "Blood separation on microfluidic paper-based analytical devices," *Lab. Chip*, vol. 12, no. 18, pp. 3392–3398, 2012.
[186] H. Liu and R. M. Crooks, "Paper-Based Electrochemical Sensing Platform with Integral Battery and Electrochromic Read-Out," *Anal. Chem.*, vol. 84, no. 5, pp. 2528–2532, Mar. 2012.
[187] Z. Nie *et al.*, "Electrochemical sensing in paper-based microfluidic devices," *Lab. Chip*, vol. 10, no. 4, pp. 477–483, 2010.
[188] H. Gullapalli *et al.*, "Flexible Piezoelectric ZnO–Paper Nanocomposite Strain Sensor," *Small*, vol. 6, no. 15, pp. 1641–1646, Aug. 2010.
[189] A. Russo, B. Y. Ahn, J. J. Adams, E. B. Duoss, J. T. Bernhard, and J. A. Lewis, "Pen-on-Paper Flexible Electronics," *Adv. Mater.*, vol. 23, no. 30, pp. 3426–3430, Aug. 2011.
[190] K. A. Mirica, J. M. Azzarelli, J. G. Weis, J. M. Schnorr, and T. M. Swager, "Rapid prototyping of carbon-based chemiresistive gas sensors on paper," *Proc. Natl. Acad. Sci.*, vol. 110, no. 35, pp. E3265–E3270, Aug. 2013.
[191] K. A. Mirica, J. G. Weis, J. M. Schnorr, B. Esser, and T. M. Swager, "Mechanical Drawing of Gas Sensors on Paper," *Angew. Chem. Int. Ed.*, vol. 51, no. 43, pp. 10740–10745, Oct. 2012.
[192] S. E. Lewis, J. R. DeBoer, J. L. Gole, and P. J. Hesketh, "Sensitive, selective, and analytical improvements to a porous silicon gas sensor," *Sens. Actuators B Chem.*, vol. 110, no. 1, pp. 54–65, Sep. 2005.
[193] B. Cho *et al.*, "Graphene-based gas sensor: metal decoration effect and application to a flexible device," *J. Mater. Chem. C*, vol. 2, no. 27, pp. 5280–5285, 2014.
[194] A. C. Romain and J. Nicolas, "Long term stability of metal oxide-based gas sensors for e-nose environmental applications: An overview," *Sens. Actuators B Chem.*, vol. 146, no. 2, pp. 502–506, Apr. 2010.
[195] A. Tamayol *et al.*, "Flexible pH-Sensing Hydrogel Fibers for Epidermal Applications," *Adv. Healthc. Mater.*, vol. 5, no. 6, pp. 711–719, Mar. 2016.
[196] P. Mostafalu, M. Akbari, K. A. Alberti, Q. Xu, A. Khademhosseini, and S. R. Sonkusale, "A toolkit of thread-based microfluidics, sensors, and electronics for 3D tissue embedding for medical diagnostics," *Microsyst. Nanoeng.*, vol. 2, p. 16039, Jul. 2016.